2020

NDRG1 AND MYELIN-RELATED DISEASE: ALCOHOLISM AND CHEMOTHERAPY-INDUCED NEUROPATHY

Guy Harris

NDRG1 AND MYELIN-RELATED DISEASE: ALCOHOLISM AND CHEMOTHERAPY-INDUCED NEUROPATHY

A dissertation submitted in partial fulfillment of the requirements for the degree of Doctor of Philosophy at Virginia Commonwealth University.

by

Guy M. Harris

Bachelor of Science, Georgia Institute of Technology, 2009

Master of Science, Louisiana State University, 2012

Director: Michael F. Miles, M.D., Ph.D.,

Professor, Department of Pharmacology and Toxicology

Virginia Commonwealth University

Richmond, VA

August 21, 2020

Acknowledgments

I would like to thank my advisor, Dr. Michael Miles, for his guidance, wisdom, and expertise. He has been an incredible resource and his creative out-of-the-box thinking has helped me learn how to approach complex problems from new angles. For that, I will always be very grateful.

I thank my committee members: Dr. Jill Bettinger, Dr. Babette Fuss, Dr. Kurt Hauser, and Dr. Ross Mikkelsen. Their unique perspectives and critical analysis of my work helped me tackle this ambitious project and has refined the way I approach the scientific method. Similarly, Dr. Jennifer Wolstenholme has been a constant positive influence on my training, offering her technical expertise, life advice, and encouragement.

I would also like to thank my wife, Amanda Harris, who has always been so supportive and always lent a sympathetic ear during the more difficult times of my training.

To my friends and former labmates, Rory Weston and Andrew van der Vaart, will always perish the long and deep discussions we had both inside and outside of lab. I could not have asked for two better partners in crime.

I would like to express my gratitude to the VCU MD-PhD program and especially to Dr. Donnenberg for his dedication to improving the program and increasing the wellbeing of its students.

I want to thank my parents for years of generosity and support throughout my education. None of would have ever been possible without their help. I also want to thank my Uncle Jerry. Our talks over the years helped to kindle the scientific fire that burned within me.

Table of Contents

Acknowledgements . . . . . **ii**

Table of Contents . . . . . **iii**

List of Tables . . . . . **vi**

List of Figures . . . . . **vii**

List of Abbreviations . . . . . **x**

Clarification of Contributions . . . . . **xii**

Abstract . . . . . **xiv**

1 Introduction **1**

2 Background and Significance **6**
2.1 Sensitivity to alcohol and future risk 6
2.1.1 Measures of sensitivity to ethanol 8
2.2 Identification of candidate genes / networks involved in risk of alcoholism 8
2.3 Myelin as a risk factor 10
2.4 N-myc Downstream Regulated Gene 1 12
2.4.1 General background 13
2.4.2 The Role of *Sgk1*-Mediated Phosphorylation 14
2.4.3 *Ndrg1*: importance in lipid dynamics and myelination 16
2.5 *Ndrg1* and chemotherapy-induced peripheral neuropathy (CIPN) 17
2.6 *Ndrg1*: involvement with signaling pathways 18
2.6.1 *Ndrg1* is an upstream regulator and a downstream target of ethanol responsive signaling pathways 21
2.7 Investigations of mPFC *Ndrg1* and alcohol 22
2.8 Closing Remarks 24

3 Characterization of cellular expression and ethanol regulation of *Ndrg1* in the mPFC 26
3.1 Introduction 26
3.2 Materials and Methods 28
3.2.1 Animals 28
3.2.2 Prepared Solutions 29
3.2.3 Intermittent Alcohol Drinking 29
3.2.4 Acute Ethanol Exposure 30
3.2.5 BEC Measurements 30
3.2.6 Antibodies and Primers 32
3.2.7 qPCR Methodology 33

3.2.8 Western Blot Methodology . . . 33
3.2.9 Immunohistochemistry Methodology . . . 34
3.2.10 Microscopy Methods . . . 36
3.2.11 Statistical Analysis Methods . . . 36
3.3 Results . . . 36
3.3.1 Basal Expression Patterns in mPFC . . . 36
3.3.2 Modulation of *Ndrg1* by Acute Ethanol . . . 40
3.3.3 Modulation of *Ndrg1* by Chronic Consumption of Ethanol . . . 46
3.4 Discussion and Conclusions . . . 53

4 Genetic Effects of *Ndrg1* knockout in myelinating cells . . . 56
4.1 Introduction . . . 56
4.2 Materials and Methods . . . 58
4.2.1 Drugs Used in Chapter . . . 58
4.2.2 Tamoxifen Treatment . . . 58
4.2.3 Tamoxifen Inducible Cre Recombinase Mouse Line . . . 58
4.2.4 Prepared Solutions . . . 60
4.2.5 Ethanol Exposure Models . . . 60
4.2.6 Loss of Righting Reflex (LORR . . . 61
4.2.7 Western Blotting . . . 61
4.2.8 Immunohistochemistry . . . 64
4.2.9 Tastant Alteration Studies . . . 65
4.2.10 Ethanol Pharmacokinetics . . . 65
4.2.11 Light-Dark (LD) Box Testing . . . 66
4.2.12 Antibodies and Primers . . . 66
4.2.13 Microscopy . . . 67
4.2.14 Mechanical Sensitivity . . . 67
4.2.15 Thermal Sensitivity . . . 67
4.2.16 Nerve Conduction Velocity Testing . . . 68
4.2.17 Rotarod Testing . . . 68
4.2.18 Paclitaxel Sensitivity Study . . . 69
4.2.19 High Dose Ethanol Neuropathy Study . . . 69
4.3 Results . . . 70
4.3.1 Validation of the *Ndrg1* Deletion in Myelinating Cells . . . 70
4.4 Control Experiments . . . 74
4.5 Deletion of *Ndrg1* in Myelinating Cells Alters Ethanol-Related Behaviors . . . 76
4.6 Deletion of *Ndrg1* Results in Peripheral Nerve Dysfunction . . . 79
4.6.1 Deletion of *Ndrg1* Leads to Long-Lasting Mechanical Hypersensitivity . . . 79
4.6.2 Homozygous Deletion of *Ndrg1* Causes Alterations of Thermal Sensitivity . . . 82
4.6.3 Heterozygous Deletion of *Ndrg1* does not Alter Sensitivity . . . 82
4.6.4 *Ndrg1* Deletion Results in Motor Skill Deficits, but Not Motor Learning . . . 83
4.6.5 *Ndrg* Deletion Adversely Affects Peripheral Nerve Conduction and Velocity 84
4.6.6 Sensitivity to Severity of Paclitaxel-Induced Neuropathies is Enhanced by*Ndrg* deletion . . . 85

4.6.7 Repeated High Doses of Ethanol do not Alter the Development of Mechanical or Cold Sensitivity Following Deletion of *Ndrg1* 87
4.7 Discussion 88

5 GCSscore: a differential expression algorithm 92
5.1 Introduction 92
5.2 Implementation 94
5.2.1 Algorithm 94
5.2.2 Statistical properties and analysis of GCSscore outputs 96
5.2.3 Workflow for generating differential expression for downstream analysis . . 96
5.3 Results 99
5.3.1 Comparison with original algorithm 99
5.3.2 Comparison with RMA analysis of ClariomD/XTA assays 100
5.3.3 Comparison with RMA analysis of ClariomS assays 108
5.4 Discussion 112

6 Discussion, Conclusions, and Future Directions 115
6.1 Ethanol and Expression of *Ndrg1* in Oligodendrocytes 115
6.2 Ethanol Modulates *Ndrg1* Expression Patterns 116
6.3 *Ndrg1* Levels Modulate Ethanol-Related Behaviors 117
6.4 *Ndrg1* Levels Modulate Peripheral Nerve Function 119
6.5 Theories for Observed Effects of *Ndrg1* Deletion 121
6.6 Concluding Remarks 122

References 124

Vita 135

List of Tables

3.1 Sequences for primers used in Chapter 3 32

5.1 Example of formatting for BATCH input into in GCSscore 98

5.2 Functional GO enrichment for GCS-score results for GEO dataset: GSE76700. Top 5 enrichments for the listed GO categories returned from ToppFun GO Suite . 105

5.3 GCS-score results for all 15 exon-level probesetids assigned to *Lcn2* 107

5.4 Functional GO enrichment for GCS-score results for GEO dataset: GSE103380. Top 5 enrichments for the listed GO categories returned from ToppFun GO Suite . 111

List of Figures

1.1 Brain regions affected by alcohol-induced neurological conditions. 2

2.1 Role of myelin in development of alcohol dependence 12

2.2 Cluster of myelin related ethanol responsive genes in the mPFC 13

2.3 NDRG1 protein domains and binding sites 15

2.4 Overview of NDRG1 interactions upstream of signaling pathways 22

2.5 Basal NDRG1 expression correlations with ethanol phenotypes 24

2.6 Ethanol phenotypes from shRNA knockdown of NDRG1 in the mPFC of B6 mice . 24

3.1 Animal models of acute and chronic ethanol exposure 31

3.2 Microscopy of sh-*Ndrg1* infected cells with neuronal marker, NeuN 37

3.3 Cell type expression of NDRG1 in mPFC: NeuN, CC1, and CNPase 38

3.4 Basal sub-cellular localization of phospho-forms of NDRG1within olgiodendrocytes of mPFC 39

3.5 Quantification of basal sub-cellular localization of phospho-forms of NDRG1 . . . 40

3.6 qPCR analysis of *Ndrg1* transcript levels following acute ethanol exposure 41

3.7 Example of Western blot imaging and quantification for Thr346-pNDRG1 in chronic drinking male mice 42

3.8 Modulation of phospho and total NDRG1 following acute ethanol dose response . . 43

3.9 Levels of Thr346-pNDRG expression in mPFC are altered by acute ethanol exposure 44

3.10 Comparison of nuclear to cytosol ratio of phospho-NDRG1 signal following acute ethanol exposure 45

3.11 Drinking patterns over time in 5 week 2-bottle choice IEA study 47

3.12 BEC measurements of select mice at the 2 hour binge reading point after 5 weeks of 2-bottle choice IEA drinking 48

3.13 qPCR analysis of *Ndrg1* transcript levels following 5 weeks of chronic ethanol exposure 49

3.14 qPCR analysis of a panel of 4 myelin genes following 5 weeks of chronic consumption of ethanol 50
3.15 Western blots for NDRG1 and MBP following chronic ethanol exposure 51
3.16 Scans of membranes stained for NDRG1 and MBP following chronic ethanol exposure in female and male mice 52
4.1 Schematic of NDRG1 KO line genetic manipulations 60
4.2 IHC validation of KO in male and female PCNdrg1 mice, 4 weeks post-Tamoxifen 70
4.3 Confocal validation of KO of NDRG1 in oligodendrocytes and myelin PCNdrg1 mice, male mouse 6 weeks post-Tamoxifen 71
4.4 Western blot validation of KO of Myelin protein expression following *Ndrg1* deletion 72
4.5 Western blot validation of KO of NDRG1 and MBP levels in peripheral nerve tissue 73
4.6 Control experiments for PCNdrg1 KO mouse line 75
4.7 Ethanol pharmacokinetics: BEC time course following 4 g/kg of acute ethanol . . . 76
4.8 Comparison of male and female average daily ethanol (g/kg) in 3-bottle choice drinking 77
4.9 Average daily ethanol intake and average preference for ethanol by each drinking week 78
4.10 Loss of Righting Reflex (LORR) onset and duration 79
4.11 Time course for development of altered mechanical sensitivity: baseline measurement 80
4.12 Time course for development of altered mechanical sensitivity: 2 weeks and 8 weeks post-Tamoxifen 80
4.13 Altered mechanical sensitivity long after Tamoxifen administration: 8 months post-Tamoxifen 81
4.14 Thermal sensitivity testing of PCNdrg1 KO mice 3 months post-Tamoxifen 81
4.15 Tracking of mechanical and cold sensitivity over time in heterozygous *Ndrg1* KO mice 83
4.16 Performance on a fixed speed Rotarod protocol over time 84
4.17 Nerve conduction and velocity testing 6 months port-Tamoxifen 85

4.18 Tracking of mechanical sensitivity over time following Tamoxifen and low-dose Paclitaxel 86
4.19 Tracking of mechanical and cold sensitivity over time following repeated high doses of following deletion of *Ndrg1* 88
5.1 Workflow diagram for GCS-score algorithm. 97
5.2 Example histogram for GCSscore output 98
5.3 Comparison of results for original S-score algorithm and GCS-score algorithm . . . 101
5.4 Fold change vs averaged GCSscore (*AvgSs*) for all publication-identified TCids in cerebral cortex from GEO dataset: GSE76700 103
5.5 Functional pathway enrichment for GCS-score results for GEO dataset: GSE76700. Top 20 pathways returned from IPA 104
5.6 Exon- level GCGscores for *Lcn2* expression in GEO dataset: GSE76700 106
5.7 Top 10 enriched pathways via Ingenuity Pathway Analysis (IPA) for GCS-score analysis of GEO dataset: GSE103380 109
5.8 Correlation of *AvgSs* values with reported linear fold change for dataset: GSE103380 110
6.1 Theories for role of *Ndrg1* in modulation of acute ethanol sensitivity and normal myelin function 120

List of Abbreviations

5-HT	Serotonin receptor
ACD	Acetaldehyde
ADH	Alcohol dehydrogenase
AFT	Acute functional Tolerance
ALDH	Aldehyde dehydrogenase
APO	Apolipoprotein
ARLD	Alcohol-related liver disease
AUD	Alcohol use disorder
B6J	C57BL/6J mice
BEC	Blood ethanol concentration
BK	Large conductance Ca2+ and voltage-activated K+ (BK) channel
BXD	RI strains of C57BL/6J crossed DBA/2J mice
Cre	Cre recombinase
Cre+	Cre recombinase positive *Ndrg1* KO
Cre-	Cre recombinase negative *Ndrg1* control
CIPN	Chemotherapy-induced peripheral neuropathy
CMT4D	Charcot-MarieTooth Disease 4D
CNS	Central Nervous System
D2	DBA/2J mice
DEG	Differentially expressed genes
DSM-V	Diagnostic and Statistical Manual of Mental Disorders
DZP	Diazepam
EtOH	Ethanol
EMT	Epithelial-Mesenchymal Transition
FDR	False Discovery Rate
FYN	Proto-oncogene tyrosine-protein kinase Fyn
GABA	Gamma aminobutyric acid
GIRK	G protein-coupled inwardly-rectifying potassium channel
GO	Gene Ontology
GSK3B	Glycogen Synthase Kinase 3 Beta
GWAS	Genome-wide association study
i.p.	Intraperitoneal injection
IEA	Intermittent ethanol access drinking protocol
IPA	Ingenuity Pathway Analysis
KCNMA1	Potassium Calcium-Activated Channel Subfamily M Alpha 1
KO	Knockout mouse line
LDLR	Low density lipoprotein receptor
LIMMA	Linear Models for Microarray Data
LORR	Loss-of-righting reflex
MBP	Myelin Basic Protein
MPZ	Myelin Protein Zero

NAc	Nucleus Accumbens core
mPFC	Medial prefrontal cortex
nACh	Nicotinic acetylcholine receptor
NDRG1	N-myc downstream regulated gene 1
NeuN	Neuronal nuclei marker
NMDA	N-Methyl- d-aspartic acid
OOV	Out of vivarium animal housing
PDE4	Phosphodiesterase-4
PFC	Prefrontal Cortex
PIPN	Paclitaxel-induced peripheral neuropathy
PLP	Proteolipid protein
PNS	Peripheral nervous system
PSRid	Probe selection region ID
qPCR	Quantitative polymerase chain reaction
RI	Recombinant Inbred mouse line
RIPA	Lysis and Extraction Buffer
RMA	Robust Multiarray Analysis
ROI	Region of interest
RORR	Recovery-of-righting reflex
SAM	Significance analysis of microarrays
SGK1	Serum/Glucocorticoid Regulated Kinase 1
SNP	Single nucleotide polymorphism
TCid	Transcription cluster ID

Clarification of Contributions

Many individuals made invaluable contributions to the body of work presented in this dissertation. All other unlisted works were exclusively by me.

Chapter 3

I performed the acute ethanol dose-response and harvested the tissue with Andrew Van der Vaart. I ran the intermittent ethanol access (IEA) experiment with the help of Andrew Van der Vaart and Phoebe Lin. Rory Weston performed cryostat sectioning for the brains used in the acute ethanol immunohistochemistry. Dalton Jun-da Huey contributed to running and the analysis of all Western blots. I ran the Analox analyses of BEC with Andrew Van der Vaart. Dr. Bernas and Frances White provided the training and resources to acquire the microscopy results presented in this chapter. The retro-orbital sinus bleeds for BEC determination were performed with the help of Dr. Jennifer Wolstenholme. The qPCR experiments were designed by me, but were run by Morgan Driver.

Chapter 4

Madison Philhower performed the cyrostat sectioning and staining of immunohistochemistry of the *Ndrg1*-knockout mice. Dalton Huey played a pivotal role in the troubleshooting, running, and analysis of the Western blots presented in this chapter. Rory Weston aided in the experimental designs regarding myelin levels following *Ndrg1* deletion validation. Ernesto Blay aided in the acquiring the Rotarod machine data. Dr. Imad Damaj and Dr. Wisam Toma were absolutely essential to the experimental design and testing of the peripheral nerve functions following *Ndrg1*-deletion. The Von Frey filament, Nerve Conduction Velocity, Acetone, and Tail Flick test were all performed by Dr. Wisam Toma. The retro-orbital sinus bleeds for BEC determination were performed with the help of Dr. Jennifer Wolstenholme.

Chapter 5 The algorithm was re-written by Shahroze Abbas under my supervision. The rewrite was based on the first R package *sscore*, which was originally written by Dr. Robert Kennedy. The original algorithm was conceived by Dr. Li Zhang and Dr. Michael Miles.

Abstract

Alcohol use disorder (AUD) is a prevalent neuropsychiatric disease with profound health, social, and economic consequences. With an estimated 50% heritability, identifying genes that engender risk and contribute to the underlying neurobiological mechanisms represents an important first step in developing effective treatments. Gene expression studies are an important source of candidate genes for studying AUD, providing windows into the molecular machinery engaged by the brain in response to ethanol. Our laboratory has implicated N-myc down-regulated gene 1 (*Ndrg1*) as a potential candidate gene that modulates ethanol-induced changes in myelin-related gene expression and acute sensitivity to ethanol. Analysis of mPFC expression data found that *Ndrg1* expression was positively correlated with voluntary ethanol intake across the BXD panel of mice and demonstrated that the basal levels of *Ndrg1* mRNA expression in the mPFC across seven different strains of mice was inversely correlated with LORR duration time. We found that mPFC *Ndrg1* expression was upregulated following 5 weeks of intermittent ethanol access in C57BL/6J (B6J) mice. We also observed an induction of *Ndrg1* in the mPFC of female B6J mice following acute ethanol exposure. After observing the regulation of *Ndrg1* in wild type mice, studies were performed in a mouse line that produces a myelinating cell-selective conditional knockout (KO) of *Ndrg1*, by inducing Cre Recombinase with tamoxifen treatment. Our findings demonstrate that *Ndrg1* expression and its functional state, as determined by phosphorylation state and localization, are clearly modulated by acute ethanol.. We also found that deletion of *Ndrg1* in myelinating cells alters ethanol-related behaviors in a way that suggests sensitivity to ethanol is modified. Additionally, we found altered ethanol concentration preferences and total ethanol preference between the KO and control groups in a 5-week drinking study. Mutations in *Ndrg1* result in a demyelinating polyneuropathy: Charcot-MarieTooth Disease 4D. Given that mutations in *Ndrg1* are known to cause peripheral neuropathies in multiple species, we characterized the peripheral nerve dysfunction that develops from conditional deletion of the gene in adult aged mice. Additionally, some evidence in clinical literature had suggested that nerve tissue levels of NDRG1 inversely correlates

with chemotherapy-induced peripheral neuropathy (CIPN) following treatment with Paclitaxel for breast cancer. We demonstrated that low dose Paclitaxel accelerates the development of neuropathy symptoms in mice that have had *Ndrg1* knocked out. The literature and our results suggest that cellular bio-lipids and lipid interactions with BK channels, such as *Kcnma1*, are key drivers for both the peripheral nerve dysfunction and the changes in ethanol sensitivity, but more studies are needed to prove this hypothesis. These results demonstrated the importance of *Ndrg1* for peripheral nerve function and demonstrated that decreasing levels of *Ndrg1* do increase the toxic effects of chemotherapeutics. Ultimately, the works presented here demonstrate the biological importance of *Ndrg1* in the maintenance of peripheral nerve function and as an ethanol-related gene that modulates ethanol sensitivity, consumption, and risk for developing an AUD.

Chapter 1

Introduction

In the United States, 17 million adults (7.2% of the population 18 years or older) met the criteria for having an Alcohol Use Disorder (AUD) in 2012 (SAMHSA 2013). AUD is a clinical diagnosis that encompasses a spectrum ranging from mild problem drinking to severe alcohol dependence, according to DSM-V (American Psychiatric Association 2013). Long term abuse of alcohol leads to end organ damage, abusive behaviors, and results in excessive and compulsive consumption (Osna and Kharbanda 2016). Alcohol abuse is the third highest cause of preventable deaths in the United States, following tobacco use and unhealthy diet (Mokdad 2004). Even though the burden of alcohol abuse on society is large, there have been few medical interventions that successfully treat the disease. In fact, it is estimated that less than 20% of alcoholics achieve sustained abstinence with current approaches (Thompson and Lande 2018).

Multiple studies in animal models and humans have made it clear that gene expression, especially in the basal state before any ethanol exposure, contributes to the molecular and behavioral response to ethanol and the propensity to develop AUD. Additionally, it is estimated that 50% of the risk for developing alcohol dependence can be attributed to genetic predisposition (Goodwin 1974; Prescott and Kendler 1999). In particular, genetic factors that alter the magnitude of gene expression, basally or in response to ethanol, are considered to be part of the mechanisms that result in a predisposition for developing alcohol dependence (Chesler et al. 2005). While much remains unknown regarding all the actions of ethanol, it is known that acute ethanol interacts directly with many ligand-gated ion channels, such as GABA and NMDA receptors. Furthermore, the gene expression of these ion channels are regulated by both acute and chronic ethanol exposure (Farris and Miles 2013). Given that these receptors play a crucial role in behavioral responses to ethanol, it suggests that genomic-level gene expression analysis can provide additional novel targets for genes that modulate ethanol behaviors and may contribute to genetic risk for AUD.

In another example of the relationship between ethanol, gene expression and mechanisms of AUD, alcoholic patients are likely to face myelin-related sequelae after years of abuse. Pathologic studies of postmortem alcoholic brains have revealed white matter atrophy, particularly in the frontal cortex (Kril et al. 1997). Early microarray analysis of postmortem frontal cortex of human alcoholics found that several myelin-related genes are significantly down regulated relative to control (Lewohl et al. 2000). Latter neuroimaging studies of living alcoholics confirmed white matter deficits in vivo (Zahr and Pfefferbaum 2017). While the greatest white matter reductions were observed in the mPFC, there are several other myelin related disorders that affect chronic alcoholics. The most common neurological disorders and the selective areas of the brain where the white matter or the gray matter damage is most severe are highlighted in Figure 1.1. This shows the deleterious effects of alcohol abuse on myelin is widespread throughout the central nervous system. In addition, chronic abuse of ethanol results in damage to a number of different tissue types, including: skeletal and cardiac muscle, liver, immune system and both the central and peripheral nervous systems (Chopra and Tiwari 2012).

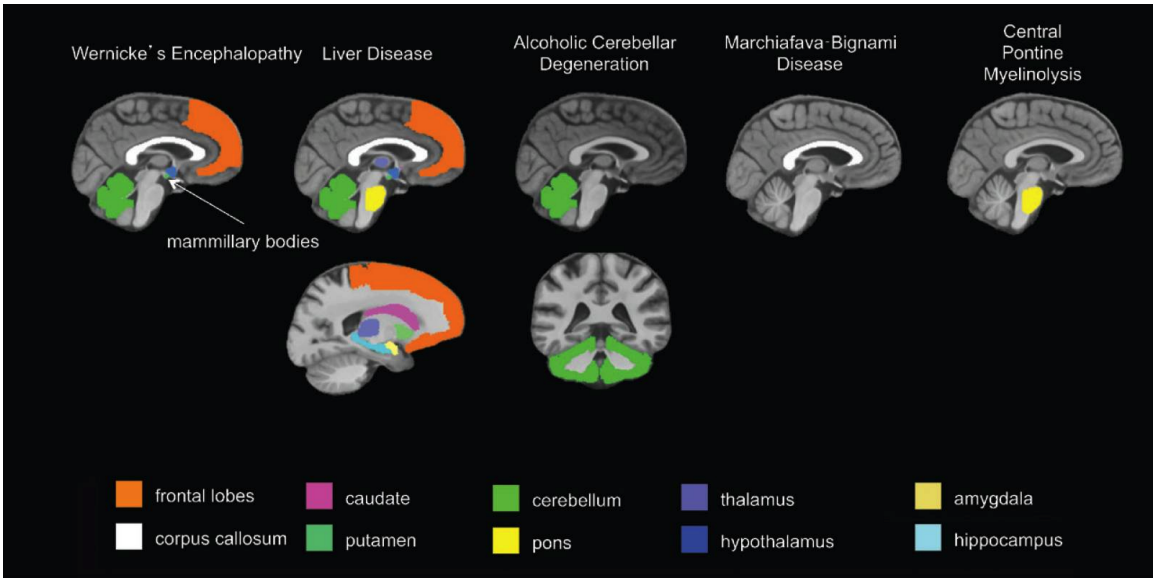

Figure 1.1: Brain areas affected by alcohol-induced neurological conditions. Of note, Marchiafava-Bignami disease (MBD), Wernicke's Encephalopathy, and Liver Disease all affect white matter within the corpus callosum. Central pontine myelinolysis (CPM) also affects white matter in a distinctly different region of the brain. Figure from: Zahr and Pfefferbaum 2017.

Chronic excessive consumption of ethanol has been shown to produce a peripheral neuropathy. In the beginning stages, patients present with complaints of pain that results in allodynia, hyperalgesia, and a burning or tearing pain, especially in the lower extremities (Koike et al. 2001). Unfortunately, alcohol-induced neuropathies respond poorly to existing pharmacotherapies (Chopra and Tiwari 2012). Alcoholism-related thiamine deficiency leads to nervous system damage in cases such as Beriberi neuropathy and Wenicke-Korsakoff disease, but is not the cause of many cases of alcohol-induced neuropathy. Interestingly, a study of patients with alcohol neuropathy and normal thiamine levels found small myelinated and unmyelinated nerve fiber density to be more severely affected than large myelinated fiber density (Koike et al. 2001). This reduced nerve fiber density, along with pathologic and eletrophyisologic evidence, suggest an axonal neuropathy (Koike et al. 2001). Additionally, thiamine-induced neuropathy has prominent subperineurial edema between the perineurium and the endoneurial compartments, while widening of the distance between nodes of Ranvier results in the segmental demyelination and remyelination (Koike et al. 2003). These findings suggest that alcohol-induced neuropathy is caused directly by the toxic actions of ethanol or the resulting metabolites, rather than thiamine deficiency.

As mentioned above, genetic factors have a major influence on susceptibility to developing an AUD (Kalsi et al. 2009). In particular, it has been hypothesized that genetic determinants modulating sensitivity to the intoxicating effects of acute ethanol exposure are an important risk factor for developing an AUD (Schuckit et al. 1994; Gilman et al. 2012). Our laboratory has identified a novel myelin-related candidate gene, *Ndrg1*, that is regulated at the level of mRNA abundance by both acute and chronic ethanol exposure (Kerns et al. 2005; Bogenpohl et al. 2019). Furthermore, NDRG1 protein phosphorylation is also regulated by acute ethanol treatment in mice (Costin, Dever, and Miles 2013). *Ndrg1* encodes the alpha/beta hydrolase: N-myc down- regulated gene 1 (NDRG1). The NDRG1 protein is typically found in the cytoplasm of many different cell types and it is thought to be involved in cellular stress responses, cancer related signaling pathways, and cell trafficking, particularly in myelin-producing cells (Berger et al. 2004). Mutations in NDRG1 in humans underlie Charcot-Marie-Tooth disease type 4D, an autosomal recessive demyelinating pe-

ripheral neuropathy and immunocytochemistry studies show high levels of NDRG1 expression in areas enriched in myelin (Okuda, Kokame, and Miyata 2008). While the exact function of NDRG1 is still unknown, multiple animal model studies have shown that modulation of *Ndrg1* expression can produce variation in myelin structure and function, particularly in the peripheral nervous system (Okuda et al. 2004), but also in the central nervous system of humans (Echaniz-Laguna et al. 2007).

The studies described above suggest that myelin basal expression is an important determinant of acute sensitivity to ethanol and hence, to the risk for abusive ethanol consumption. They further suggest that ethanol can regulate myelin expression and that *Ndrg1* is a potential key gene involved in this response. We hypothesize that *Ndrg1* expression is an important factor determining sensitivity to ethanol and that regulation of *Ndrg1* by ethanol exposure may have a role in the long term risk for abusive consumption. As individuals progress from initial ethanol exposure to clinical alcoholism, we also hypothesize that fundamental changes occur in the physiological and behavioral responses from initial versus chronic ethanol exposure. Additionally, we also hypothesize that changes in myelin related gene expression during this transition, in part, drive alterations in behavioral responses to ethanol, such as the sensitivity to both the rewarding and aversive effects of ethanol, thus resulting in escalating consumption of ethanol over time. We proposed the following specific aims to test these hypotheses: (1) To determine whether acute and chronic ethanol show differential effects on the gene expression, protein expression, or protein activity of a previously identified genetic hub of ethanol responsive myelin-relates network in mPFC, *Ndrg1*. (2) To determine whether genetic modulation of *Ndrg1* in myelin-producing cells alters ethanol-related behaviors, particularly ethanol consumption, and determine how loss of *Ndrg1* in oligodendrocytes alters brain gene expression. (3) Study the peripheral effects of *Ndrg1* deletion on sciatic nerve function and sensitivity to noxious stimuli, such as repeated high doses of ethanol and chemotherapeutics.

Additionally, this will be the first study to fully characterize the cell biology of NDRG1 in the CNS, and document ethanol regulation of *Ndrg1* in both male and female mice. Given that male and female humans have differing responses to ethanol and that there are documented differences

in the risk factors for alcohol use disorders between the sexes (Nolen-Hoeksema 2004), these studies may aid in identification of sex-specific molecular risk factors for AUD.

Chapter 2

Background and Significance

2.1 Sensitivity to alcohol and future risk

Human and animal studies have demonstrated that subjects with a "low" response to alcohol's effects following acute challenge have an increased risk for increased ethanol consumption and the later development of alcohol dependence (reviewed in Crabbe, Bell, and Ehlers 2010). The authors note that for the human participants, response to alcohol was measured by alterations in the physiological, motor, and mood responses following after drinking a standardized dose of ethanol. The degree of response relative to the ethanol dose provided can be considered as the sensitivity to effects of ethanol intoxication.

Differences in sensitivity to acute ethanol, especially the adverse effects, alters the risk of developing an AUD (Schuckit et al. 1994). In particular, individuals with low levels of response to acute ethanol are at increased risk for later development of alcohol abuse (Schuckit et al. 1994). While the immediate sensitivity to alcohol is very important in determining the response level to alcohol, the individual's capacity to develop tolerance to the acute challenge of ethanol is also an important component of the "response level" of the individual (Blednov et al. 2018). Previous work had already identified that PDE4 inhibitors, such as apremilast, led to decreases in ethanol consumption and preference in B6 mice (Blednov et al. 2014). It was determined that apremilast increased the LORR duration and recovery from the effects of ethanol on motor coordination, and the drug led to increases in conditioned place avoidance to ethanol (Blednov et al. 2018). The authors conclude that apremilast increases "level of response" to aversive effects of ethanol, and this leads to the decreases in consumption and preference that were observed in their prior publication (Blednov et al. 2018).

There is also an interplay between initial (acute) sensitivity to alcohol and acute functional tolerance (AFT) to ethanol. Acute functional tolerance is a measure of the BEC at which the

recovery of function occurs after intoxication from acute ethanol. The higher the BEC at the recover or function, the higher the AFT to the measured task. In a study with mice that have been bred for high alcohol preference and low alcohol preference, the high preference mice had a higher initial sensitivity and a very fast development of AFT to the ataxia that follows ethanol (Fritz, Grahame, and Boehm 2013). While this finding may seem counter to earlier works regarding acute sensitivity and risk of increased ethanol consumption, this a logical outcome if AFT and acute sensitivity are both elevated. For example, if one considers a subject that is very sensitive to the initial effects of ethanol, which can be both the rewarding and the adverse effects, but that quickly recovers from the adverse effects of acute ethanol. Following the AFT to the adverse effects of ethanol, the subject would continue to experience the rewarding aspects of ethanol rather since tolerance has developed to the adverse effects that would limit further consumption of ethanol during the drinking session.

It is also documented that sensitivity to the adverse effects of ethanol has a protective effect for the abuse risk. Individuals with SNPs in the genes responsible for ethanol metabolism, alcohol dehydrogenase (ADH) and aldehyde dehydrogenase (ALDH), have reduced risk of developing an AUD (Edenberg 2007). This is due in part to the fact that deficits in ethanol metabolism likely alter acute sensitivity to ethanol since the pharmacokinetics of ethanol will be altered. Acetaldehyde (ACD) is a toxic byproduct of ethanol metabolism. In addition to being a known carcinogen, ACD is responsible for many of the adverse physical effects of excess ethanol consumption in the periphery (Deehan, Brodie, and Rodd 2013). Interestingly, the authors acknowledge there is a debate if ACD crosses the blood brain barrier and if it is an important contributor to the reinforcing effects of ethanol consumption, as other literature claims these adverse central effects are mediated by both ACD and acetate (Pardo et al. 2013). This group demonstrated that the downstream metabolite of ACD, acetate, also contributes to ethanol behaviors and modulates the effects of ethanol within the CNS (Pardo et al. 2013). Interestingly, these authors found that while prolonged consumption of acetate did not alter the onset or the duration of LORR, it did significantly decrease the number of mice that actually lose their righting reflex (LORR), a test of acute ethanol sensitivity, following

a large dose of ethanol. In addition, 15 days of acetate administration amelorated ethanol induced changes in locomotor activity without altering basal open field locomotion (Pardo et al. 2013).

2.1.1 Measures of sensitivity to ethanol

There are many available methods for measuring sensitivity to ethanol in humans and mouse models. In humans, sensitivity to ethanol can be studied by measuring sway characteristics while standing on a force platform following acute exposure (Kitabayashi et al. 2004). Total locomotor activity frequently altered by acute ethanol exposure in many strains of mice. The ability to remain on the rotating stage of a Rotarod machine is impaired by moderate to high doses of ethanol. One of the important measures of sensitivity to alcohol is rodent models is the loss of righting reflex (LORR). Rodents have a remarkable ability to right themselves from the supine to the prone position almost instantly. Following a high dose of ethanol (e.g., greater than 3.8g/kg, i.p.), this ability is temporarily lost before it is regained. This test measures the onset or latency until LORR is achieved and the duration of time until the righting reflex is regained. Additionally, blood can be drawn immediately after the onset of LORR, and again immediately after the righting reflex is recovered. The time to the onset of LORR and the BEC at the onset can be considered a measure of acute sensitivity to ethanol, while the duration of LORR and the BEC at the recovery of the righting reflex (RORR) can be considered a measure of acute functional tolerance. Additionally, LORR can be performed multiple times or after voluntary drinking to get further measures of tolerance, which can be predictive of future issues with alcohol dependence.

2.2 Identification of candidate genes / networks involved in risk of alcoholism

As discussed in Chapter 1, it is estimated that 50% of the risk for developing alcohol dependence can be attributed to genetic predisposition (Goodwin 1974; Prescott and Kendler 1999). The studies above regarding the metabolism of ethanol illustrate the presence of deleterious SNPs in genes that encode for ethanol metabolism (ADH and ALDH) can have strong effects on behavioral sensitivity to ethanol. These alterations in sensitivity to the effects of ethanol exposure play a large role in predicting the risk of later development of alcohol dependence. Thus, it begged to

ask if additional SNP variants could be correlated with AUD using human genome-wide association studies (GWAS). While there is incredible utility in GWAS methods, extremely strong signals are needed to overcome the multiple test corrections that occur when probing millions of different SNPs. The effects of SNP variants in ADH and ALDH are so strong that they can be detected in human GWAS studies, partially validating the theory that an individual's genetics can predict risk of AUD (Sun et al. 2019). As of 2019, tens of ethanol consumption-related genes have been identified by GWAS and recent larger studies have produced > 10 relevant hits (Kranzler et al. 2019). Unfortunately, relatively few alcoholism-related genes that have achieved the threshold of significance in further GWAS studies (Adkins et al. 2015). Since the pathophysiology of alcohol dependence is considered polygenic, which many small changes in gene expression contribute to the risk, detecting the individual genes is extremely difficult using traditional GWAS approaches that require very strict statistical thresholds for significance.

Ethanol is known to interact with many different neural transmission receptor systems. In brief, ethanol potentiates the following receptors: GABA-A, 5-HT3, neuronal nACh, GIRK channels, and glycine receptors (Belknap et al. 2008). In contrast, ethanol inhibits NMDA receptors and voltage-gated L-type receptors (Belknap et al. 2008). While the direct actions on select individual receptors are well studied, less is known about alcohol's effect on cellular signaling, transporters, or kinase cascades. We believe that unknown fundamental mechanisms for the pathophysiology of alcohol lies in the sum of many modest effects of ethanol on multiple targets within important pathways. In order to study and detect the small effects of many genes working in concert, genetic researchers of complex traits, including mental illness and drug abuse, are utilizing network-based analyses of genome-wide expression studies (e.g. microarray and RNAseq) to find organized networks of genes that are correlated by their expression and are also correlated, at a network level with phenotypes of interest. This approach also allows functional analysis of multiple correlated genes, using gene enrichment tools and pathway analysis of clusters of genes. Thus, groups of genes with modest changes in expression can be identified and organized into functional domains for hypothesis testing in relation to a given complex trait. This approach has led to the identifica-

tion of many important clusters of co-expressed genes, giving more insight into important signal cascades and pathways, such as the PI3K/AKT pathway that will be discussed later in this chapter, that are simply not detectable with GWAS methods alone due to the very large samples sizes that are needed to detect genes having small contributions toward a trait such as AUD.

2.3 Myelin as a risk factor

There is growing interest in studying and identifying genes and mechanisms that contribute to impulsivity in alcoholics due to the clear direct link between impulsivity and AUD, where alcohol dependent subjects have increased levels of impulsivity (Sun et al. 2019). Sun and company concluded that effects of alcohol abuse related variants that affect impulsivity should be considered an important area of future research. It is well documented that as the adolescent brain matures, there are large increases in myelination in the frontal cortex (Sharma et al. 2013). During this transition, reduced myelination in the prefrontal cortex is correlated with deficits in compulsivity and impulsivity in adulthood (Ziegler et al. 2019). In particular, Ziegler et al. found that myelination in the dorsomedial and dorsolateral PFC regions are important for compulsivity, while the lateral and medial PFC regions are important for impulsivity. Thorough reviews of addiction literature clarify that both impulsivity and conpulsivity are contributors to development of addictions (i.e., drugs of abuse, gambling), including alcohol, rather than being the result of the addiction behaviors (Lee, Hoppenbrouwers, and Franken 2019).

As alluded to in Chapter 1, multiple molecular, pathological and neuroimaging studies show perturbation of myelin or myelin gene expression in alcoholic patients. This has been shown in postmortem human tissue, functional imaging studies, and in multiple animal models. Early studies using two commonly used inbred strains of mice, C57BL/6J (B6) and DBA/2J (D2), demonstrated strikingly different behavioral responses to acute ethanol exposure and ethanol consumption. For example, B6 mice drink much more ethanol than D2 mice, while D2 mice display much larger locomotor responses to acute exposure (Phillips et al. 1994; Metten et al. 1998). Prior genomic studies from our laboratory suggested possible mechanisms responsible for these differences in acute ethanol sensitivity between B6 and D2 mice (Kerns et al. 2005). K-means clustering

analysis identified a group of genes in the medial prefrontal cortex (mPFC) which contained multiple myelin-related genes. This cluster of genes showed higher basal expression in B6 mice, but demonstrated a greater degree of gene expression induction after acute ethanol exposure in D2 mice (Kerns et al. 2005). Genomic studies of *Fyn* kinase null mice also provided evidence that alterations in myelin expression underlies the increased ethanol sensitivity, as demonstrated by prolonged LORR duration in the *Fyn*-null mice (Farris and Miles 2013). Additional works by Farris et al. found that administration of a demyelinating drug, Cuprizone, resulted in dramatically reduced basal expression of myelin genes in the mPFC of B6 mice, increased LORR duration, and decreased ethanol consumption and preference in a 2-bottle choice drinking model (unpublished data / Farris thesis).

Therefore, it stands that basal levels of myelin and networks of myelin related genes in the prefrontal cortex in particularly important for behavioral deficits that raise the risk of developing alcohol dependence. We previously discussed how both myelin density and gene expression is markedly downregulated in in the PFC of chronic alcoholic patients (Lewohl et al. 2000). Thus, the regulation of myelin related genes is paramount for both the risk of developing abusive alcohol behaviors and, as will be discussed, chronic ethanol abuse leads to later dysregulation of myelin genes. This dysregulation of myelin genes then contributes to further escalations in abusive behaviors and drives the pathophysiology of cognitive deficits and brain matter loss following years of alcohol abuse. To summarize, we hypothesize that basal expression of myelin related genes in the prefrontal cortex can function as risk factors for AUD by altering initial sensitivity to ethanol (e.g. impulsivity and compulsivity). Additionally, the dysregulation of myelin related gene expression following chronic ethanol exposure also affects the risk of developing an AUD and contributes to the neurological sequelae that result from years of abuse (see Figure 2.1). Given the potential importance of myelin genes for the pathophysiology driving the development of AUD, studies on ethanol regulation of myelin-related gene expression networks could be of critical importance to the alcohol research field.

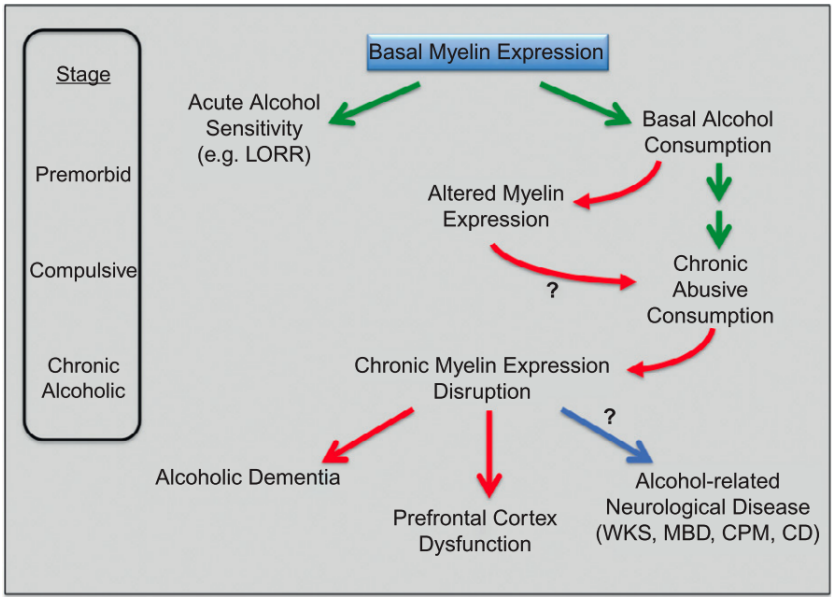

Figure 2.1: Role of myelin in development of alcohol dependence. Figure from: Costin and Miles 2014.

2.4 N-myc Downstream Regulated Gene 1

As described above, Kerns and company found clusters of co-expressed genes when comparing basal and differential gene expression changes in response to acute alcohol in D2 and B6 mice (Kerns et al. 2005). One of the clusters of genes in the mPFC was highly enriched for myelin related genes, as shown is Figure 2.2. Within this cluster, a novel ethanol responsive, myelin-related gene, N-myc Downstream Regulated Gene 1 (*Ndrg1*), was identified.

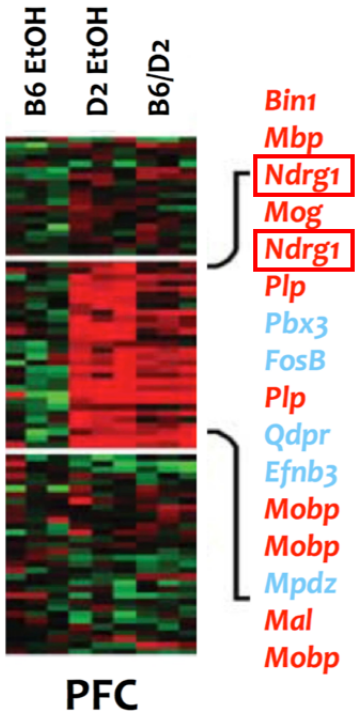

Figure 2.2: Cluster of myelin related ethanol responsive genes in the mPFC. Microarray probesets for *Ndrg1* are highlighted in red. Figure adapted from: Kerns et al. 2005.

2.4.1 General background

NDRG1 is part of the N-myc downregulated gene (NDRG) family, which contains 4 NDRG proteins. All family members belong to the alpha/beta hydrolase superfamily. In humans, the NDRG1 protein is 53% homologous to NDRG2 and 62% homologous to both NDRG3 and NDRG4 (Sun et al. 2013). Furthermore, human NDRG1 is 94% homologous to the mouse homolog, and the NDRG1 sequence is highly conserved in many other organisms (Sun et al. 2013). Relative to other members of the NDRG family, NDRG1 has a unique 10 amino acid that repeat 3 times in tandem near the C-terminus, as shown in Figure 2.3 (Murray et al. 2004). The NDRG1 protein is typically found in the cytoplasm of many different cell types and it is thought to be involved in cellular stress responses, cancer related signaling pathways, and cell trafficking, particularly in myelin-producing cells (Berger et al. 2004). For example, *Ndrg1* is required for cells to undergo p53-induced apoptosis (Stein et al. 2004), by playing a role in p53-mediated checkpoint at the mitotic spindle (Kim et al. 2004). There is evidence that other acute cellular stresses, such as hypoxia,

can result in dramatic increases in *Ndrg1* mRNA expression and protein phosphorylation over a 24-hour window of observation in tumor cell lines (Sibold et al. 2007). While the exact function of NDRG still remains unknown, several studies have suggested that phosphorylation of the protein affects its functional roles (Sun et al. 2013).

2.4.2 The Role of *Sgk1*-Mediated Phosphorylation

NDRG1 has been identified as substrates for phosphorylation by two important serine/threonine kinases, Serum/Glucocorticoid Regulated Kinase 1 (SGK1) and Glycogen Synthase Kinase 3 Beta (GSK3B) (Murray et al. 2004). The authors found that NDRG1 is phosphorylated on several residues in the 10 amino acid tandem repeat near the C-terminus, as shown in Figure 2.3. Furthermore, initial phosphorylation of the SGK1 targets primes the protein for additional phosphorylation by GSK3B (Murray et al. 2004). Furthermore, initial phosphorylation of the SGK1 targets primes the protein for additional phosphorylation by GSK3B (Murray et al. 2004). When phosphorylated at the thr-346 residue, NDRG1 colocalizes with γ-tubulin on centromeres during mitosis and with microtubule bundles at late in the telophase stage in HCT116 cells (McCaig et al. 2011). Interestingly, this phosphorylated NDRG1 does not localize with centromeres at all during the cell growth phase (McCaig et al. 2011). Recently, investigations of *Ndrg1* in the peripheral nervous system also have noted that a reversible phosphorylation of the thr-346 residue determines the subcellular localization of the protein in Schwann cells (Skedsmo et al. 2019). The authors suggest that signaling cascades responsible for the phosphorylation event are important for the regulation of the subcellular location of *Ndrg1* in myelinating cells (Skedsmo et al. 2019). In specific, the authors note that thr346-NDRG1 is only present in the abaxonal cytoplasm of Schwann cells (Skedsmo et al. 2019). Based on the literature, there appear to be multiple mechanisms that control the subcellular localization of NDRG1 beyond phosphorylation. For instance, in human trophoblasts, cellular stressors result in a redistribution of NDRG1 into the nucleus and to areas of the cytoplasm involved with endoplasmic reticulum and microtubule functions (Shi et al. 2013).

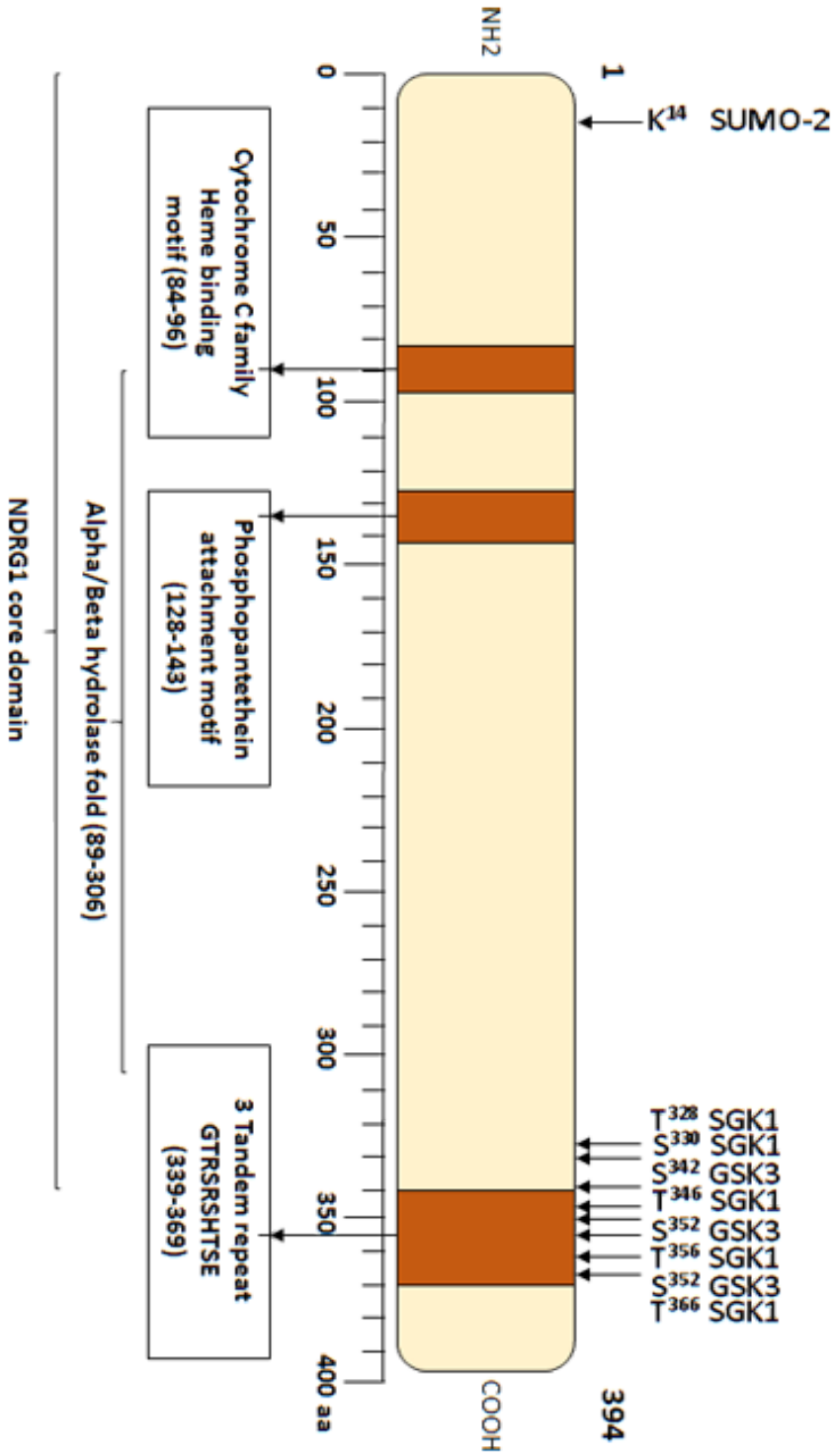

Figure 2.3: NDRG1 protein domains and binding sites. Note the residues phosphorylated by SGK1 and GSK3B near the C-terminus. The phospho-sites within the 3 tandem repeat are unique to Ndrg1. Figure adapted from: http://atlasgeneticsoncology.org/

Interestingly, this redistribution of NDRG1 is ameliorated if the phosphopantetheine attachment site (see Figure 2.3) contains loss of function mutations (Shi et al. 2013). The evidence suggests that multiple domains of the NDRG1 protein are involved in determining the sub-cellular localization of NDRG1, and that the driving mechanism is determined by the cell type.

2.4.3 *Ndrg1*: importance in lipid dynamics and myelination

As stated in Chapter 1, mutations involving *Ndrg1* in humans underlie Charcot-Marie-Tooth disease type 4D, an autosomal recessive demyelinating peripheral neuropathy that results in widespread demyelination and the appearance of onion bulb formations when viewing the cross sections of myelinated axons (King et al. 2011). More extensive immunohistochemistry studies of the NDRG family found high levels of NDRG1 expression in areas enriched with myelin, with little to no expression outside of myelin or the myelinating cells of the nervous system (Okuda, Kokame, and Miyata 2008). Constitutive deletion of *Ndrg1* in mice results in degradation of peripheral myelin starting at week 5 that progresses into a severe polyneuropathy (Okuda et al. 2004). As mentioned above, thr346-pNDRG1 is only present in the abaxonal cytoplasm of Schwann cells in healthy control dogs. Alaskan malamutes, a breed with known *Ndrg1*-induced neuropathies, with defective *Ndrg1* lack this phosphorylation event (Skedsmo et al. 2019). While phosphorylation and cellular sub localization of NDRG1 is certainly important, reviewing the literature suggests that *Ndrg1*-induced neuropathies are largely due to *Ndrg1*'s effects on cellular lipid dynamics. Studies have shown that patients with defects in NDRG1 frequently developed hypercholesterolemia and defects in reversed transport of cholesterol in addition to the neuropathy symptoms (Dacković et al. 2008). It has been shown that NDRG1 co-localizes and directly interacts with apolipoproteins, APO-AI and A-II, which suggests that the lack of functional NDRG1 in Schwann cells, and the resulting defects in lipid synthesis, transport, and trafficking, are the major driver of the pathology observed in CMT4D (Hunter et al. 2005). It was later determined that knocking down expression of NDRG1 in epithelial cells reduces the cell surface density of LDL receptors, resulting in reduced uptake of LDL (Pietiäinen et al. 2013). The authors also knocked down NDRG1 in rodent oligodendrocytes and found similar reductions in cellular uptake of LDL and reduced expression of

the oligodendrocyte differentiation factor, *Olig2* (Pietiäinen et al. 2013). The authors determined that NDRG1 modulates the formation of multivesicular bodies and LDL receptor trafficking, and they ultimately conclude that part of the pathophysiology of CMT4D can be attributed to impaired control of cellular lipid dynamics, since functional *Ndrg1* is required for proper myelination in the PNS due to its role in biolipid synthesis and transport, and through reductions in differentiation signals in myelinating cells (Pietiäinen et al. 2013). The importance of NDRG1 in cellular lipid dynamics is not restricted to myelinating cells. *Ndrg1* expression levels in breast cancer cells affect the aggressiveness of cells by altering the cell's lipid profile (Sevinsky et al. 2018). The authors found that *Ndrg1* expression modulates both the cellular uptake of lipids, by affecting how neutral lipids store fatty acids, and endogenous cellular lipid biosynthesis (Sevinsky et al. 2018). Multiple works have provided evidence that NDRG1 directly interacts with both E-cadherin and B-catenin, and these interactions suggest the role of *Ndrg1* in cancer metastasis and aggressiveness may be in part to modulations in the epithelial-to-mesenchymal transition (EMT) that are mediated by the Wnt pathway (Tu et al. 2007; Liu et al. 2012; Jin et al. 2014; Cen et al. 2017). The evidence suggests that at least part of NDRG1's effects on lipid metabolism are mediated through the Wnt signaling cascade, given that the Wnt pathway has recently been implicated in altering the lipid metabolism profile in the hepatocytes of zebrafish following toxic insults and injuries (Yao et al. 2018).

2.5 *Ndrg1* and chemotherapy-induced peripheral neuropathy (CIPN)

One of the most important chemotheraputics used in the treatment of breast of cancer is Paclitaxel (Perez 1998). Paclitaxel is considered a first-line treatment for metastatic breast cancer, as an adjuvant treatment following surgery, and for anthracycline-resistant cancer (Perez 1998). Paclitaxel is a member of the taxane family, a class of drugs that have antimicrotubule functions. Paclitaxel is distinguished from others taxanes in that it indirectly prevents depolymerization of microtubules by inducing tubulin dimerization (Rowinsky, Cazenave, and Donehower 1990). As noted by Rowinsky, Cazenave, and Donehower 1990, the two common toxicity side effects of Paclitaxel are neutropenia and peripheral neuropathy. While many agents lead to chemotherapy in-

duced peripheral neuropathy (CIPN), Paclitaxel is one of the few that causes symptoms both while undergoing treatment or immediately following treatment (Zajaczkowską et al. 2019). While CIPN is a sensory and a motor neuropathy, the first symptoms to appear are sensory and occur in the distal ends of limbs, which results in "stocking and glove" complaints in the feet and the hands, respectively (Zajaczkowską et al. 2019). Given that CIPN can result in permanent neuropathic symptoms that reduce quality of life following treatment, research to identify genetic variants that modulate the risk and severity of CIPN is of critical clinical importance. A study investigating the association of single nucleotide polymorphisms with CIPN in an Asian population found that an NDRG1 SNP, *rs2233335*, correlated with Paclitaxel induced peripheral neuropathy (PIPN) (Sundar et al. 2014). Furthermore, they found that additional NDRG1 SNPs in linkage disequilibrium with *rs2233335* were localized to intronic regions, suggesting that some regulatory mechanisms for the expression of NDRG1 may be driving the association of NDRG1 with PIPN (Sundar et al. 2014). This group followed up by investigating the levels of NDRG1 expression in nerve bundles in the resected breast tissue following mastectomy or lumpectomy that includes the nipple (Sundar et al. 2016). Following surgery, all women received up to 12 cycles of weekly Paclitaxel unless toxicity developed. The authors found a strong inverse correlation of the amount of nerve *Ndrg1* expression and severity of CIPN symptoms experienced by the patients (Sundar et al. 2016). While the authors acknowledge that performing nerve biopsies for predicting sensitivity to and severity of CIPN is not practical, they provide evidence that investigating nerve bundles within resected tumor tissue could be a useful biomarker for predicting severity of PIPN (Sundar et al. 2016).

2.6 *Ndrg1*: involvement with signaling pathways

Even though is no reported detectable NDRG1 in axons or neurons, NDRG1-related neuropathies in humans, rodents, and dogs all have clinical signs and pathological evidence that imply an axonal neuropathy (Skedsmo et al. 2019). In the peripheral nervous system, axonal Neuregulin1 acts on the PI3K/AKT pathway such that NDRG1 protein levels are upregulated, and an induction of myelination follows (Heller et al. 2014). In contrast, a later interaction of axonal $\alpha 6\beta 4$ integrin results in *Sgk1* activation in the Schwann cells, inducing thr-346 phosphorylation of NDRG1 at the

Cajal bands within the abaxonal compartments, which results in down-regulation of myelination (Heller et al. 2014). This work demonstrates that axonal-glial junction cross-talk regulates the induction and reduction of myelination by acting through differing parts of the PI3K/AKT pathway. The theory is supported by the fact that many different cell types have the PI3K/AKT pathway activated by the binding of ligands to various integrins located on the cell surface (Matsuoka et al. 2012).

It has been shown that the PI3K/AKT signaling pathway in involved in alcohol pathology, in multiple organ systems. One study found that low dose and high dose acute alcohol exposure in cardiac myocytes had opposing effects on cardiac output, and constitutively active or inhibited PI3K either blocks or enhances the effects on cardiac function (Umoh et al. 2014). The authors suggested that cardiac response to acute alcohol is driven by the effects of the pathway on oxidative stress (Umoh et al. 2014). Additionally, it is known that alcohol-related liver disease (ARLD) is driven in large part by oxidative stress (Liu et al. 2019). ARLD is responsible for many cognitive issues, especially in the frontal cortex (Zahr and Pfefferbaum 2017). Within the CNS, PI3K/AKT pathway plays an important role in modulating maladaptive alcohol behaviors via the mesocorticolimbic circuity. Initial studies found that the mammalian target of rapamycin complex 1 (mTORC1) signaling pathway is activated in the nucleus accumbens (NAc) after ethanol exposure (Neasta et al. 2010). Since AKT is the primary upstream activator of the mTORC1 pathway, the authors followed up and found that the AKT pathway is activated in the NAc of rats following an alcohol paradigm involving multiple cycles of excessive consumption and withdrawal (Neasta et al. 2011). Furthermore, the authors found that intra-NAc delivery of an inhibitor for either AKT or its activator, PI3K, reduces the excessive voluntary consumption and operant responding for alcohol (Neasta et al. 2011). These examples show that perturbations of the PI3K/AKT pathway can play a large role in CNS responses to ethanol, especially in the acute setting.

Additionally, the Wnt/B-cantenin pathway has been implicated in CNS responses to ethanol exposure, especially in the context of acute tolerance. In fact, the rapid acute function tolerance, both molecular and behavioral, is thought to be mediated by the internalization of large conduc-

tance Ca2+ and voltage-activated K+ (BK) channels (Treistman and Martin 2009). The internalization of the BK channels, and the rapid tolerance to acute ethanol that follows, occurs on the scale of minutes after the initial exposure to ethanol (Treistman and Martin 2009). Furthermore, this mechanism is conserved across multiple species and animal models, which suggests that this is a fundamental regulator of tolerance to the effects of ethanol and the increased consumption and preference that follows (Bettinger and Davies 2014). In relation to the Wnt/B-cantenin pathway, studies in cultures of hippocampal neurons suggest that the Wnt pathway regulates the ethanol-induced internalization of BK channels by phosphorylation of the channel by GSK3B, which drives the development of acute tolerance to ethanol (Velázquez-Marrero et al. 2016). Furthermore, Treistman et al. 2009 suggests that lipid environment of the cell membrane in the vicinity of the BK channel is a strong modulator of effects of ethanol on the channels. It has been shown that the activation of BK channels by ethanol is affected by the cholesterol/phospholipid ratio of the cell's lipid bilayer (Crowley, Treistman, and Dopico 2003). In addition, studies have found that the cell's bilipid membrane thickness modulates to response of BK channels to ethanol: BK channels in thinner membranes have stronger responses to ethanol, while response of BK channels in thicker membranes is blunted (Yuan et al. 2007). BK channels, such as KCNMA1, have been directly observed on the surface of axons and the synaptic terminals of glutamatergic connections in the hippocampus and the GABAergic connections in the cerebellum (Misonou et al. 2006). Also of note, BK channels are concentrated at the paranodal junctions of myelinated axons in Purkinje cells, where they help regulate action potentials (Hirono et al. 2015). Given that NDRG1 is also a member of the Wnt signaling pathway that is responsive to axon-glial cross-talk, and it is known modulate to lipid and cholesterol uptake and metabolism. It is possible that the main effect that NDRG1 may have on acute sensitivity may be mediated through Wnt signaling and alterations in the lipid composition along the axon-glial junction.

Probing the BioGrid repository for mass-spec affinity captured, protein-protein interactions of NDRG1 reveals that the top interaction with the most evidence is with KCNMA1 (Kathiresan et al. 2009). The NDRG1-KCNMA1 interaction came out of a publication on the protein-protein net-

work for *Kcnma1* in mouse cochlea, which is a transition zone of the PNS and the CNS (Kathiresan et al. 2009). 161 unique protein interactions with KCNMA1 were identified in this study. Running this list of genes through Toppgene reveals several interesting GO enrichment categories. Notably, cellular component GO results include: myelin sheath, synapse, secretory vesicle, supramolecular fiber, microtubule, and endocytic vesicle. GO results for mouse phenotype also includes myelin and axon related pathologies, such as: axon degeneration, abnormal metabolism, abnormal tricarboxylic acid cycle, hindlimb paralysis, abnormal myelination, and abnormal action potential. Even more striking are the human phenotype GO results, which include: segmental peripheral demyelination/remyelination, spastic paraplegia, onion bulb formation, abnormality of the cerebral subcortex, Abnormal corpus callosum morphology, Hypertrophic nerve changes, Aplasia/Hypoplasia of the corpus callosum, Abnormality of peripheral nerve conduction, Abnormality of the cerebral white matter, abnormality of peripheral nerves, and peripheral axonal degeneration

These GO results, along with the 161 protein-protein interactions, suggest that KCNMA1 along the axon directly interacts with myelin and/or lipid-related proteins, such as MBP, MPZ, APOA1, APOE, and NDRG1. This raises the possibility that NDRG1 could modulate acute tolerance and sensitivity to ethanol through the axon-glial cross-talk, perhaps by altering the lipid composition at the axon-glial junction, which then modulates the magnitude of action potential and the rate of internalization the KCNMA1 channel.

2.6.1 *Ndrg1* is an upstream regulator and a downstream target of ethanol responsive signaling pathways

As discussed above, *Ndrg1* plays an important role in at least 2 ethanol-responsive signal pathways: PI3K/AKT and Wnt/β-cantenin. A thorough review of *Ndrg1* by Sun et al. 2013 demonstrated that *Ndrg1* has direct interactions with additional signaling cascades, including: TGF-β, Ras/Raf, and NF-$\kappa\beta$, as shown in Figure 2.4.

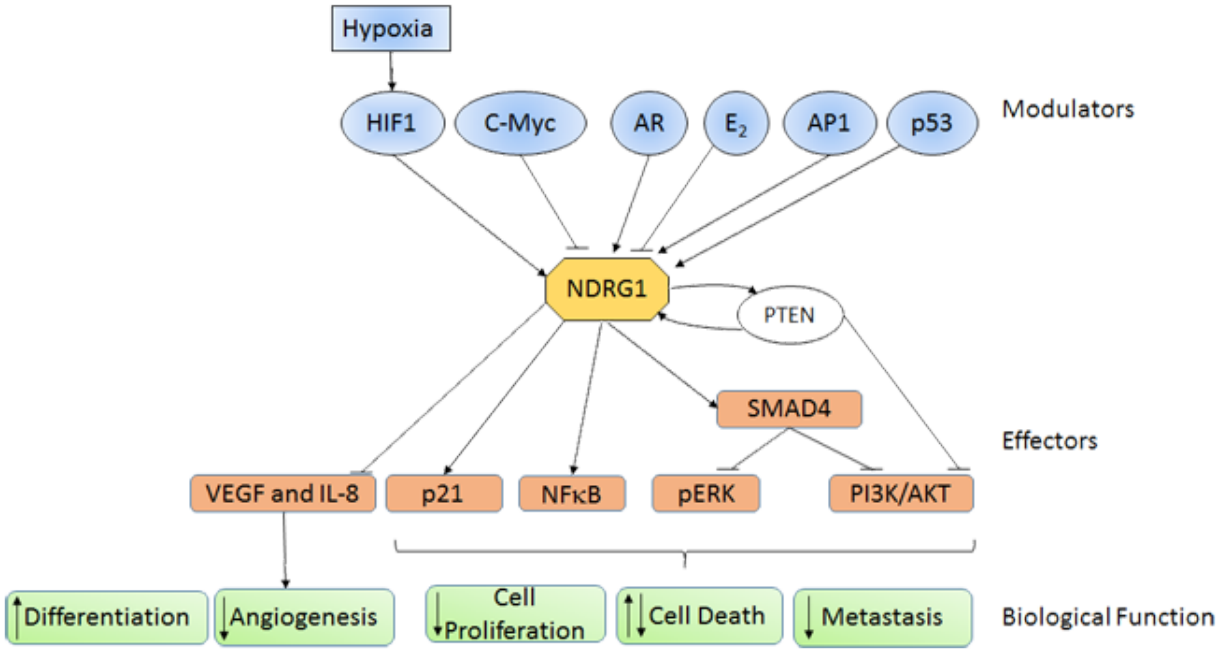

Figure 2.4: Overview of NDRG1 interactions upstream of signaling pathways. Figure adapted from: http://atlasgeneticsoncology.org/

It is thought that *Ndrg1* acts on each pathway in an independently, but it might also promote cross-interactions (Sun et al. 2013). It has been reported that the actions of *Ndrg1* on the NF-kB pathway is dependent on SGK1-mediated phosphorylation of NDRG1 residues, Ser330 and Thr346 (Murakami et al. 2010). *Ndrg1* plays a role in upstream inhibition of the PI3K/AKT via NDRG1 activation of SMAD4 and PTEN. The relationship between PI3K/AKT pathway and *Ndrg1* is complex, as shown in Figure 2.5. In peripheral nerves, *Ndrg1* is a downstream target of the PI3K/AKT as it is phosphorylated by both *Sgk1* and *Akt1* (Heller et al. 2014). This demonstrates that *Ndrg1* has roles both upstream and downstream in the PI3K/AKT pathway, suggesting a possible feedback role in regulation of this pathway.

2.7 Investigations of mPFC *Ndrg1* and alcohol

To reiterate, both *Sgk1* and Gsk3β, kinases that phosphorylate *Ndrg1* as discussed above, are members of the PI3K/AKT pathway and both have been found to be ethanol responsive kinases in the mPFC of rodents following acute exposure (Kerns et al. 2005; Wolen et al. 2012; Costin, Dever, and Miles 2013; van der Vaart et al. 2018). The regulation of *Sgk1* in the mPFC of D2

mice has been studied in greater detail in prior work in our laboratory (Costin, Dever, and Miles 2013). Costin and company found that acute ethanol leads to a dose-dependent upregulation of Sgk1 mRNA expression 4 hours following exposure and increases the level of phosphorylated SGK1 (Ser-422 and Thr-256) and phosphorylated NDRG1 (Ser330) 15 minutes after exposure (Costin, Dever, and Miles 2013). This work provided evidence that acute ethanol does in fact regulate the phosphorylation of NDRG1 in the mPFC, but it only provides a single time point, 15 mins after exposure, and a single dose (4 g/kg, i.p.). As discussed above, multiple previous studies have demonstrated that phosphorylation of NDRG1 by SGK1 and GSK3B leads to changes in the cellular sub-localization of NDRG1. Taken together, these works certainly suggest that cellular stresses can lead to increased phosphorylation of NDRG1 and subsequent changes in NDRG1 sub-cellular localization, potentially altering the activity and physiological function of the protein. At this time, there have been no studies concerning the effect of chronic ethanol exposure on *Ndrg1* expression and protein phosphorylation. This information could elucidate whether or not *Ndrg1* plays a role in the alterations in mPFC-mediated neurobiology that leads to myelin alterations and lead to addictive behaviors following chronic exposure to ethanol. Bioinformatic analysis of mPFC expression data found that *Ndrg1* expression was positively correlated with voluntary ethanol intake across the BXD panel of mice and demonstrated that the basal levels of *Ndrg1* mRNA expression in the mPFC across seven different strains of mice was inversely correlated with LORR duration time, as shown in Figure 2.5.

Additionally, in unpublished data from the Miles laboratory, modulation of mPFC *Ndrg1* was achieved via stereotaxic injection of lentivirus containing shRNA that targets the *Ndrg1* transcript. This site-specific knock down of *Ndrg1* in the mPFC produced alterations in ethanol phenotypes that are related to ethanol sensitivity. First, the knock down mice experienced prolonged LORR duration relative to scrambled shRNA controls. Interestingly, after 4 weeks of intermittent access to a 3-bottle choice drinking model (15%, 30%, water), NDRG1 knock-down mice showed a markedly decreased preference for the 30% ethanol relative to the 15% ethanol, as displayed in Figure 2.6, while overall ethanol consumption was unchanged between the control and the knockdown ani-

mals. We have postulated that the knockdown animal's decreased preference for 30% is due to an altered sensitivity to the intoxicating or adverse effects of the higher concentration of ethanol.

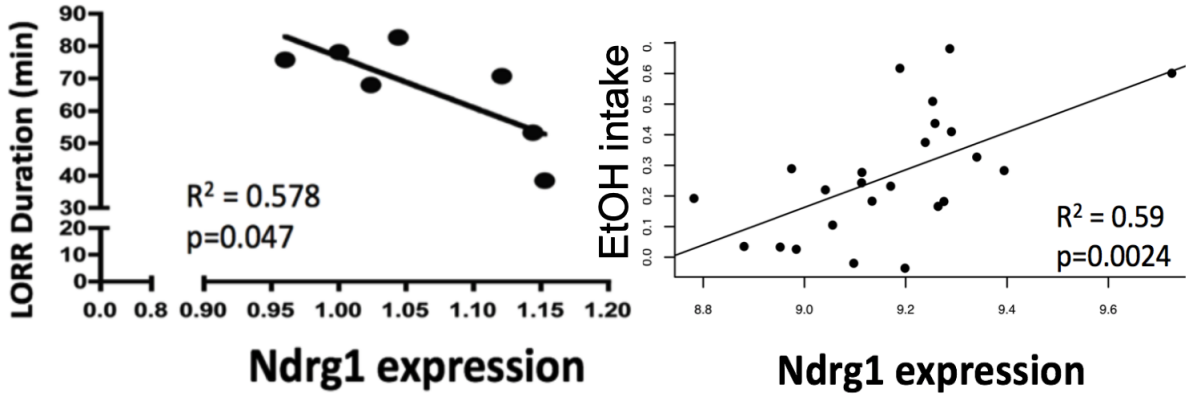

Figure 2.5: Basal NDRG1 expression is inversely correlated to LORR duration across 7 different laboratory mice strains (left). Correlation of alcohol consumption with NDRG1 basal expression across the panel of BXD mice (right). Figures adapted from Farris thesis / unpublished manuscript.

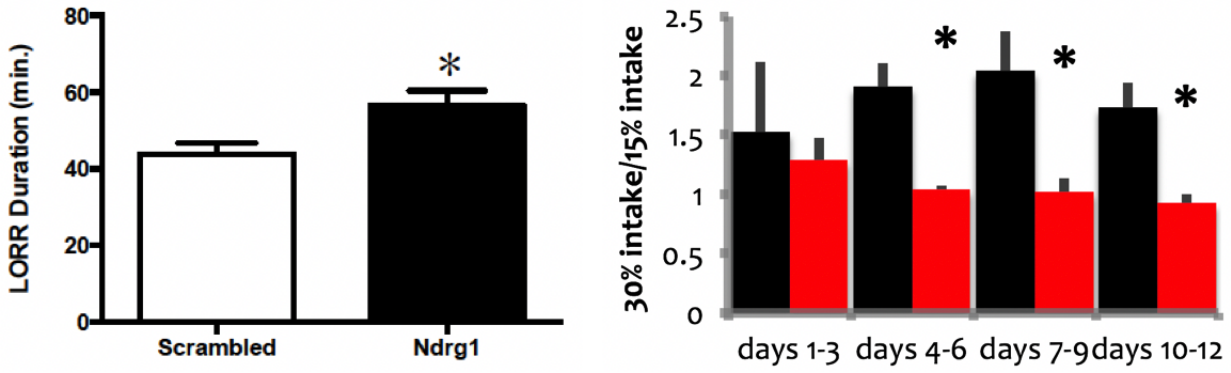

Figure 2.6: Ethanol phenotypes from shRNA knockdown of NDRG1 in the mPFC of B6 mices. The knockdown mice display significantly longer LORR durations (left). Knockdown mice (red) reduced their intake of 30% relative to 15% ethanol the course of the drinking study, while scramble injected controls (black) escalated their consumption of 30% over the 15% ethanol (right). (* $P < 0.05$). Figures adapted from: Farris thesis / manuscript in preparation.

2.8 Closing Remarks

The works discussed in this chapter suggest that basal myelin expression is an important determinant of acute sensitivity to ethanol and hence, to the risk for abusive ethanol consumption. They further document that ethanol can regulate myelin expression in the mPFC and that *Ndrg1* is a potential key gene involved in this response. We hypothesize that *Ndrg1* expression is an

important factor determining sensitivity to ethanol and that regulation of *Ndrg1* by ethanol may have a role in the long term risk for abusive consumption. Furthermore, given the direct role of *Ndrg1* in peripheral neuropathies and suggested role in severity of chemotherapy-induced peripheral neuropathy, we hypothesize the sensitivity for the development of alcoholic neuropathy may modulated by *Ndrg1* expression in the Schwann cells of the peripheral nervous system.

Chapter 3

Characterization of cellular expression and ethanol regulation of *Ndrg1* in the mPFC

3.1 Introduction

Ndrg1 expression is induced and is strongly correlated with a cluster of myelin-related genes in the mPFC of male D2 mice 4 hours after acute ethanol (2 g/kg, ip) (Kerns et al. 2005). A significant increase of Ser330-pNDRG1 levels occurs in the mPFC of male D2 mice 15 minutes after a large dose of acute ethanol (4 g/kg, ip) (Kerns et al. 2005). *Ndrg1* expression was modulated in rhesus macaques mPFC following 1 year of chronic ethanol consumption (Bogenpohl et al. 2019). Network analysis found that *Ndrg1* was a member of network that was enriched for myelin-related genes and that *Ndrg1*'s connectivity within this module is dramatically increased in rhesus macaques that underwent the year of drinking (Bogenpohl et al. 2019).

The sub-cellular localization of *Ndrg1* is affected by it's phosphorylation state at *Sgk1*-mediated residues in multiple cell cancer lines (Park et al. 2018). However, other works have reported no changes in sub-cellular localization based on the phosphorylation state in Hela cells (Murray et al. 2004). It is thought that the phosphorylation of *Ndrg1* at *Sgk1*-mediated residues is important for the function of the NDRG1 protein (Murray et al. 2004). It was not known if oligodendrocytes in the CNS would demonstrate sub-cellular localization of NDRG1 based on its phosphorylation state. Furthermore, it was also unknown if either acute or chronic ethanol would induce changes in the levels or the sub-cellular localization of phospho-NDRG1 in the CNS. If the phosphorylation state of *Ndrg1* does in fact play a role in protein function, it would be a vital addition to the current knowledge base of *Ndrg1* expression in the CNS, both basally and in the context of acute and chronic ethanol exposure.

The previous findings regarding *Ndrg1* in mouse models were generated in the D2 strain. It is advantageous to investigate this further using the reference B6J mouse strain. This is especially important since we plan to modulate the expression of *Ndrg1* through genetic interventions in Chapter 4, as nearly all existing genetically modified mouse lines are created on a B6J background. Furthermore and even more importantly, D2 mice are known to consume significantly less ethanol per body weight than B6J mice due to alterations in taste perception. Given that we plan to use a genetically modified mouse line and we plan to study drinking behaviors in the context of *Ndrg1*, we utilized mouse lines bred over a B6J-reference background for all studies throughout this dissertation. As such, this thesis work will add vitally important data on the regulation of *Ndrg1* following both acute and chronic ethanol exposure in reference mouse strain, B6J.

Outside of the preliminary lentiviral data discussed in Chapter 2, there are no reports or studies published concerning the effect of chronic ethanol exposure on *Ndrg1* expression in any organ system. We will begin our investigation by determined the predominant cell type that is infected by the lentivirus in this preliminary study using immunofluorescence methods. We will then further test to see if the predominantly infected cell type is localizes with NDRG1 protein to determine if *Ndrg1* is in fact expressed in this cell type. It is entirely unknown what effects long-term ethanol exposure with have on the transcript expression or proteomics dynamics for *Ndrg1*. It is also unknown if any changes in *Ndrg1* phosphorylation following acute ethanol are also observed following chronic ethanol drinking. In other words, mice repeatedly exposed to ethanol that escalate their voluntary usage could have enhanced, diminished, or no change in ethanol-induced phosphorylation of NDRG1compared to naive mice that received an equivalent ethanol dose. This could be crucial to providing information on how the response of *Ndrg1* may adapt after acute exposures turns into chronic usage. As eluded to in Chapter 2, any compensations in response to ethanol exposure could play a vital role in the development of the pathophysiology behind maladaptive alcohol usage.

To establish the basal expression patterns of *Ndrg1* in the mPFC, we will use immunofluorescence methods to determine the cell type localization of total NDRG1 protein. We will also use

IHC to determine the sub-cellular localization of multiple phosphorylated forms of NDRG1 protein in the mPFC of B6J mice. To characterize to the effect of acute ethanol on *Ndrg1*expression or protein activity of NDRG1, we utilize an acute ethanol dose response model with 4 different doses administered via intraperitoneal injection. Additionally, sub-cellular localization of 2 forms of phosphorylated NDRG1 (Ser330-pNDRG1 and Thr346-pNDRG1) will be investigated following a single dose of ethanol in a smaller subset of male mice using super resolution microscopy techniques

Likewise, we sought to determine the effects of chronic ethanol on the gene expression and protein activity of *Ndrg1* by establishing an escalating alcohol consumption using an Intermittent Ethanol Access (IEA) model. We will track and compare the amount of ethanol relative to tap water consumed both 2 hours into the session (binge-like behavior) to the 24 hour measurements at the end of session. We will compare consumption and preference for male and female B6J mice. In addition, we will confirm the binge-like alcohol consumption by determining the blood ethanol content (BEC) at the 2 hour mark in a smaller subset of the mice in the drinking study. And finally, since *Ndrg1* expression is known to be co-expressed and correlated with other myelin related genes in the mPFC (Kerns et al. 2005; Bogenpohl et al. 2019), we will also determine protein or transcript alterations of myelin genes following both the acute and the chronic ethanol models.

3.2 Materials and Methods

3.2.1 Animals

For all experiments conducted in this Chapter, C57BL/6J mice of both genders were ordered from Jackson laboratories (Bar Harbor, Maine) and delivered at 8 weeks of age. All mice were housed in a temperature vivarium space that was set to a 12 hour light cycle. At 9 weeks of age, the mice utilized for drinking studies were habituated to housing in a different out of vivarium (OOV) space for 1 week prior to the beginning of drinking. The mice in the OOV space were singly housed in open air cages on SaniChip wood chip-based bedding. For the acute ethanol studies, mice remained group housed (N=3 or 4 per cage) on corn cob-based bedding the vivarium

for the duration of the studies. Habituation to acute intraperitoneal injections began at 10 weeks of age. The group housed mice were maintained in static rack-mounted cages with active air circulation. All cages were changed once a week for the duration of the studies. All mice had ab libitum access to standard chow (Teklad food pellets, Envigo, Hungtingdon, UK) and tap water. All procedures performed on the animals within our laboratory protocol, which was approved by the VCU Institutional Animal Care and Use Committee and were compliant with the NIH Guide for the Care and Use of Laboratory Animals. Unless noted otherwise, all experiments within this chapter contained equal numbers off male and female mice. For the study that characterizes the basal expression of NDRG1 in the mPFC, 3 male B6J of 12-weeks of age were used.

3.2.2 Prepared Solutions

The injection solution for the IHC studies was either 0.9% normal saline or ethanol diluted to 20% (v/v) in normal saline. The drinking solutions provided for the IEA study were either tap water or ethanol diluted to 20% (v/v) in tap water. For the acute dose-response study, all ethanol solutions were diluted to 18% (v/v) in normal saline. The formaldehyde solution (4% w/v) was created by dissolving powdered para-formaldehyde into 0.9% saline using heat (65°C) and by adding 1N NaOH to bring the solution pH to 10. Once the para-formaldehyde powder was fully dissolved under the described conditions, the solution was cooled and 1N HCL acid was added drop wise to bring the formaldehyde solution to physiologic conditions (pH = 7.4).

3.2.3 Intermittent Alcohol Drinking

For studies on consumption with intermittent ethanol access (IEA), B6J mice (N=21/sex/group) were transferred to an out-of-vivarium space, housed 1 animal/cage, and given one week to habituate to the new environment. The mice were then provided access to 2 graduated glass conical tubes with ball bearing sippers, and containing either 20% ethanol (v/v), diluted into tap water, or plain unadulterated tap water. In brief, our protocol entailed providing 24-hour access to both bottles within 1 hour of the beginning of the 'dark' cycle on Monday, Wednesday, and Fridays. Volume readings were marked as the bottles went on, 2 hours into the drinking sessions, and at the 24-hour time point when the bottles are removed after each session. For further details concerning

the paradigm, consult Figure 3.1B. Drinking measurements were acquired for 5 weeks. 24 hours following the final ethanol drinking session, chronic consumption mice were sacrificed by rapid cervical dislocation and decapitation and harvested for tissue collection. Micro-dissection of the individual brain regions was performed as previously described (Kerns et al. 2005).

3.2.4 Acute Ethanol Exposure

We used male and female B6 mice to determine the effect of acute ethanol on protein and gene expression of *Ndrg1*. Following 3 days of habitation to saline injections, the mice were intraperitoneally injected with one of the following doses of ethanol: 0.0 g/kg (saline control), 0.5 g/kg, 2.0 g/kg, and 4.0 g/kg. In all studies that utilized acute ethanol administration, mice were habituated to injections all normal saline for the three days leading up to the experimental injections (see Figure 3.1A). For the acute ethanol studies, the mice were sacrificed via cervical dislocation at one of two time points. The animals utilized for protein studies (IHC, WB) were sacrificed 30 minutes post-injection to detect phosphorylation state changes. The animals utilized for transcript studies (qPCR) were sacrificed 4 hours post-injection, as previously described (Kerns et al. 2005).

3.2.5 BEC Measurements

Near the conclusion of the drinking paradigm, blood was obtained for a subset of female and male mice (N= 5 EtOH drinkers per sex, and N=1 water drinkers per sex) 2 hours following start of the drinking session (see Figure 3.1B). Blood was extracted using the cheek punch method with Goldenrod sterile lancets (Braintree Scientific, Braintree, MA), as previously described (Regan et al. 2016). Blood was collected into EDTA-coated BD tubes (Fisher Scientific, Waltham, MA) before it was spun down in a refrigerated centrifuge (4°C) at 1500g for 15 minutes. The plasma was extracted from the resulting supernatnate and stored at -80°C until quantification. The measurement of the blood ethanol content of the plasma was performed using an Analox AM1 alcohol analyzer (Analox Instruments Ltd, UK) according to the manufacturer provided instructions. Of note, of the male ethanol drinking samples could not be analyzed due to insufficient plasma collection.

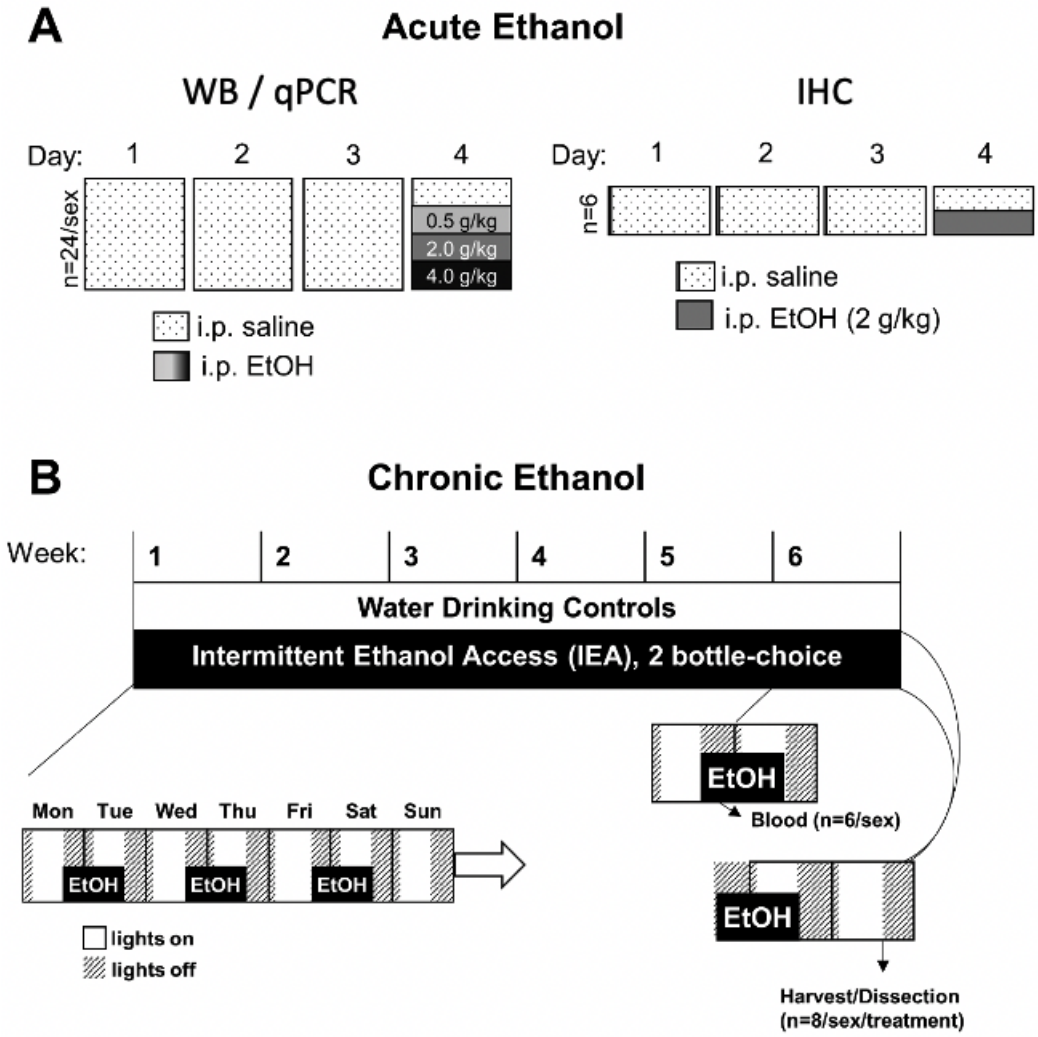

Figure 3.1: Animal models of acute and chronic ethanol exposure. (A) Acute ethanol paradigms. Left: acute dose response experiment. Right: acute IHC experiment. (B) Chronic ethanol paradigm: Intermittent Ethanol Access (IEA) model. Left: Demonstrates the light schedule and bottle schedule per week. Right: Details of the blood and tissue collection at the end of the drinking study. Adapted from: Van der Vaart 2018

3.2.6 Antibodies and Primers

Antibodies utilized for immunofluorescence studies:

Primary: anti-NDRG1 (1:500, Abcam, ab124689), anti-Thr346-pNDRG1 (1:400, Cell Signaling Technology (CST), #3217), anti-Ser330-pNDR1 (1:400, Abcam, ab124713), anti-CNP [11-5B] (1:400, Abcam, ab6319), anti-NeuN Antibody [A60] (1:500, Millipore, MAB377).

Secondary: AlexaFluor 488 anti-mouse IgG1 (1:1000, ThermoFisher, A-2112), AlexaFluor 568 anti-rabbit (1:500, ThermoFisher, A-11036)

Antibodies utilized for Western blotting studies:

Primary: anti-NDRG1 (1:1000, Abcam, ab124689), anti-Thr346-pNDRG1 (1:1000, Cell Signaling Technology (CST), #3217), anti-Ser330-pNDRG1 (1:1000, Abcam, ab124713), anti-MBP (1:1000, Abcam, ab7349), anti-GAPDH [6C5] (1:7500,Millipore, MAB374).

Secondary: 680LT Mouse IgG1 (1:50000; LiCor #926-68050), 800CW Rabbit (1:30000; LiCor #926-32211), 800CW Rat (1:30000; LiCor #926-32219)

Genes targeted for qPCR analysis:

Ndrg1, *Ublcp1*, *B2m*, *Mbp*, *Mag*, *Mobp*, *Mal*.

The sequences for each primer pair used are provided in Table 3.1.

Gene	Forward	Reverse
Ndrg1	ATGAATGTGAACCCCTGTGC	TATCTCCTCCTTGCCGAAGA
Ublcp1	ATCTCTCACCCTTGCCCTTT	CCCATTTTGTGTGCTTTCGT
B2m	GGAGAATGGGAAGCCGAACA	TCTCGATCCCAGTAGACGGT
Mbp	ACACACGAGAACTACCCATTATGG	AGAAATGGACTACTGGGTTTTCATCT
Mobp	AACTCCAAGCGTGAGATCGT	CTCGGTCACTTCTTCCTTGG
Mal	TCTTCACCACCTTCCCTGAC	GCCACAAAGCAGAACACAGA

Table 3.1: Sequences for primers used in Chapter 3.

3.2.7 qPCR Methodology

Total RNA was extracted from mPFC microdissected tissue using the RNeasy Mini Kit (Qiagen, #74104). RNA purity and concentration assessed by NanoDrop 2000 (ThermoFisher, ND-2000) spectrophotometry and only samples with 260/280 ratios > 1.8 were analyzed further. cDNA was synthesized using an iScript cDNA Synthesis Kit (BioRad, #1708891). PCR reactions were performed using iQ SYBR Green Supermix (BioRad,#1708880) reagent and and a CFX Connect Thermocycler (BioRad). Normalized expression values were calculated with the delta-delta Ct method, where non ethanol-responsive genes, *Ublcp1* and *B2m*, were used as reference genes. Tukey's HSD post-hoc testing was utilized for analysis of acute exposure data, while unpaired Student's t-test were applied for the chronic ethanol exposure data.

3.2.8 Western Blot Methodology

For all western blot studies in this chapter, tissue homogenization was performed using 1X RIPA lysis buffer (50 mM Tris, 150 nM NaCl, 1% NP40, 5 mM EDTA, and 0.5% SDS). Microdissected tissue was homogenized using 2 to 4 short pulses with an ultrasonic sonicator over ice. To prevent protease and phospatase activity in the homogenized samples, 100X HALT Protease and Phosphatase Inhibitor Cocktail (ThermoFisher, #78440) was diluted to 1X in all RIPA buffers prior to homogenization. The homogenized solutions were partitioned into aliquots and immediately frozen at $-80°$C. Total protein concentration was determined by utilizing a Pierce BCA Protein Assay Kit (ThermoFisher, #23225), to allow for equal protein loading. Before performing an immunoblot, the proteins in the homogenized samples were denatured by heating the sample dissolved in NuPage Reducing Agent (ThermoFisher, NP0004) and 4X Protein Sample Loading Buffer (LiCor, #928-40004) in a heat block for 10 minutes at 70°C. Both the electrophoresis and the transfer steps were performed using the Xcell Surelock Mini Cell System (ThermoFisher, EI0001). The denatured protein samples were loaded into NuPage 4-12% Bis-Tris 17-well gels (ThermoFisher, NP0329BOX). Once equal amounts of total protein are loaded onto the gel, the proteins are first separated by size using electrophoresis at 100V. The size separated gels were then transferred onto Immobilon-FL PVDF Membrane (Millipore, IPFL00005) by applying 12V at 4C

for 16 hours using NuPage Transfer Buffer (ThermoFisher, NP0006). Following transfer, the membranes were briefly rinsed in milliQ water and were air dried for at least 1 hour to promote permanent binding of transferred proteins. The membranes were then re-hydrated using 100% methanol and rinsed with milliQ water. The membranes were then blocked in Licor Intercept Blocking Buffer (Licor, #927-60001) for 1 hour before the immediate application of primary antibodies, diluted in 1X blocking buffer containing .2% Tween-20. The primary antibodies were incubated overnight at 4C before the solution is washed 4 times with 1X TBS with 0.1% Tween-20. The membranes were then incubated with secondary antibodies were diluted into 1X blocking buffer with 0.2% Tween-20, and then applied for 1 hour at room temperature. The membranes were then washed 4 times with 1X TBS with 0.1% Tween-20, followed by rinses in 1X TBS to remove the residual tween-20 from the washes. The membranes were stored submerged in 1X TBS in the dark at 4C until ready to image. Imaging was performed using the Odyssey Infrared Imaging System (Licor, #9120). The experimental proteins were stained using the species-specific 800CW secondary at 1:30,000 dilution. The loading control and normalization protein, GAPDH, was stained using the 680LT anti-mouse antibody specific to mouse IgG1 at a concentration of 1:50,000. All scans were analyzed and quantified using the FiJi image analysis software package (ImageJ, NIH).

Because the membrane was thoroughly dried following transfer, the membranes can be safely stripped of the primary/secondary antibodies multiple times without noticeable protein loss. The stripping of the membranes was performed using 1X NewBlot IR Stripping Buffer (Licor, #928-40028) for 20 minutes with vigorous shaking, followed by multiple wash steps. A new aliquot of the secondary antibody staining solution is then incubated on the stripped membrane and re-imaged to determine efficacy of the stripping of the signal. Using this methodology, we were able to measure both phospho-forms of NDRG1, total NDRG1, and myelin related genes using a single membrane in most cases.

3.2.9 Immunohistochemistry Methodology

All mice were perfused with transcardial administration of a 4% formaldehyde solution (in 1X PBS) while anesthetized with high doses of isoflurane. The mice were first flushed with pure

1X PBS to remove the remaining blood before the 4% formaldehyde was injected. The perfused brains were then removed from the skull and transferred to a vial of fresh 4% formaldehyde for an overnight post-fixation step. The brains are then placed into a 30% sucrose solution dissolved in 1X PBS for dehydration of the remaining water. Once the brains were fully dehydrated and sunk to the bottom of the sugar solution, they were snap frozen in a vial of isopentane that was cooled to -80C using dry ice and then stored at -80C until they are ready to proceed. The frozen brains are then cut into 20um thick coronal sections using a Leica CM3050 cryostat (Leica Biosystmes, Wetzlar, Germany). The sliced sections stored as free-floating sections that were submerged in a 1X PBS solution containing 0.02% sodium azide to preserve and prevent bacterial growth. The slices were stored in order along the wells of a 24-well plate.

Prior to staining of the coronal slices, the antigens that are masked by protein cross linking are recovered by placing the slices in Citrate Acid Buffer (pH = 6.0) and heating at 80C for 20 minutes with shaking, followed by a 30 minute cool-down step at room temperature with vigorous shaking. Following this antigen retrieval process, the sections are then permabolized and blocked in 10% goat serum with 0.2% Triton X100 for 30 minutes are room temperature. The sections were then incubated overnight at 4C with primary antibodies that are dissolved in 1XPBS with 0.2% Triton-X with gentle rocking. The slices are then washed 4 times in an abundance of 1X PBS for 5 minutes with vigorous shaking. Following the fourth wash, the slices are then incubated with secondary antibodies dissolved in 1X PBS with 0.2% TritonX for 1 hour at room temperature with gentle rocking. Following the secondary incubation, the slices were washed 4 times in an excess of 1X PBS for 5 minutes with vigorous shaking.

These stained slices are then mounted and dried onto SuperFrost Plus Gold Slides (ThermoFisher). The dried slices are then coated with Vibrance anti-fade mounting media (VectaShield, H1800) and sealed under a .17mm thickness glass cover slip. The mounting media is dried and hardened overnight at room temperature in the dark. Following the curing of the mounting media, the edges are sealed with clear nail polish for long term storage either at 4C or room temperature, per the manufacturer instructions.

3.2.10 Microscopy Methods

Confocal images presented in this chapter were taken using either the Zeiss LSM710 or the Zeiss LSM880. All images taken with the LSM710 were taken at a scan area and an airy unit equal to 1. All images taken on the LSM880 utilized the AiryScan super resolution mode, while the scan area varied depending on desired field of view and resolution. All images on both Zeiss microscope utilized the 63X oil objective. Additional validation of cell-type localization images were performed on a Zeiss IM inverted microscope using a 40X water objective or 32X air objective and a Retiga 2000R CCD camera (Qimaging, USA).

3.2.11 Statistical Analysis Methods

All statistics were performed using R v3.6.3 (CRAN development group, 2019) and all resulting figures were generated using the ggplot2 package (Wickham 2016) unless noted. An alpha of 0.05 and a beta of 0.80 were used for the determination if results are statistically significance. The exact statistical tests will be defined when presenting the results for this chapter. Tukey's Honest Significant Difference (HSD) is utilized for multiple test corrections when applying post hoc analysis of significant main effects or interactions in ANOVA-based statistical models.

3.3 Results

3.3.1 Basal Expression Patterns in mPFC

The literature has reported that CNS expression of *Ndrg1* is limited to oligodendrocytes (Okuda, Kokame, and Miyata 2008; Costin, Dever, and Miles 2013). Imunolabeling of the viral injection site of mice infected with sh-*Ndrg1* lentivirus demonstrated that nearly all viral GFP+ cells co-stained with NeuN, a maker that labels the nuclei most types of neurons (see Figure 3.2).

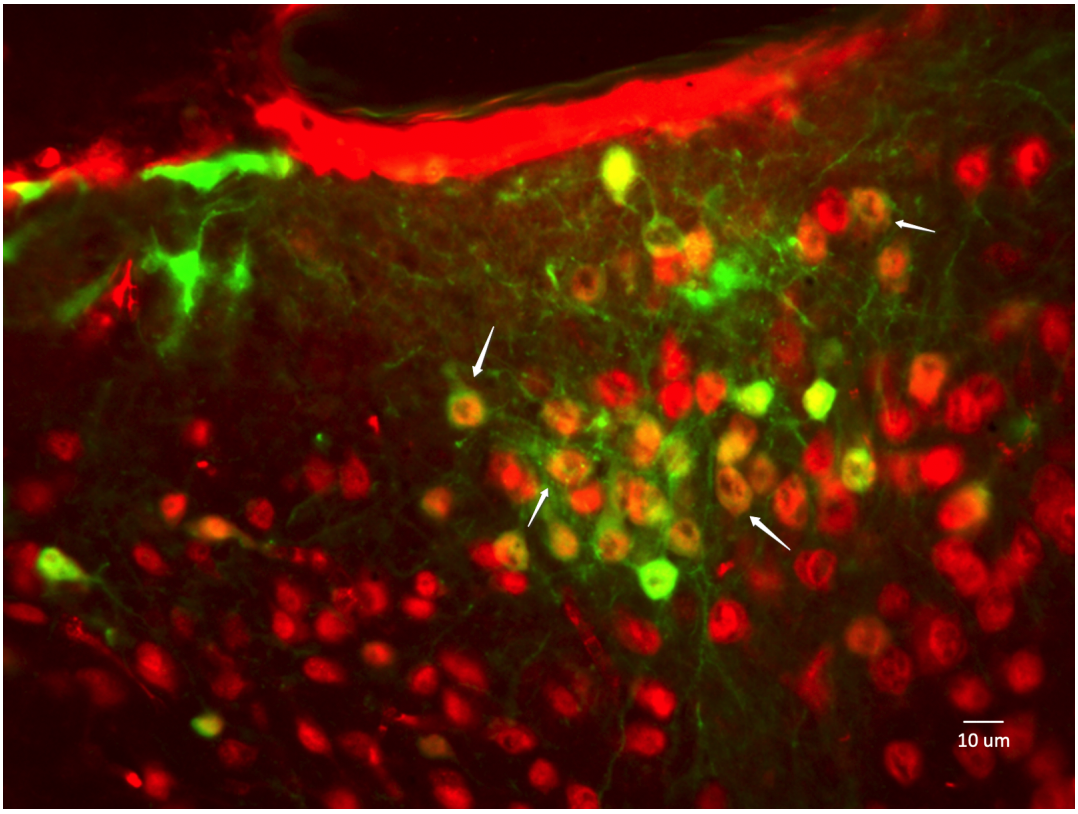

Figure 3.2: Microscopy of sh-*Ndrg1* infected cells with neuronal marker, NeuN. Imaged at 32X. Green: GFP+ cells express the tag when infected with lentivirus. Red: Labeling of NeuN+ cells. White arrows highlight cells that demonstrate strong overlap of NeuN and GFP signal.

Given the significantly increased LORR duration and decreased EtOH consumption observed following *Ndrg1* knockdown, we investigated if neuronal expression of *Ndrg1* is possible in the mPFC of the CNS, a region not previously studied for *Ndrg1* expression. We found that NDRG1 did not colocalize with mPFC neurons, but that it did colocalize with both CC1and CNPase (see Figure 3.3). Thus we conclude that NDRG1 expression in the mPFC is limited to oligodendrocytes.

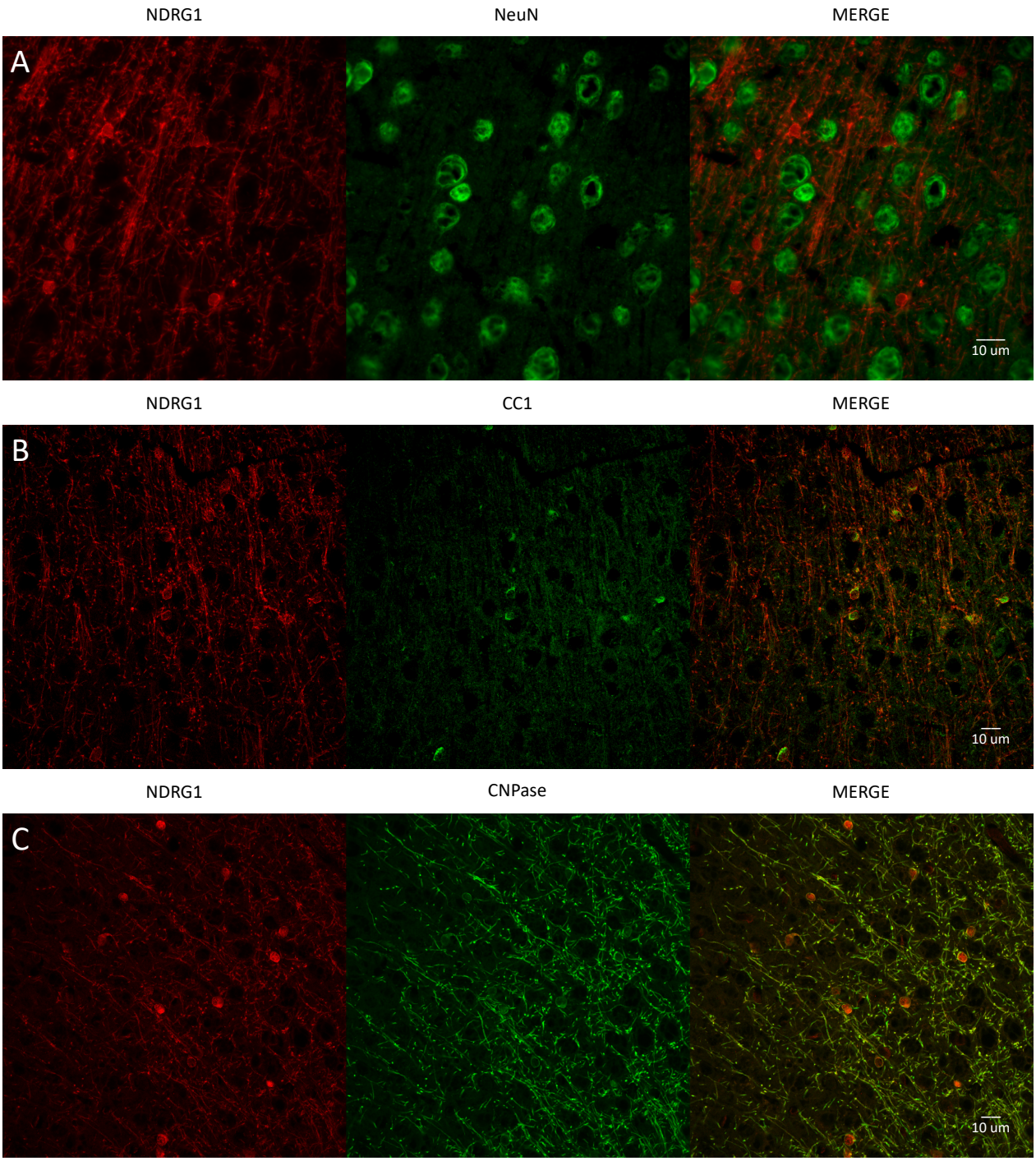

Figure 3.3: Cell type expression of NDRG1 in mPFC. A (top row): overlap with neuronal marker, NeuN. B (middle row): overlap with cytosol marker for oligodendrocytes, CC1. C (bottom row): over with oligodendrocyte membrane and myelin process marker, CNPase. Note the overlap of NDRG1 signal with both the oligodendrocyte cell body (see B and C) and within the myelin process (see C).

Additionally, we sought to characterize the sub-cellular localization of NDRG1 within the oligodendrocyte cell type. We found that the Ser330 phospho-form of NDRG1 (Ser330-pNDRG1) was predominately nuclear with some expression in the cytosol and less in the processes (see Figure 3.4B). In contrast, the Thr346 phospho-form of NDRG1 (Thr346-pNDRG1) was predominately expressed in the cytosol and in the myelin processes, with some nuclear expression as well (see Figure 3.4A). Remarkably, this phosphorylation specific localization pattern is consistent with that observed in multiple cancer cell lines (Park et al. 2018).

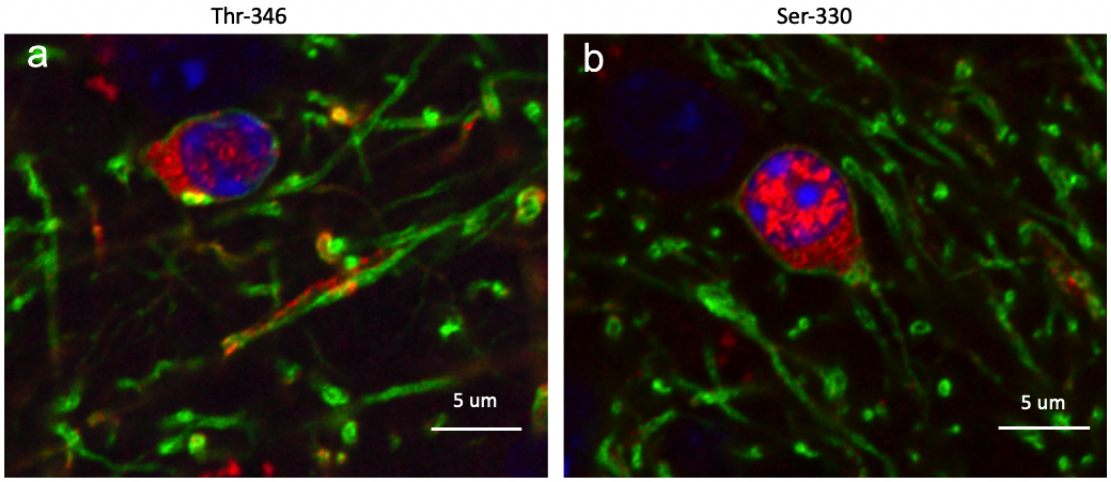

Figure 3.4: Basal sub-cellular localization of phospho-forms of NDRG1within olgiodendrocytes of mPFC. A: Thr346-pNDRG1 co labeled with CNPase (green) and DAPI (blue). B: Ser330-pNDRg1 co labeled with CNPase (green) and DAPI (blue)

As demonstrated in Figure 3.5, we used the quantification abilities of the ImageJ software package to compare the mean intensities of pNDRG1 signals for a region of interest (ROI) surrounding 2 cellular compartments. (1) the nucleus: as defined by the outline of the DAPI signal within the cell (blue). (2) the cyostol: as defined by the outlines of he CNPase signal (green) and the DAPI signal (blue). Here, we demonstrate a greater mean intensity of Thr346-pNDRG1 signal in the cytosol relative to the nucleus (see Figure 3.5A). Conversely, we found a greater intensity of Ser330-pNDRG1 signal in the nucleus relative to the cytosol(see Figure 3.5B).

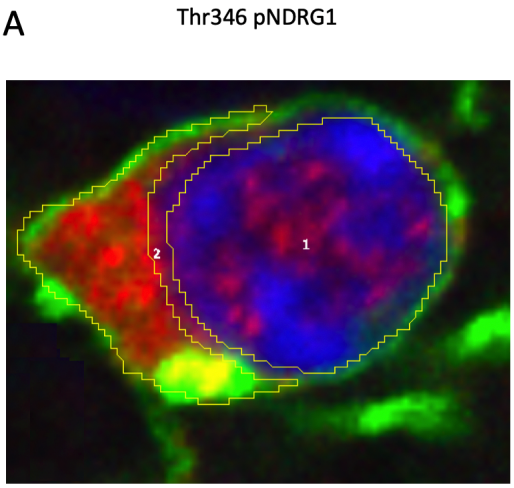

	Area	Mean	IntDen	RawIntDen
1	23.951	10256.277	245644.604	14143406
2	11.793	20838.591	245748.761	14149403

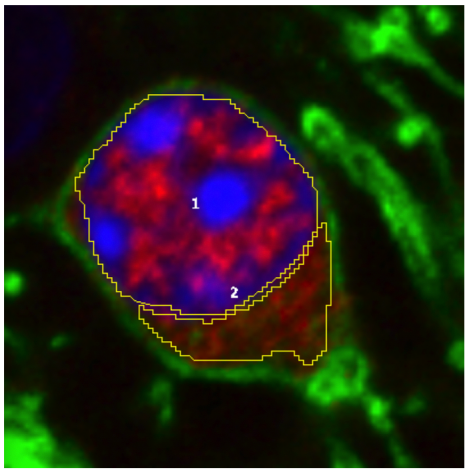

	Area	Mean	IntDen	RawIntDen
1	32.635	19010.426	620400.097	35720591
2	8.875	16229.920	144042.448	8293489

Figure 3.5: Comparison of mean intensities of pNDRG1 signal for a region of interest (ROI) surrounding 2 cellular compartments. (1) the nucleus: as defined by the outline of the DAPI signal withing the cell (blue). (2) the cyostol: as defined by the outlines of he CNPase signal (green) and the DAPI signal (blue). Quantification of basal sub-cellular localization of phospho-forms of NDRG1. (A) Thr346-pNDRG1 (B) Ser330-pNDRG1.

3.3.2 Modulation of *Ndrg1* by Acute Ethanol

To begin our ethanol studies, we sought to determine if acute exposures to ethanol would alter the *Ndrg1* transcriptome and/or proteome. First, we utilized qPCR to measure modulation of *Ndrg1* mRNA abundance in the mPFC 4 hours after receiving one of the following doses of ethanol: 0.0 g/kg (saline control), 0.5 g/kg, 2.0 g/kg, 4.0 g/kg. We normalized the calculated expression values for all samples in the study relative to a single female control sample, which allowed us to consider the difference in basal levels of *Ndrg1* expression between male and female mice in the analysis. The 2-way ANOVA analysis revealed significant main effects of (1) ethanol dose ($P = 5.7E\text{-}6$) and (2) sex ($P = 1.52E\text{-}14$) and their interaction ($P = 0.0013$) on the detected levels of *Ndrg1* expression (see Figure 3.6). A post hoc Tukey HSD analysis of all sex and ethanol dose comparisons was performed to correct the p-values of all comparisons. Post hoc testing revealed a significant induction of *Ndrg1* expression in female mice at the highest dose (4.0 g/kg) relative to the saline control group ($P < 0.0001$), as shown in Figure 3.6A. Conversely, the male

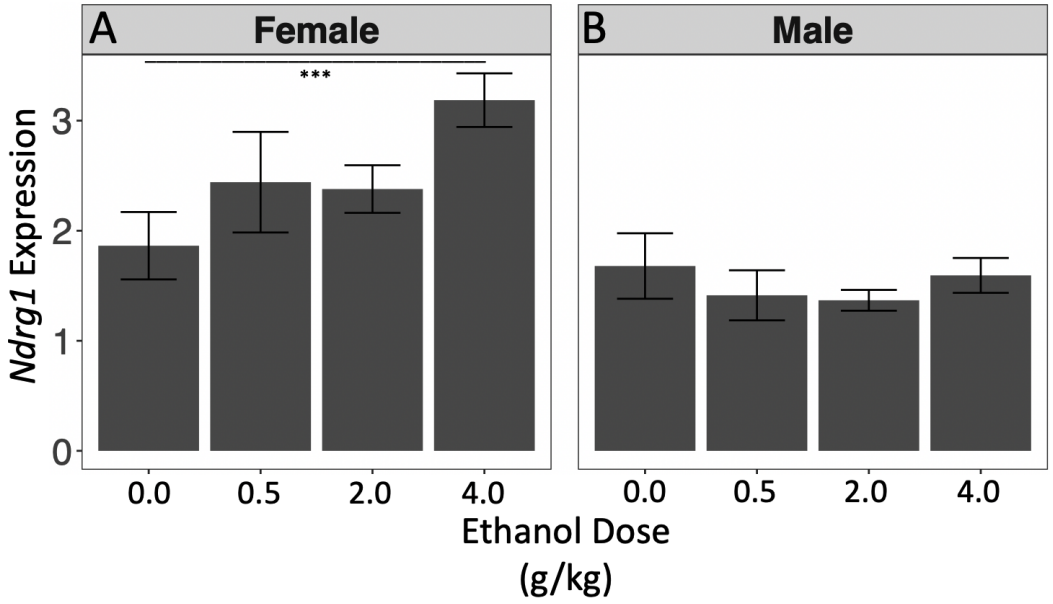

Figure 3.6: qPCR analysis of *Ndrg1* transcript expression 4 hours after one of the following acute ethanol exposures: 0.0 g/kg (saline control), 0.5 g/kg, 2.0 g/kg, 4.0 g/kg. (A) dose response for female mice. (B) dose response for male mice.

mice (Figure 3.6B) did not display any alterations in *Ndrg1* expression following acute ethanol ($P > 0.89$ for all ethanol dose comparisons). Additionally, no difference was detected between basal levels (0.0g/kg) of *Ndrg1* in female and mice in the saline control groups ($P = 0.465$). Likewise, no differences were detected between the group of saline control female mice and any of the 3 ethanol dosed groups of male mice ($P > 0.19$ for all comparisons).

After considering the transcript response to acute ethanol, we utilized Western blotting to measure changes in two different phospho-forms of NDRG 30 minutes following one of the following doses of ethanol: 0.0 g/kg (saline), 0.5 g/kg, 2.0 g/kg, 4.0 g/kg. In the following acute ethanol Western blotting analyses, we utilized a 2-way ANOVA design that considered the main effects and interactions of ethanol dose and sex. For demonstration of concept of our Western blotting quantification setup, we briefly show the imaged membrane Thr346-pNDRG1 staining for male mice following chronic ethanol drinking (see Figure 3.7). In particular, we note variation of the quantification protein signal, Thr346-pNDRG1 (see Figure 3.7A) across the samples. However, we see no variation of normalization control gene, GAPDH (see Figure 3.7B), indicating that our Western blotting quantification system is valid for our experimental design.

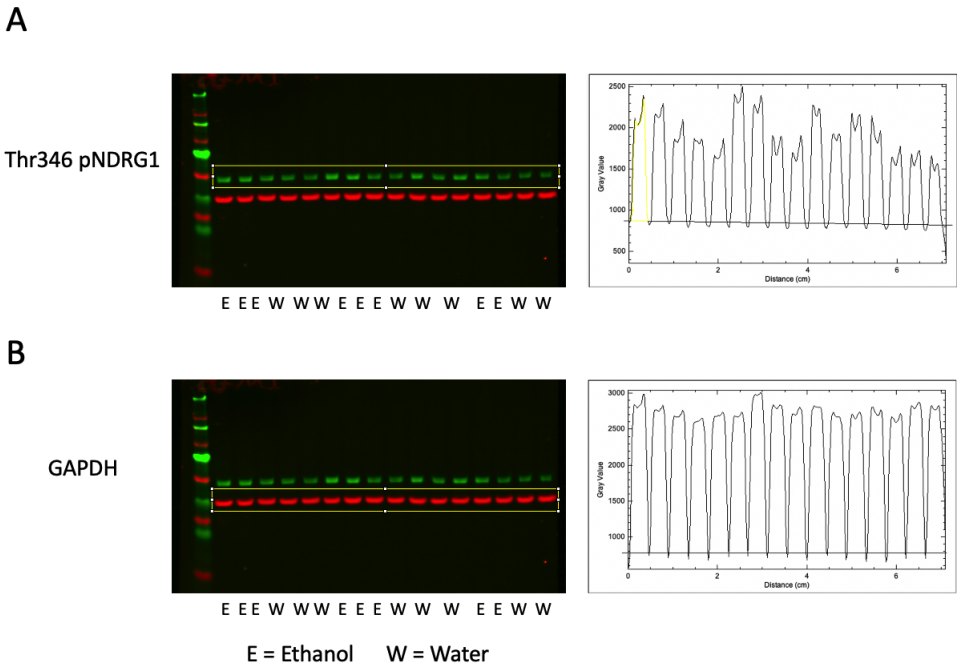

Figure 3.7: Example of Western blot imaging and quantification for Thr346-pNDRG1 in chronic drinking male mice. (A) shows the signal of the 800CW secondary antibody for Thr346-pNDRG1 (in green). The intensity quantification of the Thr346-pNDRG1 displays variation of signal between samples (right of A). (B) shows the signal 680LT secondary antibody for the normalization control, GAPDH (in red). Note the constant, non-varying signal of GAPDH across the samples (right), indicating that GAPDH is an appropriate normalization gene for these Western blotting studies.

As expected, we found no significant main effects of ethanol dose ($P_{EtOHdose}$ = 0.198) or sex (P_{Sex} = 0.846) and no significant interactions of between the main effects ($P_{EtOHdose:Sex}$ = 0.970) for the total NDRG1 signal following acute ethanol (see Figure 3.8C). Here, the total NDRG1 signal is first normalized using the GAPH signal as a loading/normalization control. The signals for each ethanol treated samples is then normalized by dividing by the average NDRG1 signal of the saline control group in both sexes. This last step results in the control group having a normalized expression of 1.0 for each sex (see Figure 3.8C). Next, we analyzed the two phospho-forms of pNDRG1 by normalizing the phospho-signal to the normalized total NDRG1 signal for each sample. Finally, the signals for each ethanol treated sample is then normalized by dividing by the average pNDRG1 signal of the saline control group in both sexes to normalize the control groups to an average of 1.0 for each sex (Figure 3.8A,B).

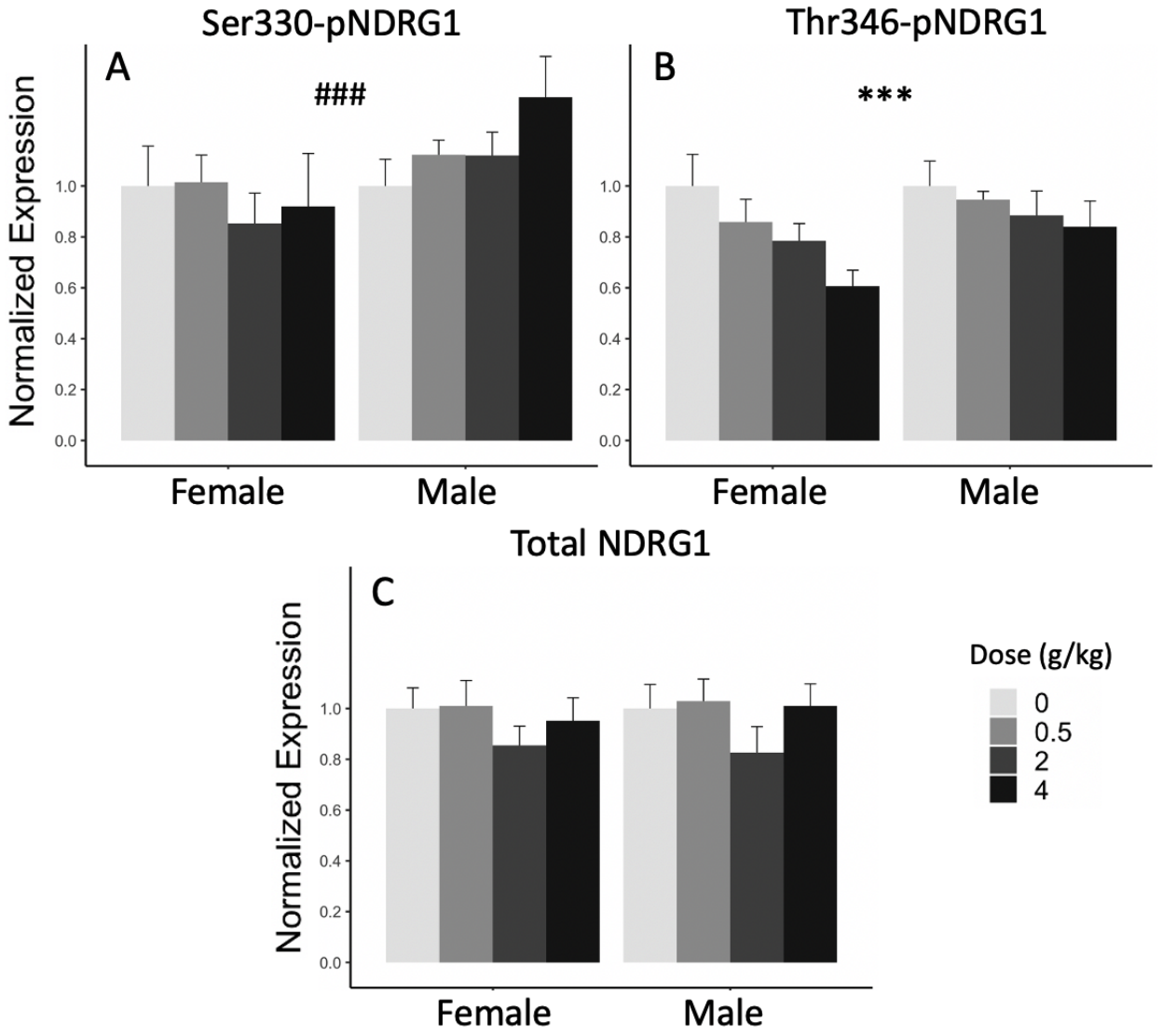

Figure 3.8: Modulation of phospho and total NDRG1 following acute ethanol dose response. Graphical representation of 2-way ANOVA investigating effects of ethanol dose and sex. (A) Ser330-pNDRG1 results: significant main effect of sex (### < 0.05) detected. (B) Thr346-pNDRG1 results: significant main effect of ethanol dose (*** < 0.05) detected. (C) Total NDRG1 results: no significant effects or interactions detected

Following these normalization steps, we found a main effect of sex ($P_{Sex} = 0.046$) was observed for the Ser330 phospho-form of NDRG1, but there was no main effect of ethanol dose ($P_{EtOHdose} = 0.653$) or any significant interactions ($P_{EtOHdose:Sex} = 0.423$) the between the main effects (see Figure 3.8A) . Conversely, the signal Thr346 phospho-form of NDRG1 demonstrated a main effect of ethanol dose ($P_{EtOHdose} = 0.027$), but was unaffected by either the main effect of sex ($P_{Sex} =$

0.105) or an interaction ($P_{EtOHdose:Sex}$ = 0.6302) between the main effects (see Figure 3.8). Therefore, we collapsed the sexes to increase our statistical power and reduce the dimensions to a 1-way ANOVA that only considers the effect of the ethanol treatment dose (see Figure 3.9). Post-hoc testing of the effect of ethanol treatment dose on Thr346-pNDRG1 expression was conducted in a pairwise fashion. Following multiple test corrections with Tukey's HSD, it was determined that there was a significant down regulation ($P_{adjusted}$ = 0.017) of the Thr346 phospho-form of NDRG1 at the highest dose (4.0 g/kg) relative to the control saline animals (see Figure 3.9).

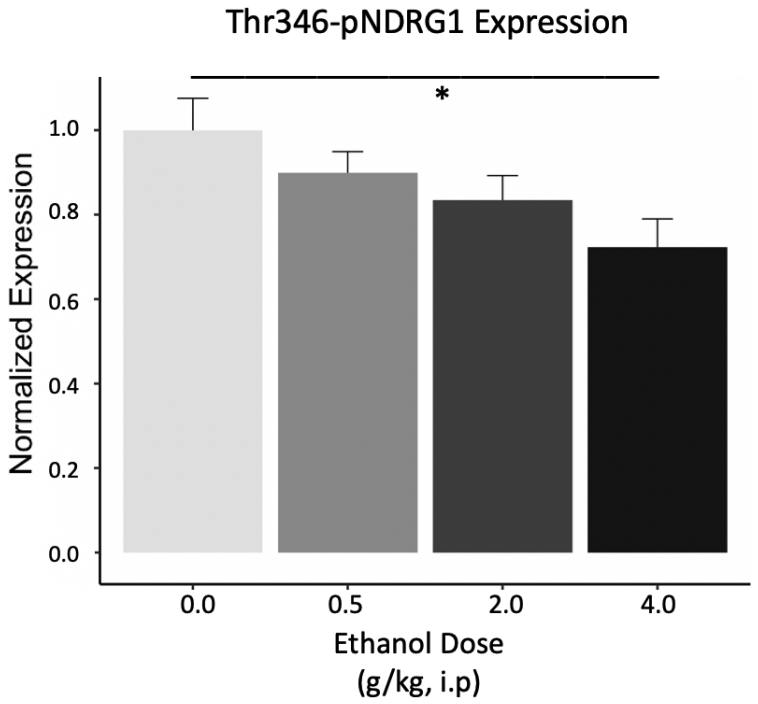

Figure 3.9: Levels of Thr346-pNDRG expression in mPFC are altered by acute ethanol exposure. Sexes are collapsed in this analysis, based on the results of the 2-way ANOVA. Post hoc analysis with Tukey's HSD revealed that a significant decrease in Thr346-pNDRG1 was detected in the 4.0 g/kg ethanol dose group relative to the saline treated control group ($P_{adjusted}$ = 0.017).

Additionally, rather than simply asking if levels of phospho-NDRG1 are altered following acute ethanol, we utilized IHC methods to determine if sub-cellular distribution of phospho-NDRG1 forms is altered by acute ethanol. We delivered a dose of 2.0 g/kg and the mice were transcardially perfused 30 minutes following the ethanol injection. The dose of 2.0 g/kg was chosen as a more accurate representation of human levels of intoxication and the time point was set to be

the same as previously used in the acute ethanol dose response experiment. Both phospho-forms were investigated using the super resolution AiryScan functionality of the Zeiss LSM880. The phospho-NDRG1 forms are co stained with CNPase, as a marker of oligodendrocyte cell membranes and the myelin processes, and DAPI, as a marker of nuclear compartment. As described above and demonstrated in Figure 3.5, we used FiJi to quantify signal intensity of the phospho-NDRG1 in the cytosol and the nucleus by drawing ROIs based on the compartments that are defined using the CNPase and DAPI costains. We imaged a total of 90 cells per treatment group by 3 coronal slice are used per animal, where 5 well shaped oligodendrocytes are imaged in the mPFC region per hemisphere. We found that 2.0 g/kg of acute ethanol significantly alters the ratio of nuclear/cytosol mean intensities signals for Ser330-pNDRG1 ($P < 0.01$), but not for Thr346-pNDRG1 (see Figure 3.10). In specific, we determined that acute ethanol results in higher levels of nuclear Ser330-pNDRG1 signal relative to cytoplasmic signal (see Figure 3.10A).

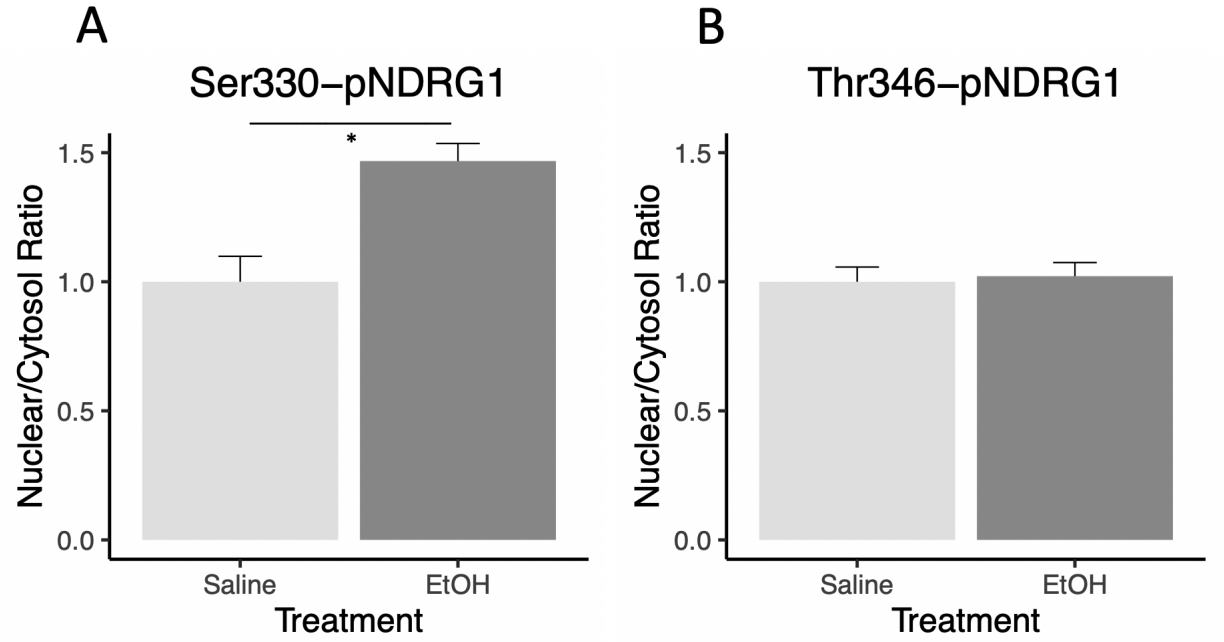

Figure 3.10: Comparison of nuclear to cytosol ratio of phospho-NDRG1 signal following acute ethanol exposure (30 minutes after 2 g/kg, ip). (A) Ser330-pNDRG1. (B) Thr346-pNDRG1. N = 3 per treatment (ratio values for each N is derived from an average of 30 imaged cells over 3 coronal slices). Student's t-test (* $P < 0.05$)

3.3.3 Modulation of *Ndrg1* by Chronic Consumption of Ethanol

Recent studies from the Miles laboratory have shown marked increase in *Ndrg1* correlation with myelin gene expression in mPFC following one year of chronic ethanol consumption in rhesus macaques (Bogenpohl et al. 2019). To complement our data on acute ethanol exposure, we set out to determine if *Ndrg1* was altered at the transcript or protein level following 5 weeks of chronic intermittent consumption of ethanol in a mouse model. We also determined expression profiles of myelin genes at both the transcript and the protein level. As documented in the dissertation by Van der Vaart 2018, the IEA protocol produced a number of ethanol drinking phenotypes. While there is no change in total daily ethanol consumption or preference over the course of the study, the binge readings measured an increased preference for ethanol (see Figure 3.11B) and ethanol consumed (see Figure 3.11A) in the first 2 hours over the course of the 5-week study. As expected, the female mice consumed higher amounts of ethanol than males over a 24-hour period (see Figure 3.11E). Additionally, BEC measurements of the 12 selected mice at the 2 hour time mark showed that both males and female had significantly elevated BEC levels (180 mg/dL), indicating the mice were indeed consuming intoxicating levels of ethanol soon after the drinking bottle was provided (see Figure 3.12A). Both the male and the female mice had and average BEC of approximately 100mg/dL after 2 hours of access to the ethanol (see Figure 3.12B). Consistent with this finding, we report that both male and female mice escalated their ethanol consumption (Figure 3.11C) and preference (Figure 3.11D) to very similar levels by the 15th access day in the study.

After validating the effectiveness of our IEA drinking paradigm, we investigated *Ndrg1* at transcript level expression using qPCR following the 5 weeks of chronic ethanol exposure. Here, we found a borderline significant main effect of treatment ($P = 0.051$) on expression levels of *Ndrg1* when utilizing a 2-way ANOVA model that considered both treatment and sex (see Figure 3.13A). We did not observe any effects of sex, so data was collapsed across sexes and analyzed by simple t-test based statistics. Once collapsed, we observed a statistically significant induction of *Ndrg1* mRNA in the mPFC ($P = 0.041$) following 5 weeks of chronic ethanol drinking (see Figure 3.13B).

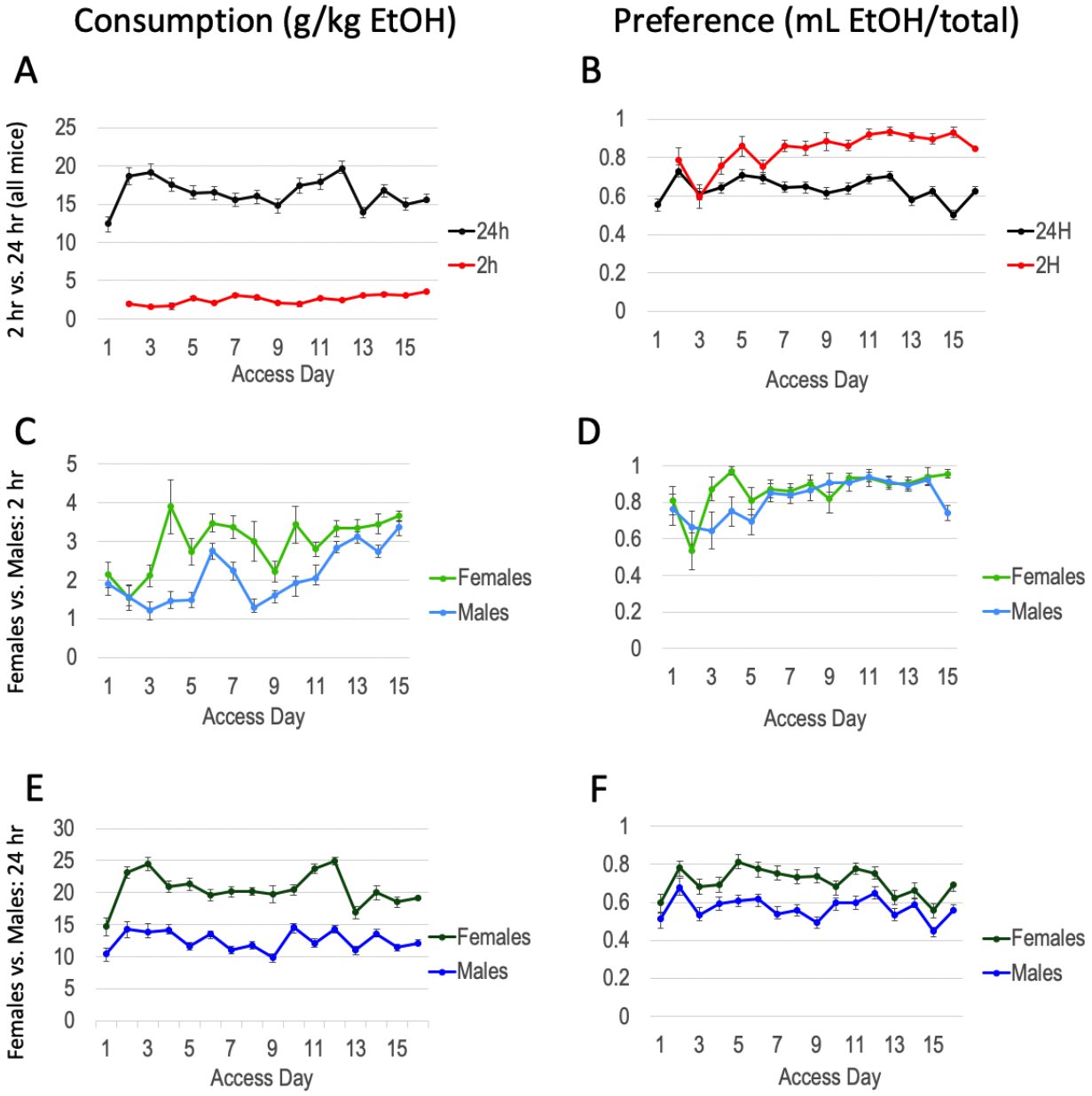

Figure 3.11: Drinking patterns over time in 5 week 2-bottle choice IEA study. Displays both the ethanol consumption (A, C, D) and preference (B, D, F). 24 hour measurements are compared with 2 hour binge measurements in A, B. Male and female measurements at the 2 hour binge measurement are compared in C, D. Male and female measurements at the 24 total daily measurement are compared in E, F.

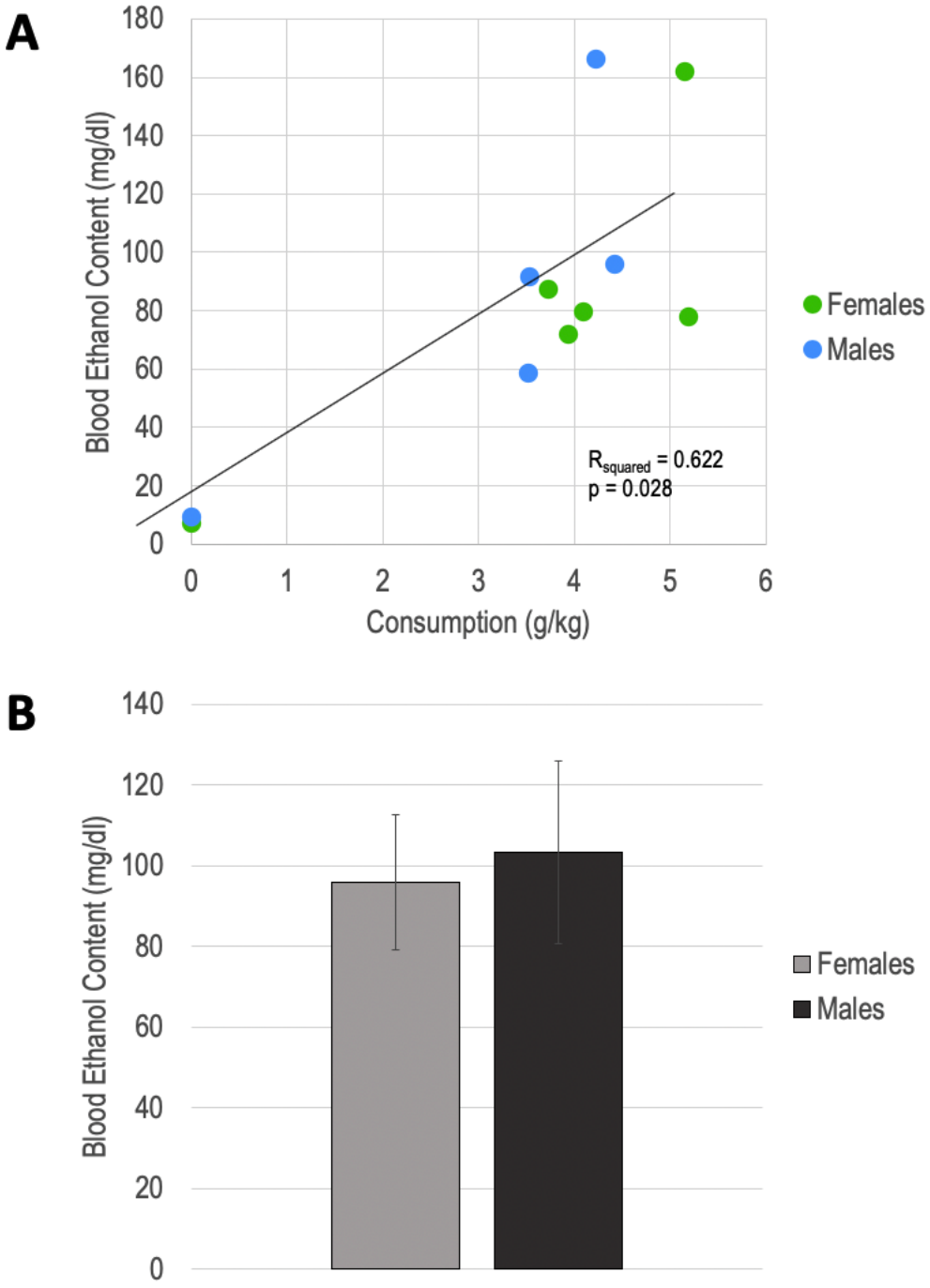

Figure 3.12: BEC measurements of select mice at the 2 hour binge reading point after 5 weeks of 2-bottle choice IEA drinking. Blood draws occurred during the second to last drinking session. (A) Individual BEC measurements for all selected mice. (B) Average BEC values per sex.

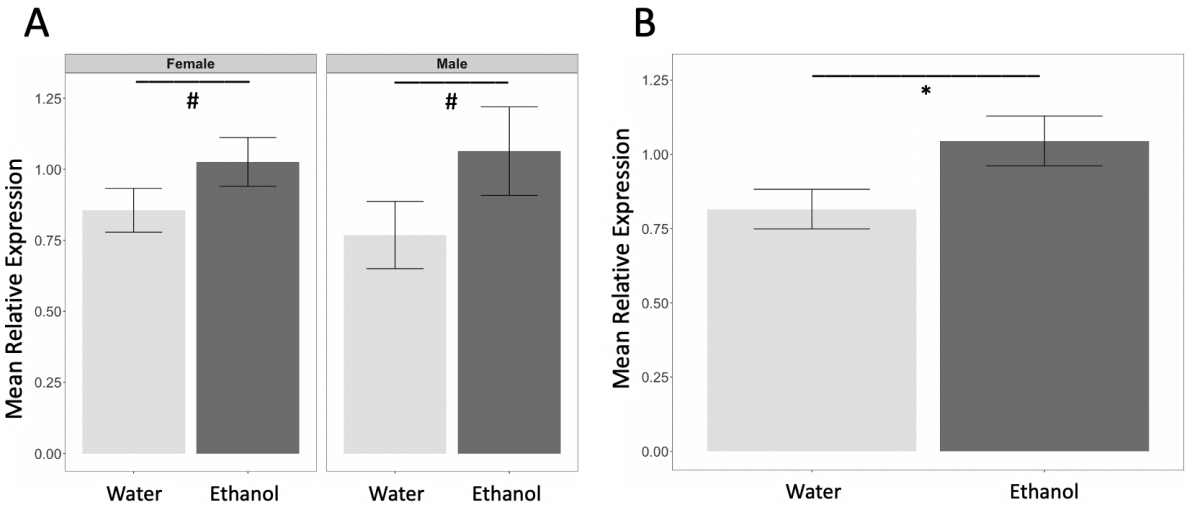

Figure 3.13: qPCR analysis of *Ndrg1* transcript levels following 5 weeks of chronic ethanol exposure. (A) Graphical representation of 2-way ANOVA model investigating the effects of ethanol drinking and sex. A borderline main effect of main effect of ethanol drinking was detected (#, P = 0.051), while no effects of sex were detected. (B) Sexes are collapsed to increase statistical power. Results in a significant induction of *Ndrg1* transcript following chronic ethanol drinking

We next determined if myelin-related transcripts were altered by the chronic ethanol exposure, since dysregulation of myelin genes are thought to contribute in part to the pathology of alcohol abuse. We measured the expression of a panel of myelin genes which have been shown to be altered in brain tissue from human alcoholics (Mayfield et al. 2002; Liu et al. 2006) or animal models (Kerns et al. 2005; Wolstenholme et al. 2017): *Mag*, *Mbp*, *Plp1* and *Mobp*. Sexes were collapsed to increase power since there was no main effect or interaction with the treatment group for any gene. In short, we observed no changes in our panel of 4 myelin genes between the ethanol drinkers and the water controls when the treatment groups are compared by simple Students t-tests.

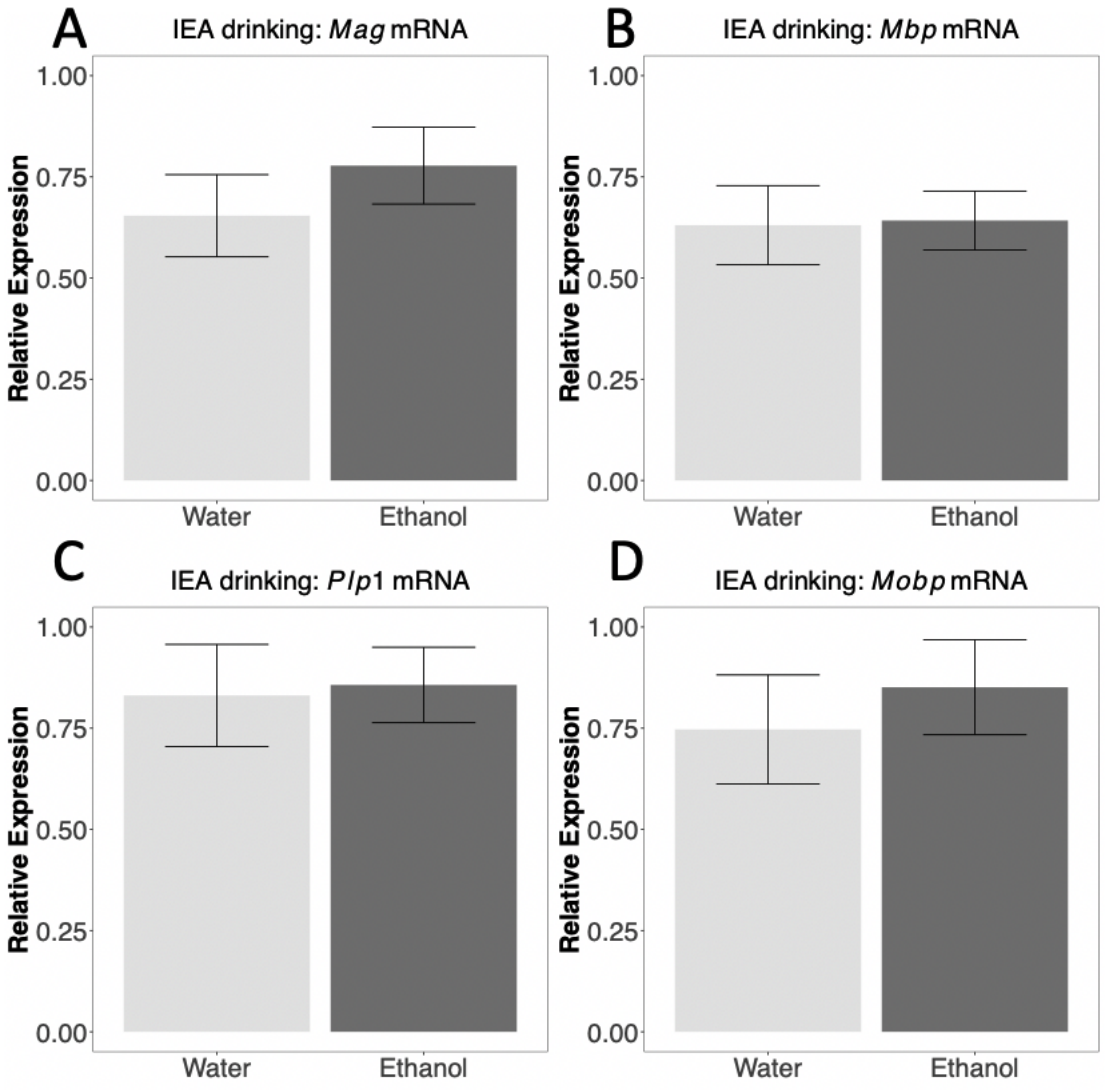

Figure 3.14: qPCR analysis of a panel of 4 myelin genes following 5 weeks of chronic consumption of ethanol. No effects or interactions of sex or ethanol treatment were detected with a 1-way ANOVA analysis after collapsing both sexes. (A) *Mag* (B) *Mbp* (C) *Plp1* (D) *Mobp*

After documenting the modest induction of *Ndrg1* transcripts, we investigated the effects of chronic alcohol consumption on NDRG1 protein levels in the mPFC using Western blotting. At the same time, we also quantified the predominant and main protein in CNS myelin, MBP, to get a snapshot of general levels of myelin expression in the mPFC. In brief, we found no significant changes in any phospho or total form of NDRG1 or MBP, in males or females, following 5 weeks of chronic ethanol drinking (see Figure 3.15 and Figure 3.16).

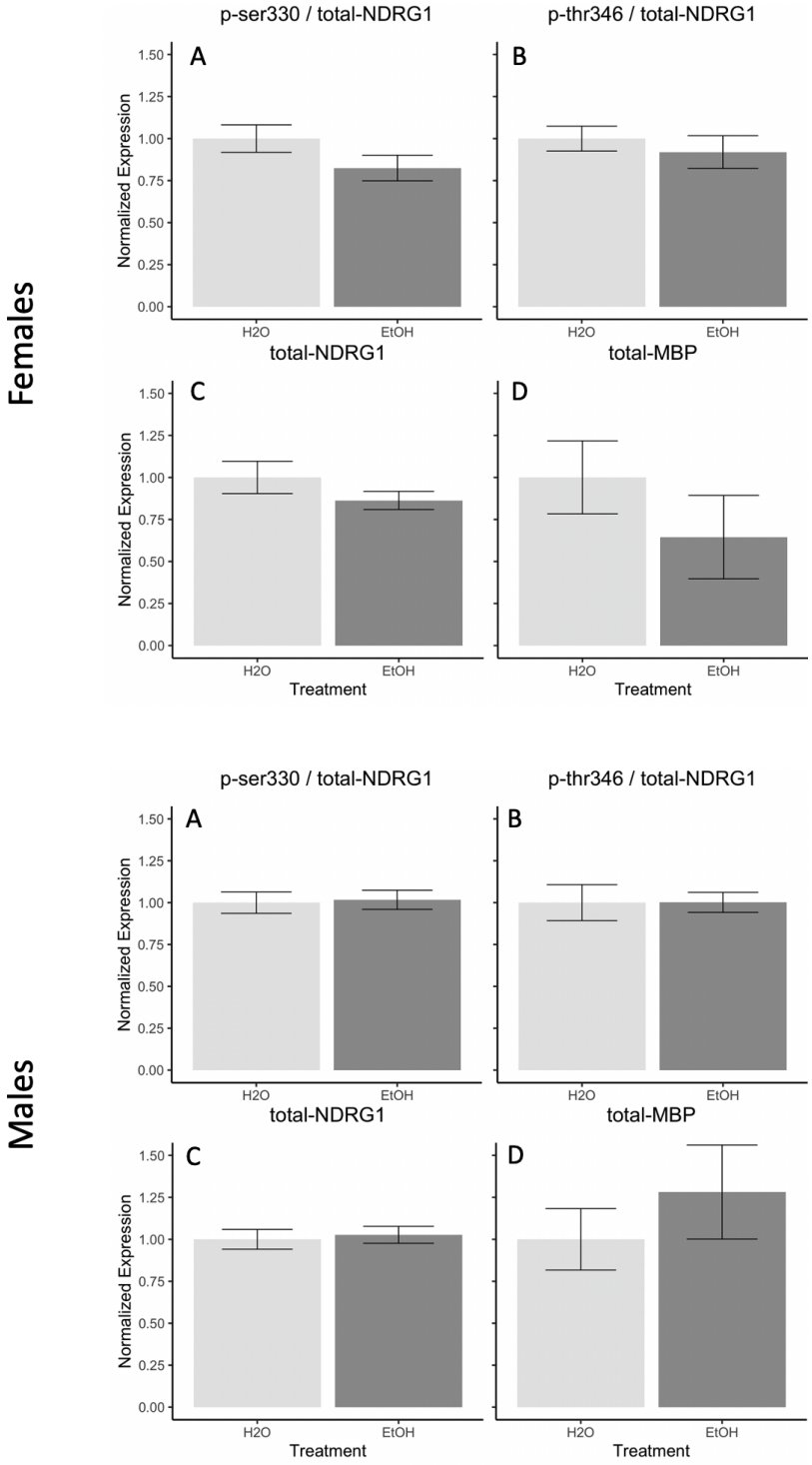

Figure 3.15: Western blots for NDRG1 and MBP following chronic ethanol exposure in female and male mice. Top panel: female results. Bottom panel: male results. No effects or interactions of sex or ethanol treatment were detected with a 2-way analysis. (A) Ser330-pNDRG1 (B) Thr346-pNDRG1 (C) total NDRG1 (D) total MBP

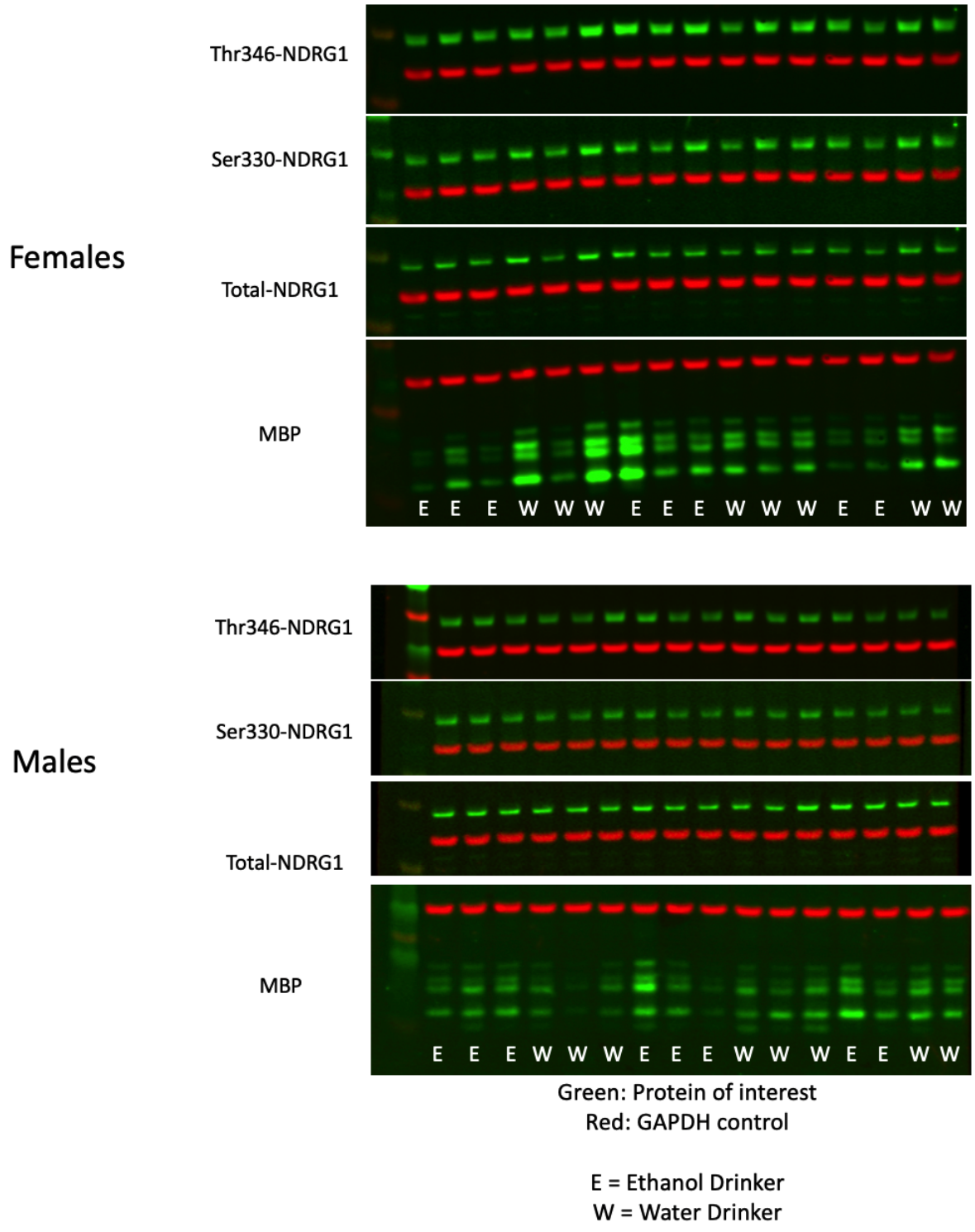

Figure 3.16: Scans of membranes stained for NDRG1 and MBP following chronic ethanol exposure in female and male mice. Top panel: female results. Bottom panel: male results. Stains and imaging of membranes are performed in the following order: (1) Thr346-pNDRG1, (2) Ser330-pNDRG1, (3) total NDRG1 (4) total MBP

3.4 Discussion and Conclusions

The prior literature and the findings presented here provide strong evidence that *Ndrg1* is only expressed in oligodendrocytes in the mPFC region of the cortex. We also found for the first time in brain tissue that the sub-cellular localization of Ser330-pNDRG1 and Thr346-pNDRG1 in CNS oligodendrocytes are consistent with that observed in many studied cancer cell lines (Park et al. 2018). This suggests that the mechanisms behind the phospho-protein distributions are conserved in many cell types that express *Ndrg1*. Our studies on ethanol regulation of *Ndrg1* showed that acute ethanol altered both the mRNA transcript abundance and the sub-cellular distribution of *Ndrg1*, while chronic ethanol consumption also altered *Ndrg1* transcript abundance.

Since we determined original lentiviral knockdown of *Ndrg1* that altered ethanol related phenotypes (see Figure 2.6) mainly appeared to infect *NeuN* expressing neurons (see Figure 3.2), it suggests one of the those possibilities: enough oligodendrocytes are in fact being infected by the lentiviral vector to drive the phenotype, *Ndrg1* expression in neurons was below the sensitivity of our IHC studies, or that the shRNA for *Ndrg1* has unexpected off-target effects in mPFC neruons. Some of our reported findings displayed sex specific effects, such as where the induction of *Ndrg1* after acute ethanol only occurred in the female mice (see Figure 3.6A). In many cases the reported phenotypes were observed in both sexes, such as the induction of *Ndrg1* transcript following 5 weeks of ethanol consumption (see Figure 3.13) or the decrease in total mPFC levels of Thr346-pNDRG1 that occurred following acute ethanol (see Figure 3.9). These results highlight the fundamental importance of utilizing both female and female mice to more fully understand the intricate dynamics of *Ndrg1* regulation in the context of ethanol exposure in the mPFC. While our acute ethanol immunofluorescence study only used male mice, a noted increase in the ratio of nuclear-to-cyostol signal of Ser330-pNDRG1 in mPFC oligodendrocytes was observed (see Figure 3.10). It would be very interesting to expand this particular study with both male and female mice.

While the induction of *Ndrg1* transcript did occur after 5 weeks of ethanol access, we did not see alterations myelin transcripts (see Figure 3.14). Furthermore, we did not detect any differences

total NDRG1, phospho-NDRG1, or MBP protein abundances (see Figure 3.15). Given that the Rhesus macaques were given 1 year of access to ethanol in the study before *Ndrg1* was strongly correlated with myelin gene expression (Bogenpohl et al. 2019), it is likely that any altered *Ndrg1* expression would become more correlated to myelin gene expression if the IEA study continued for 3-6 months rather than just 5 weeks. The lack of additional literature regarding *Ndrg1* and ethanol drinking in mouse models leaves us to speculate that additional time in our IEA protocol would induce further alteration of *Ndrg1* expression, leading to alterations in the expression of the myelin genes tested in this chapter.

On the whole, the results do demonstrate that *Ndrg1* is modulated by both acute and chronic ethanol exposures. We observed inductions of *Ndrg1* at the mRNA in in the acutely and chronically. We noted decreases in Thr346-pNDRG1 levels after acute ethanol, and we have evidence that a translocation of Ser330-pNDRG1 into the nucleus occurs following moderate doses of acute ethanol. It is also interesting that there is a decrease in the abundance of Thr346-pNDRG1 at the western blot level following the highest doses of ethanol, yet the Ser330-pNDRG1 form showed the alterations in cellular distribution following a moderate dose of ethanol. To followup, it would be interesting to perform acute ethanol IHC at higher doses of ethanol. Perhaps Thr346-pNDRG1 does not show translocation effects until the very high doses where total Thr346-pNDRG1 abundance is significantly decreased (Figure 3.9).

While the male mice in the acute dose response experiment did not display increased amounts of Ser330-pNDRG1 at any dose(see Figure 3.8A), there were significant alterations in the sub-cellular localization of Ser330-pNDRG1 in male mice following 2 g/kg of acute ethanol. These data combine to suggest that there is a translocation of Ser330-pNDRG1 to the nucleus from the cytosol rather than new phosphorylation of NDRG1 that resides in the nucleus. Conversely, the Thr346-pNDRG1 results suggest that the decreases in mPFC levels of Thr346-pNDRG1 following acute ethanol result in equal levels of dephosphorylation in both the nucleus and the cytosol.

It is curious that we saw a modest induction of *Ndrg1* mRNA transcript following chronic ethanol exposure, but there was no change in the amount of NDRG1 at the protein level. There

was also no change in relative amounts of either of the two phospho-NDRG1 forms. It could be possible that a compensatory mechanism prevents additional mRNA from being translated as repeated consumption of ethanol. Since we sacrificed the mice 24 hours after their final drinking session, it could also be that the phospho-NDRG1 staining patterns seen acutely are still occurring each day, but that the effect is completely washed out 24 hours later.

The data thus far suggests the myelin genes in the mPFC are not influenced by acute or chronic exposure to ethanol. But, it is not surprising that we found no changes in myelin gene expression following just 5 weeks of ethanol consumption. It would probably take a significantly longer drinking study that spanned months to detect perturbations in mPFC myelin gene expression from voluntary ethanol consumption.

Chapter 4

Genetic Effects of *Ndrg1* knockout in myelinating cells

4.1 Introduction

In Chapter 3, we confirmed that *Ndrg1* expression is limited to oligodendrocytes in the mPFC and likely the whole of the CNS. In multiple different models of ethanol exposure, we observed regulation of *Ndrg1* at the from the transcript levels down to the phosphorylation localization of the protein. In particular, the recently performed network analysis has identified *Ndrg1*as a hub gene in the low drinking line (Colville et al. 2017). However, the authors suggested that none of the hub genes, including *Ndrg1*, were directly linked to ethanol preference. As discussed in Chapter 2, additional unpublished data in our lab has determined that lentiviral mediated knockdown of *Ndrg1* expression in the mPFC of mice altered sensitivity-related phenotypes and reduced preference for higher concentrations of ethanol in a 3-bottle drinking paradigm (Wohlstenholme/Farris, in preparation). There is substantial data suggesting *Ndrg1* is both regulated by ethanol, and may modulate ethanol behaviors. We therefore wanted to devise a mouse model to better test how *Ndrg1* levels modulate ethanol behaviors by deleting the gene specifically in myelin producing cells, which we hypothesize are solely responsible for effects of *Ndrg1* deletion or mutation on ethanol behaviors.

The interactions between central nervous system *Ndrg1* and myelination are largely unanswered questions. In contrast, *Ndrg1*'s importance in peripheral myelination and nerve function is much more well understood and studied. As previously discussed, multiple studies show that mutant forms of *Ndrg1* result in CMT4D-like neuropathy in humans, dogs, and mice. As described in Chapter 2, linkage disequilibrium studies with human breast cancer patients that found SNPs in regulatory elements of *Ndrg1* correlated with severity of Paclitaxel-induced peripheral neuropathy

(PIPN) (Sundar et al. 2014). Follow-up work found that nerve levels of *Ndrg1* in excised breast tissue inversely correctly with the severity of PIPN that is experienced (Sundar et al. 2016). Peripheral neuropathy is one of the most common end-organ toxicities of chronic ethanol consumption (Chopra and Tiwari 2012). While there currently is no known link between *Ndrg1* expression levels and ethanol-induced neuropathy, our findings on ethanol regulation of *Ndrg1* and prior reports linking the gene to genetic or Paclitaxel-induced peripheral neuropathies, certainly support such a hypothesis. Thus, *Ndrg1* levels in the peripheral nerve could alter the likelihood for development of ethanol induced neuropathy symptoms.

A typical downside to constitutive deletion models is the potential for compensatory mechanisms that can form when a gene is deleted in all cells from the start of conception. These compensatory mechanisms can easily confound the results of such studies, making it unclear whether any observed biological alterations are driven by the lack of gene function or as a result of compensatory changes in the transcriptome from the gene knockout. To circumvent these shortcomings, we designed and bred a mouse line that allowed us to conditionally knockout *Ndrg1* in all myelinating cells. We utilized this mouse line to have fine control of the exact time point when *Ndrg1* is knocked out. Because the knockout is in all myelinating cells, we were able to devise experiments to investigate the effects of conditional deletion in the context of the CNS and the PNS.

First, we sought establish a more clear link between the effects of *Ndrg1* deletion on frontal cortex myelin, and ethanol related behaviors. We hypothesized that conditional knockout of *Ndrg1* in early adulthood would increase acute ethanol sensitivity, which would result in decreased consumption and preference, particularly for higher concentrations of ethanol. Second, we hypothesized that *Ndrg1* deletion would have deleterious peripheral effects that would worsen with time that it would increase sensitivity to toxic insults, such as Paclitaxel administration. In the end, we will conclude with an experiment that attempts to begin the investigation for the cross-play that occurs between these central and peripheral actions of *Ndrg1* deletion. In this final experiment, we hypothesized that repeated high doses of ethanol would induce signs of peripheral nerve dysfunction in a much shorter time scale than would be expected.

4.2 Materials and Methods

4.2.1 Drugs Used in Chapter

Tamoxifen (Sigma Aldrich, #T5648) was dissolved in Sunflower oil to a concentration of 20mg/mL using 30 minutes of sonication in a Branson ultrasonic cleaner at 37C. The tamoxifen solution was sterile filtered and stored at 4C in the dark for the duration of the study.

Ethanol solutions in the chapter dissolved 100% pharmacological grade ethanol into either tap water or normal saline (0.9%) to the indicated concentration.

Paclitaxel (Torcis, Bristol, United Kingdom) was dissolved in a 1:1:18 mixture of ethanol : Emulphor-620 (Rhone- Poulenc, Inc., Princeton, NJ) : distilled water.

4.2.2 Tamoxifen Treatment

Each mouse was injected with the prepared tamoxifen solution for a per weight dose of approximately 75 mg/kg, every 48 hours over a 5 day period (3 total injections). Validation of deletion was performed via immunohistochemistry and Western blotting. Utilizing the described mouse lines, myelinating cell specific deletion of *Ndrg1* was induced by delivering tamoxifen (Signa-Aldritch, T5648) dissolved in sunflower oil (Signa-Aldritch, S5007) by i.p injection. The injection volume of 100uL was used and all experimental mice began the tamoxifen regiment between 8 weeks and 16 weeks of age.

4.2.3 Tamoxifen Inducible Cre Recombinase Mouse Line

In order to drive Cre expression only in myelinating cells, we utilized a Tamoxifen inducible mouse line where Cre expression is driven by the promoter of the most abundant major myelin protein in the CNS, myelin proteolipid protein protein (PLP). This *Plp*-promoter tamoxifen inducible Cre mouse line (Plp-Cre-ERT, Jackson Laboratory #005975) based on a pure B6J-background. Expression of promoter driven Cre line as Proteolipid protein (PLP) is exclusive to myelinating cells.

Our floxed-*Ndrg1* mouse line was derived from ES cells of a B6N background that were acquired from the UC Davis Knockout Mouse Project KOMP Repository (https://www.komp.org,

#38738). These "knockout first" mice, as shown in Figure 4.1, were first bred to a *Flipase*-producing line to delete the entire region between the two FRT sites – leaving a modified gene with just two loxP sites that flank exons 6 and 7 (see Figure 4.1). The resulting mice were then crossed with a *Plp*-promoter tamoxifen inducible Cre mouse line (Plp-Cre-ERT, Jackson Laboratory #005975) based on a B6J-background. Following this cross, the resulting mouse line then backcrossed against the B6J reference for multiple generations for colony generation. Using this method, 3 *PCNdrg1*mouse lines were established after the 3rd, 4th, and 7th generation of backcrossing. The lines created from the 3rd the 7th generations was homozygous for the floxed-*Ndrg1* allele, generating a full knockdown of *Ndrg1* in *Plp* expressing cells. while the 4th generation was heterozygous for the floxed-*Ndrg1* allele. All mice were either heterozygous for the Cre expressing allele or *null/null*. The Cre-*null/null* are used as the experimental control since these mice is unable to produce the Cre gene product needed to delete the floxed-*Ndrg1* alleles.

For all experiments conducted in this chapter, mice of both genders were bred in the VCU Transgenic Core and delivered to our vivarium at 8 weeks of age. All mice brought into the vivarium remained group housed (N=3 or 5 per cage) on corn cob-based bedding in ventilated rack-mounted cages. The vivarium room was temperate controlled and maintained a 12 hour on-off light cycle. To begin every experiment in this chapter, all mice receive 1 week of tamoxifen injections in their original group housing, as described above. All ethanol drinking studies were performed in the OOV, while the control drinking studies were performed in free standing cages with Sani-Chip bedding. For all other behavioral studies, mice remained group housed (N=3 or 4 per cage) on corn cob-based bedding the vivarium for the duration of the studies. Habituation to acute intraperitoneal injections began at 10 weeks of age. The group housed mice were maintained in static rack-mounted cages with active air circulation. All cages were changed once a week for the duration of the studies. All mice had *ab libitum* access to standard chow (Teklad food pellets, #7912) and tap water. All procedures performed on the animals within our laboratory protocol, which was approved by the VCU Institutional Animal Care and Use Committee and

were compliant with the NIH Guide for the Care and Use of Laboratory Animals. Unless noted otherwise, all experiments within this chapter contained equal numbers off male and female mice.

Figure 4.1: Schematic of NDRG1 KO line genetic manipulations. Grey boxes indicate the location of the numbered exons. Figure adapted from KOMP website. During the first breeding step to *Flipase* expressing mice removes the lacZ expression reporter and the NEO cassette, along with the loxP site contained between the FRT sites. This generates a line of a line of floxed-*Ndrg1* with 2 loxP sites that flank exons 6 and 7 of *Ndrg1* (see red box on diagram)

4.2.4 Prepared Solutions

The injection solution for the IHC studies was either 0.9% normal saline or ethanol diluted to 20% (v/v) in normal saline. The drinking solutions provided for the IEA study were either tap water or ethanol diluted to 20% (v/v) in tap water. For the acute dose-response study, all ethanol solutions were diluted to 18% (v/v) in normal saline. The formaldehyde solution (4% w/v) was created by dissolving powdered para-formaldehyde into 0.9% saline using heat (65°C) and by adding 1N NaOH to bring the solution pH to 10. Once the para-formaldehyde powder was fully dissolved under the described conditions, the solution was cooled and 1N HCL acid was added drop wise to bring the formaldehyde solution to physiologic conditions (pH = 7.4).

4.2.5 Ethanol Exposure Models

The drinking data presented in this chapter was generated using a modified 3-bottle version of the Intermittent Ethanol Access (3B-IEA) that was described in Chapter 3 (see Figure 3.1). In brief, the main modifications to the protocol were the switch to 3-bottle choice and removal of the 2 hour binge drinking measurements. As described previously, he mice were given access to 3 bottles (water, 15%,30% (v/v) EtOH) for 24 hours every other day for 5 weeks of drinking. The drinking bottles were provided with access to the drinking bottles are provided within 30 minutes of the beginning of the 12 hour dark cycle.

4.2.6 Loss of Righting Reflex (LORR

Mice were given a high dose ethanol (3.8 g/kg, i.p.) injection of 20% ethanol v/v in normal saline. The mice were then rotated in a clear plastic tube every 5 seconds until they are unable to right themselves. At this point, time for LORR onset was recorded. Animals were then placed supine in wedge-shaped troughs and monitored until they are unable to right themselves within 30 seconds being rotated back onto their back. Once the mouse meets this criteria, duration for return of righting reflex was recorded. Animals with onset times greater than 4 minutes were considered LORR failures and removed the study. Statistical analysis was performed within-sex using unpaired Student's t-tests to compare Cre+ and Cre- animals. Sample sizes for the PCNdrg1 mice included 10 per group.

4.2.7 Western Blotting

For all western blot studies in this chapter, tissue homogenization was performed using 1X RIPA lysis buffer (50 mM Tris, 150 nM NaCl, 1% NP40, 5 mM EDTA, and 0.5% SDS). Microdissected tissue was homogenized using 2 to 4 short pulses with an ultrasonic sonicator over ice. To prevent protease and phospatase activity in the homogenized samples, 100X HALT Protease and Phosphatase Inhibitor Cocktail (ThermoFisher, #78440) was diluted to 1X in all RIPA buffers prior to homogenization. The homogenized solutions were partitioned into aliquots and immediately frozen at $-80°$C. Total protein concentration was determined by utilizing a Pierce BCA Protein Assay Kit (ThermoFisher, #23225), to allow for equal protein loading. Before performing an immunoblot, the proteins in the homogenized samples were denatured by heating the sample dissolved in NuPage Reducing Agent (ThermoFisher, NP0004) and 4X Protein Sample Loading Buffer (LiCor, #928-40004) in a heat block for 10 minutes at 70°C. Both the electrophoresis and the transfer steps were performed using the Xcell Surelock Mini Cell System (ThermoFisher, EI0001). The denatured protein samples were loaded into NuPage 4-12% Bis-Tris 17-well gels (ThermoFisher, NP0329BOX). Once equal amounts of total protein are loaded onto the gel, the proteins are first separated by size using electrophoresis at 100V. The size separated gels were then transferred onto Immobilon-FL PVDF Membrane (Millipore, IPFL00005) by applying 12V at 4C

for 16 hours using NuPage Transfer Buffer (ThermoFisher, NP0006). Following transfer, the membranes were briefly rinsed in milliQ water and were air dried for at least 1 hour to promote permanent binding of transferred proteins. The membranes were then re-hydrated using 100% methanol and rinsed with milliQ water. The membranes were then blocked in Licor Intercept Blocking Buffer (Licor, #927-60001) for 1 hour before the immediate application of primary antibodies, diluted in 1X blocking buffer containing .2% Tween-20. The primary antibodies were incubated overnight at 4C before the solution is washed 4 times with 1X TBS with 0.1% Tween-20. The membranes were then incubated with secondary antibodies were diluted into 1X blocking buffer with 0.2% Tween-20, and then applied for 1 hour at room temperature. The membranes were then washed 4 times with 1X TBS with 0.1% Tween-20, followed by rinses in 1X TBS to remove the residual tween-20 from the washes. The membranes were stored submerged in 1X TBS in the dark at 4C until ready to image. Imaging was performed using the Odyssey Infrared Imaging System (Licor, #9120). The experimental proteins were stained using the species-specific 800CW secondary at 1:30,000 dilution. The loading control and normalization protein, GAPDH, was stained using the 680LT anti-mouse antibody specific to mouse IgG1 at a concentration of 1:50,000. All scans were analyzed and quantified using the FiJi image analysis software package (ImageJ, NIH).

Because the membrane was thoroughly dried following transfer, the membranes can be safely stripped of the primary/secondary antibodies multiple times without noticeable protein loss. The stripping of the membranes was performed using 1X NewBlot IR Stripping Buffer (Licor, #928-40028) for 20 minutes with vigorous shaking, followed by multiple wash steps. A new aliquot of the secondary antibody staining solution is then incubated on the stripped membrane and re-imaged to determine efficacy of the stripping of the signal. Using this methodology, we were able to image multiple targets on a single membrane, including: anti-NDRG1, anti-MBP, and finally with anti-PLP.

For all protein studies presented in this chapter, tissue homogenization was performed in 1X RIPA lysis buffer. To prevent protease and phospatase activity in the homogenized samples, 100X HALT inhibitor (Thermo Fisher) was diluted to 1X in all RIPA buffers prior to homogenization.

For the frontal cortex studies, the frontal lobe dissection tissue was first homogenized with a Polytron blade-type homogenizer (Brinkmann, PT2000) homogenizer, and then followed by 2-3 short bursts with the sonication probe. For the sciatic nerve studies, 2 pooled sections of sciatic nerve from the left and the right hind leg are homogenized in a Beadbug6 homogenizer using 1.5mm stainless steel beads. In both cases, the remaining tissue debris is spun down at 10,000g for 10minutes and the resulting supernatant is extracted.

In all cases, the homogenized solutions were aliquoted and immediately frozen at -80C. Before performing an immunoblot, the proteins in the homogenized samples were denatured by heating the sample dissolved in NuPage Reducing Agent (Thermo Fisher) and 4X Protein Sample Loading Buffer (LiCor, Lincolin, NE) in a heat block for 10 minutes at 70C. Both the electrophoresis and the transfer steps were performed using the Xcell Surelock Mini Cell kit (Thermo Fisher). The denatured protein samples were loaded into NuPage 4-12% Bis-Tris 17-well gels (Thermo Fishger). Once loaded, the proteins are first separated by size using electrophoresis at 100V while submersed in 1X LiCor MES Running Buffer (LiCor). The separated gels were then transferred onto Immbolin FL PVDF membrane using 12V at 4C for 16 hours using NuPage Transfer Buffer (Thermo FIsher). Following transfer, the membranes were briefly rinsed in milliQ water and were air dried for at least 1 hour to promote permanent binding of transferred proteins. The membranes are then rehydrated using 100% methanol and rinsed with milliQ water. The membranes were then blocked in Licor Intercept Blocking Buffer (Licor) for 1 hour before the immediate application of primary antibodies, diluted in 1X blocking buffer containing .2% Tween-20. The primary antibodies were incubated overnight at 4C before the solution is washed 4 times with 1X TBS with 0.1% Tween-20. The membranes were then incubated with secondary antibodies were diluted into 1X blocking buffer with 0.2% Tween-20, and then applied for 1 hour at room temperature. The membranes were then washed 4 times with 1X TBS with 0.1% Tween-20, followed by rinses in 1X TBS to remove the residual tween-20 from the washes. The membranes were stored submerged in 1X TBS in the dark at 4C until ready to image. Imaging was performed using the Licor Odessy classic scanner (Licor). The experimental proteins were stained using the species-specific 800CW

secondary at 1:30,000 dilution. The loading control / normalization protein was stained using the 680LT anti-mouse antibody specific to mouse IgG1 at a concentration of 1:50,000. All membranes were probed with 3 different antibodies in the following order: anti-NDRG1, anti-MBP, and finally with anti-PLP. Between each probing, the membranes were stripped of primary and secondary antibodies using LiCor NewBlot IR Stripping Buffer (#92840028)) All scans were analyzed and quantified using the FiJi image analysis software package(ImageJ, NIH).

4.2.8 Immunohistochemistry

All mice were perfused with transcardial administration of a 4% formaldehyde solution (in 1X PBS)while anesthetized with high doses of isoflurane. The mice were first flushed with pure 1X PBS to remove the remaining blood before the 4% formaldehyde was injected. The perfused brains were then removed from the skull and transferred to a vial of fresh 4% formaldehyde for an overnight post-fixation step. The brains are then placed into a 30% sucrose solution dissolved in 1X PBS for dehydration of the remaining water. Once the brains were fully dehydrated and sunk to the bottom of the sugar solution, they were snap frozen in a vial of isopentane that was cooled to -80C using dry ice and then stored at -80C until they are ready to proceed. The frozen brains are then cut into 20um thick coronal sections using a Leica CM3050 cryostat (Leica Biosystmes, Wetzlar, Germany). The sliced sections stored as free-floating sections that were submerged in a 1X PBS solution containing 0.02% sodium azide to preserve and prevent bacterial growth. The slices were stored in order along the wells of a 24-well plate.

Prior to staining of the coronal slices, the antigens that are masked by protein crosslinking are recovered by placing the slices in Citrate Acid Buffer (pH = 6.0) and heating at 80C for 20 minutes with shaking, followed by a 30 minute cool-down step at room temperature with vigorous shaking. Following this antigen retrieval process, the sections are then permeabilized and blocked in 10% goat serum with 0.2% Triton X100 for 30 minutes are room temperature. The sections were then incubated overnight at 4C with primary antibodies that are dissolved in 1XPBS with 0.2% Triton-X with gentle rocking. The slices are then washed 4 times in an abundance of 1X PBS for 5 minutes with vigorous shaking. Following the fourth wash, the slices are then incubated with secondary

antibodies dissolved in 1X PBS with 0.2% TritonX for 1 hour at room temperature with gentle rocking. Following the secondary incubation, the slices were washed 4 times in an excess of 1X PBS for 5 minutes with vigorous shaking.

These stained slices are then mounted and dried onto SuperFrost Plus Gold Slides (ThermoFisher). The dried slices are then coated with Vibrance anti-fade mounting media (VectaShield, H1800) and sealed under a .17mm thickness glass cover slip. The mounting media is dried and hardened overnight at room temperature in the dark. Following the curing of the mounting media, the edges are sealed with clear nail polish for long term storage either at 4C or room temperature, per the manufacturer instructions.

4.2.9 Tastant Alteration Studies

A single cohort of ethanol-naive PCNdrg1 mice was utilized for both tastant studies. The mice were first given access to continuous free access to two bottles: one containing tap water and the other containing water with quinine (0.05 mM concentration) for 4 days. After the 4th day, the mice were then giving access to another two bottles: one containing tap water and the other containing saccharin (2 mM, 0.037% w/v). Volume consumed readings were taken every 24 hours. When the bottles are measured and refilled, the placement of the bottles on the cage top is alternated to prevent the development of cage side preference.

4.2.10 Ethanol Pharmacokinetics

Alterations in ethanol metabolism were tested using a large dose bolus of acute ethanol. The mice were dosed with 4 g/kg of 20% (v/v) ethanol in 0.9% normal saline. Following the injections, retro-orbital bleeds were collected in lavender topped EDTA-treated BD collection tubes (Becton Dickson 365974) with glass capillaries. These bleeds were carried out at 15, 30, 60, and 90 minutes post injection. The collected blood was spun down in a refrigerated centrifuge at 1500g for 15 minutes. The plasma was extracted from the resulting supernatnate and stored at -80C until quantification. The measurement of the blood ethanol content of the plasma was performed using an Analox AM1 alcohol analyzer (Analox Instruments Ltd, UK).

4.2.11 Light-Dark (LD) Box Testing

To begin, the mice were habituated to the testing room for 1 hour prior to the testing. Following habituation, the mice were individually placed locomotor boxes with the dark side insert installed (Med Associates, ENV-515). This insert occupies exactly half of the total box area and it contains a small hole in the middle to allow free passage between the 'dark' side and the 'light' side. A higher output 180mA stimulation bulb is used to produce a brighter open chamber that the mice perceive as a greater risk of exposure to potential predators, which produces a higher level of anxiety in the 'light' side. The mice were placed and released into the testing field by placing the mouse such that head of the mouse was positioned just inside the entry to the 'dark' side while the rest of the body was placed into the 'light' side of the chamber. The mice were then allowed to freely roam the testing area for a single 10-minute trial, which is split into two 5-minute bins. The Med Associates software utilized 16 infrared beam breaks to track the time spent and the distance traveled in each side of the testing area. Percent time spent and in the dark and percent time spent in the light were calculated and total locomotor distance traveled was documented. The analysis only considered first 5 minute bin and Student's t-testing to compare the Cre+ knockout mice against the Cre- control mice.

4.2.12 Antibodies and Primers

Antibodies utilized for immunofluorescence studies:

Primary: anti-NDRG1 (1:500, Abcam, ab63989), anti-CNP [11-5B] (1:400, Abcam, ab6319), anti-NeuN Antibody [A60] (1:500, Millipore, MAB377).

Secondary: AlexaFluor 488 anti-mouse IgG1 (1:1000, ThermoFisher, A-2112), AlexaFluor 568 anti-rabbit (1:500, ThermoFisher, A-11036)

Antibodies utilized for Western blotting studies:

Primary: anti-NDRG1 (1:1000, Abcam, ab124689), anti-MBP (1:1000, Abcam, ab7349), anti-GAPDH [6C5] (1:7500,Millipore, MAB374).

Secondary: 680LT Mouse IgG1 (1:50000; LiCor #926-68050), 800CW Rabbit (1:30000; LiCor #926-32211), 800CW Rat (1:30000; LiCor #926-32219), 800CW Mouse IgG2a (1:30000; LiCor #926-32351)

4.2.13 Microscopy

All confocal images were taken with the LSM710 using a 63X oil objective, at a scan area and an airy unit equal to 1. Additional validation of cell-type localization images were performed on a Zeiss IM inverted microscope using a 40X water objective or 10X air objective and a Retiga 2000R CCD camera (Qimaging, USA).

4.2.14 Mechanical Sensitivity

30 minutes prior to testing, the mice were placed in a Plexiglas cage with mesh metal flooring and allowed to acclimate. A series of von Frey filaments (Stoelting, Wood Dale, IL) with logarithmically incremental stiffness ranging from 2.83 to 5.88 grams of force. The filaments were applied to the directly onto the paw and pushed until the filament bends and then held for 2-3 seconds. If there is no paw withdrawal response to the initially selected filament, a thicker filament corresponding was then applied. If there was a paw withdrawal event, the next weaker stimulus filament was then tested. The stimulation of the same intensity was applied 5 times to the hind paw at intervals of a few seconds. The mechanical threshold was recorded as Log10 of [force in (mg)] for the force of the Von Frey filament that elicited an animal reaction, such as: paw withdrawal, licking or shaking. This assay was performed by Dr. Wisam Toma of the laboratory of Dr. Imad Damaj.

4.2.15 Thermal Sensitivity

Testing for thermal sensitivities utilized the acetone test and the tail flick assay. In brief, the acetone test involves squirting 20uL of acetone onto the left and right hind paws. The number of seconds spent licking the paws over the course of 1 minute. The average of the left and the right paws are then taken for the comparison. The tail flick assay involved placing the tail of a mouse in

a water bath at 50C. The time until the mouse 'flicks' its tail out of the heated water is recorded in seconds. This assay was performed by Dr. Wisam Toma of the laboratory of Dr. Imad Damaj.

4.2.16 Nerve Conduction Velocity Testing

Nerve conduction velocity (NCV) and sensory nerve action potential amplitudes (SNAP) of the caudal nerve were recorded with a PowerLab 4/35 electromyography system (ADInstruments, Inc, CO, USA). This test measures amplitude and latency of the evoked response, which is used to calculate nerve conduction velocity. Anesthesia was carried out using a VetFlo anesthesia machine, (KentScientific, CT, USA) induced in a chamber with 4% isoflurane carried in oxygen followed by 2.5% isoflurane by nose cone for maintenance during the procedure. A couple of needle recording electrodes (cathode and anode) were inserted 5 mm distal from the base of the tail, and the stimulating electrodes 5.0 cm apart from the recording points (distance measured from cathode to cathode) with a ground electrode in-between the stimulation and recording electrodes. The nerve was stimulated with single square-wave pulses of 0.1 ms duration at 7 mA, and a repeat rate of 1Hz. The neurophysiological measures were conducted under standard conditions in a temperature-controlled room. NCV was calculated by dividing the distance between the recording and stimulating electrodes (0.05 m) by the latency between the stimulus artifact and the onset of the first peak of the elicited action potential latency of the sensory nerve action potential. NCV was measured in m/s, and SNAP in uV. This assay was performed by Dr. Wisam Toma of the laboratory of Dr. Imad Damaj.

4.2.17 Rotarod Testing

The mice were habituated the the testing room for 1 hour prior to the start of the experiment. The testing was performed on Rotarod motor performance testing apparatus. All testing utilized the Fixed Speed Rotarod Rate (FSRR) protocol. The FSRR protocol involves placing the mice onto the spinning rod while it was rotating at 10 RPM. Once the mouse has been released, the test begins. The software records the time until the mouse either falls off of the rotor or the mouse clings to the rotor and is completely rotated in a circle. The time (in seconds) at which either of these two stop points occurs is the recorded measure. The trial will run for up to 300 seconds, at

this point the trial is complete and the recorded measure will be 300 seconds. On all testing days, each mouse was tested in 3 separate trials.

4.2.18 Paclitaxel Sensitivity Study

Prior to delivery of tamoxifen to induce KO of *Ndrg1*, mice were measured for baseline mechanical sensitivity. Following this baseline, the mice were split into one of the following treatment groups: Cre+/Paclitaxel, Cre+/Vehicle, Cre-/Paclitaxel, Cre-/Vehicle. Starting the following day, all mice began to receive the standard dosing of Tamoxifen to induce Cre recombinase in the Cre+ animals (75mg/kg, i.p, every other day for 5 days (3 total treatments)). After the day after the 3rd and final Tamoxifen treatment, the mice were again tested with Von Frey Filaments. Following the second baseline, the Paclitaxel treatment regiment was started. In this protocol, a low dose of Paclitaxel (1 mg/kg, i.p.) is administered every other day for a total of 4 treatments. The day after the 2nd Paclitaxel injection, the mechanical sensitivity of the mice was recorded again. Two days after the final injection, the mice were again testing for mechanical sensitivity using the Von Frey filaments. The mechanical sensitivity testing then continued once a week for one month.

4.2.19 High Dose Ethanol Neuropathy Study

Similar in design to the Paclitaxel study, prior to delivery of tamoxifen to induce KO of *Ndrg1*, mice were measured for baseline mechanical sensitivity. Following this baseline, the mice were split into one of the following treatment groups: Cre+/Ethanol, Cre+/Vehicle, Cre-/Ethanol, Cre-/Vehicle. Starting the following day, all mice began to receive the standard dosing of Tamoxifen to induce Cre recombinase in the Cre+ animals (75mg/kg, i.p., every other day for 5 days (3 total treatments)). After the day after the 3rd and final Tamoxifen treatment, the mice were again tested with Von Frey Filaments. Following the second baseline, the ethanol treatment regiment was started. In this protocol, a high dose of ethanol (3.8 g/kg, i.p.) is administered every other day for a total of 4 treatments. The day after the 2nd ethanol injection, the mechanical sensitivity of the mice was recorded again. Two days after the final injection, the mice were again tested for mechanical sensitivity using the Von Frey filaments. The mechanical sensitivity testing then continued once a week for one month.

4.3 Results

4.3.1 Validation of the *Ndrg1* Deletion in Myelinating Cells

By 4 weeks post-Tamoxifen administration, there a robust knockout of *Ndrg1* in the mPFC. We observed a very dramatic reduction in immunosignal for NDRG1 in both male and female Cre+ PCNdrg1 mice (see Figure 4.2). Furthermore, when *Ndrg1* is co-stained with oligodendrocyte and myelin process marker, *CNPase*, we confirm that the loss of both cellular and myelin process NDRG1 by 6 weeks post-Tamoxifen (see Figure 4.3). The 'speckling' pattern of NDRG1 staining that is observed in the KO mice (see Figure 4.3C) is non-specific staining. We suggest that the polyclonal anti-NDRG1 antibody (ab639890) utilized for IHC in this chapter was likely responsible, as this 'speckling' staining pattern was not observed in the IHC presented in Chapter 3 that was performed with the monoclonal anti-NDRG1 (ab124689) (see Figure 3.3).

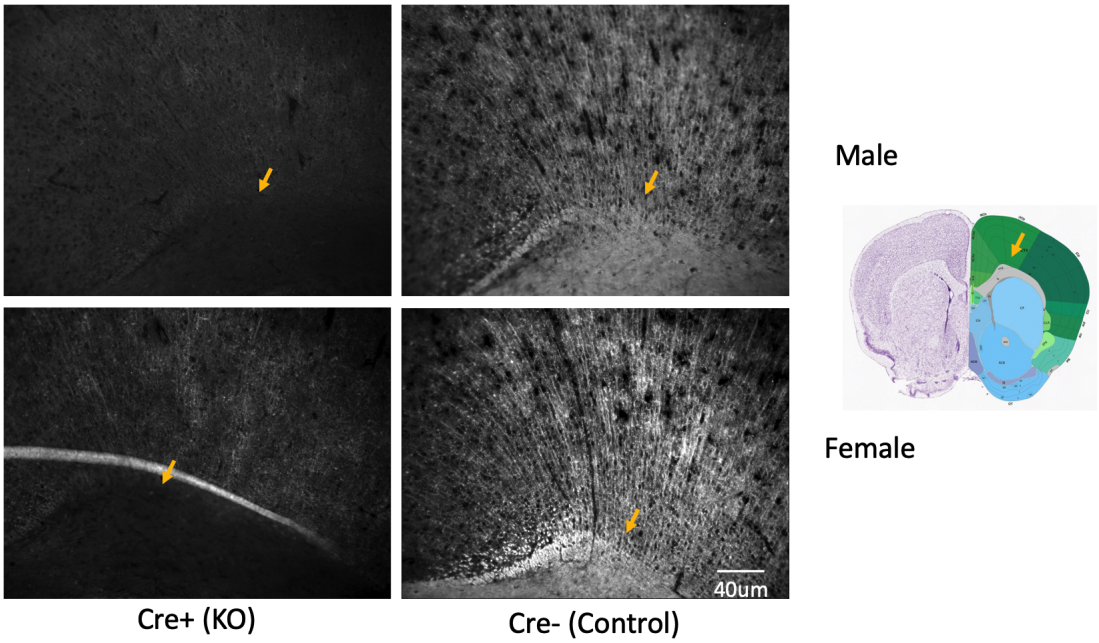

Figure 4.2: IHC validation of KO in male and female PCNdrg1 mice, 4 weeks post-Tamoxifen. Orange arrows indicates the horn of the corpus callosum, as shown on the rightmost image. All slices received the same IHC staining protocol. All images were taken at the same microscope illumination intensity and camera exposure time on a 10X air objective with a Zeiss IM micrscope.

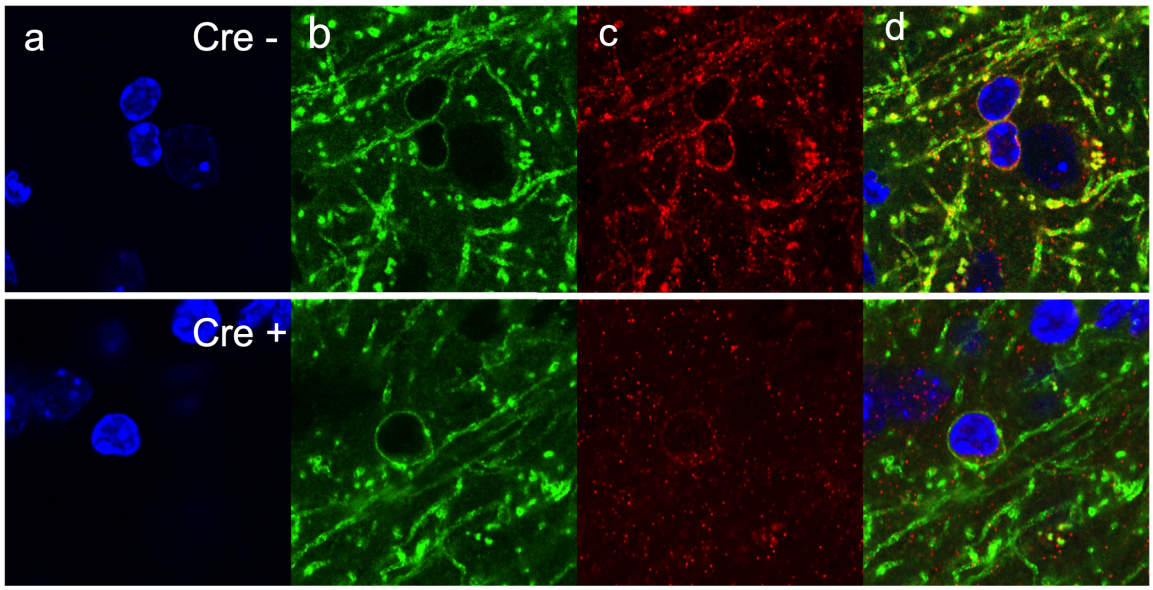

Figure 4.3: Confocal validation of KO of NDRG1 in oligodendrocytes and myelin PCNdrg1 mice, male mouse 6 weeks post-Tamoxifen. 63X microscopy image of oligodendrocytes and myelin processes in the mPFC (top shows Cre- control, bottom shows Cre+ knockout): a) DAPI b) CNPase c) NDRG1 d) Composite overlay

Western blotting of the frontal cortex dissections at both 1 month and 6 months post-Tamoxifen revealed a dramatic reduction of total NDRG1 protein levels. The 1 month and the 6 month data were analyzed separately and initial analyses were conducted with a 2-way ANOVA model that considered genotype and sex. The sciatic nerve tissue and the frontal cortex tissue were harvested from the group of experimental mice. There were 20 total mice utilized in the presented study (N=5 per sex / per genotype).

In the frontal cortex, at one month post KO, the 2-way ANOVA revealed a main effect of genotype (F = 231.0, P = 6.27E-11), but no effect or interaction with sex was present (F = 0.028, P = .869). Thus, we collapsed the sexes and performed a simple Student's t-test. At one month, there was a 90% reduction in total *Ndrg1* signal (T = 16.093, P = 2.15E-08). Furthermore, we found that both PLP and MBP (T = 4.007, P = 0.0018) levels were significantly downregulated in the frontal cortex 1 month following deletion (see Figure 4.4)

At 6 months post KO in the frontal cortex, the 2-way ANOVA revealed a main effect of genotype (F = 39.775, P = 1.04E-05), but no effect or interaction with sex was present (F = 0.237,

P = .633). Thus, we collapsed the sexes and performed a simple Student's t-test. There was a 65% reduction in immunosignal (T = 6.592, P = 9.34E-06) at the 6 month time point. While a very significant reduction was maintained for at least 6 months, there might to be some recovery of NDRG1 signal in oligodendrocytes at 6 months post-tamoxifen compared to just 1 month (see Figure 4.4). Likewise, we found that MBP levels (T = 2.598, P = 0.0184) in the frontal cortex were still decreased at 6 months post KO, while the PLP levels (T = 0.566, P = 0.580) had recovered to normal levels by the 6-month time point (see Figure 4.4).

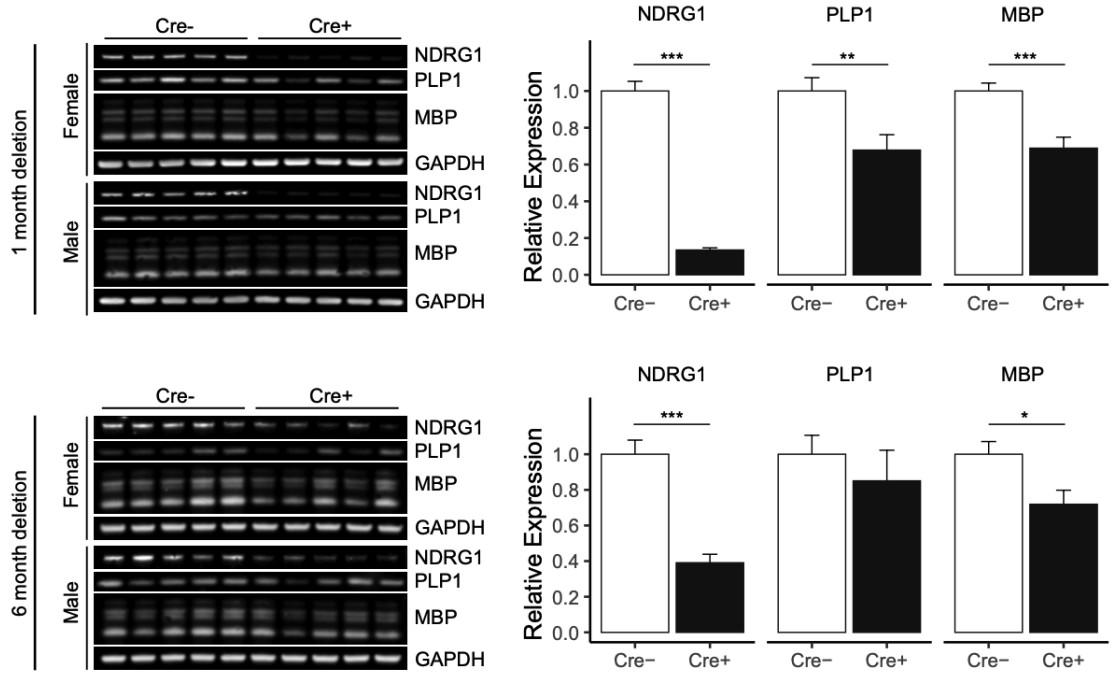

Figure 4.4: Western blot analysis of frontal lobes after conditional deletion of *Ndrg1* in oligodendrocytes at 1 month (top) and 6 month (bottom) time points for NDRG1, MBP, and PLP1. Panels on right display mean expression for each target was normalized to GAPDH and to the wild type controls (error bars = SE) (bottom). N = 5 per genotype / per sex. Student's t-test were used for statistical analysis. (*, P < 0.05; **, P < 0.005 ; ***, p < 0.0001)

Similarly, western blotting of the sciatic nerve dissections at both 1 month and 6 months post-Tamoxifen revealed a dramatic reduction of total NDRG1 protein levels (see Figure 4.5). At one month, the there was a 50% reduction (T = 7.038. P = 5.167E-06) in total *Ndrg1* signal, while there was still a 40% reduction (T = 3.328, P = 0.00574) in immunosignal at the 6 month time-point. While a very significant reduction was maintained for at least 6 months, but there might

to be some recovery of NDRG1 signal at 6 months post-tamoxifen compared to just 1 month (see Figure 4.5). Likewise, we found no different in total levels at either 1 or 6 months post-Tamoxifen, but there is a trend towards decreased levels of total MBP (T = 1.309, P = 0.209) in the sciatic nerve as more time passes post-Tamoxifen (see Figure 4.5).

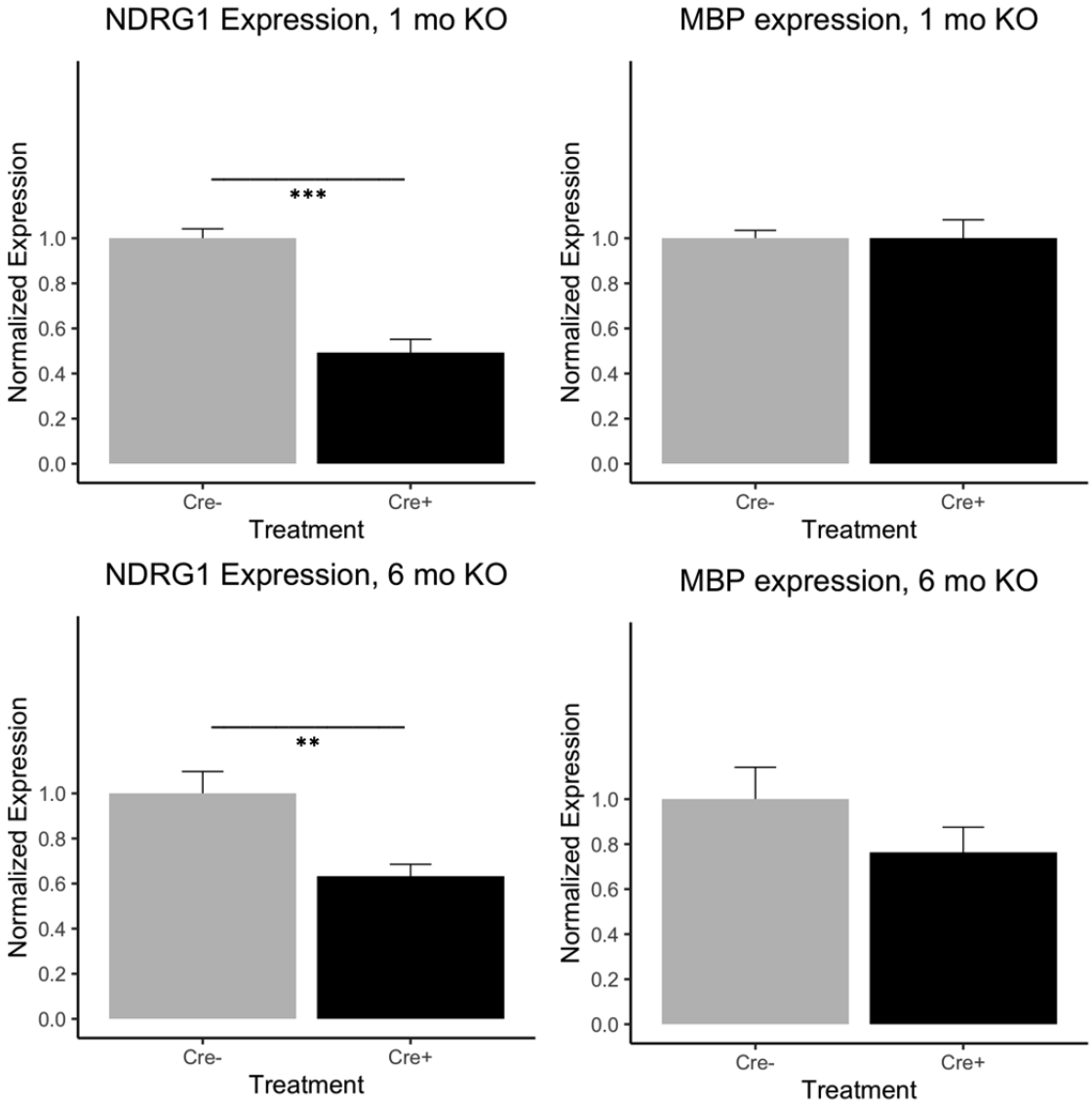

Figure 4.5: Western blot validation of KO of NDRG1 and MBP levels in peripheral nerve tissue. Left side of panel shows the total NDRG1 signal at 1 month (top) and 6 months (bottom) post-Tamoxifen. The total signal for MBP is displayed in the same fashion on the right side of the panel. Student's t-test (** $P < 0.01$)

4.4 Control Experiments

We ran multiple control studies to characterize whether tamoxifen-regulated *Ndrg1* deletion caused any changes in basal locomotor or anxiety-like behaviors, ethanol pharmacokinetics or tastant preferences, since such confounders could obscure interpretation of results for ethanol behavioral responses. For these experiments, we utilized a single cohort of male and female mice (N = 5 per sex / per genotype). Statistical analysis was performed with Student's t-test for comparison between the knockout and control genotypes. First, we found no differences in anxiety-like behavior (time in the light: T = 0.35, P = 0.704; time in the dark: T = -0.358, P = 0.724) or total locomotor activity in the light-dark (LD) box (see Figure 4.6A, B, C). It is notable here is the beginning of a trend towards decreased total locomotor distance traveled (T = 1.837, P = 0.0842)in the knockout (Cre+) mice, but there was no significant differences between the knockout and the control mice at 2 months post-Tamoxifen. Next, we observed no alteration in perception of bitter (quinine) and sweet (saccharin) tastants between the KO and control mice. Finally, we found no differences in the pharmacokinetics of ethanol metabolism (F = 0.035, P = 0.873) following a high dose of ethanol (see Figure 4.6).

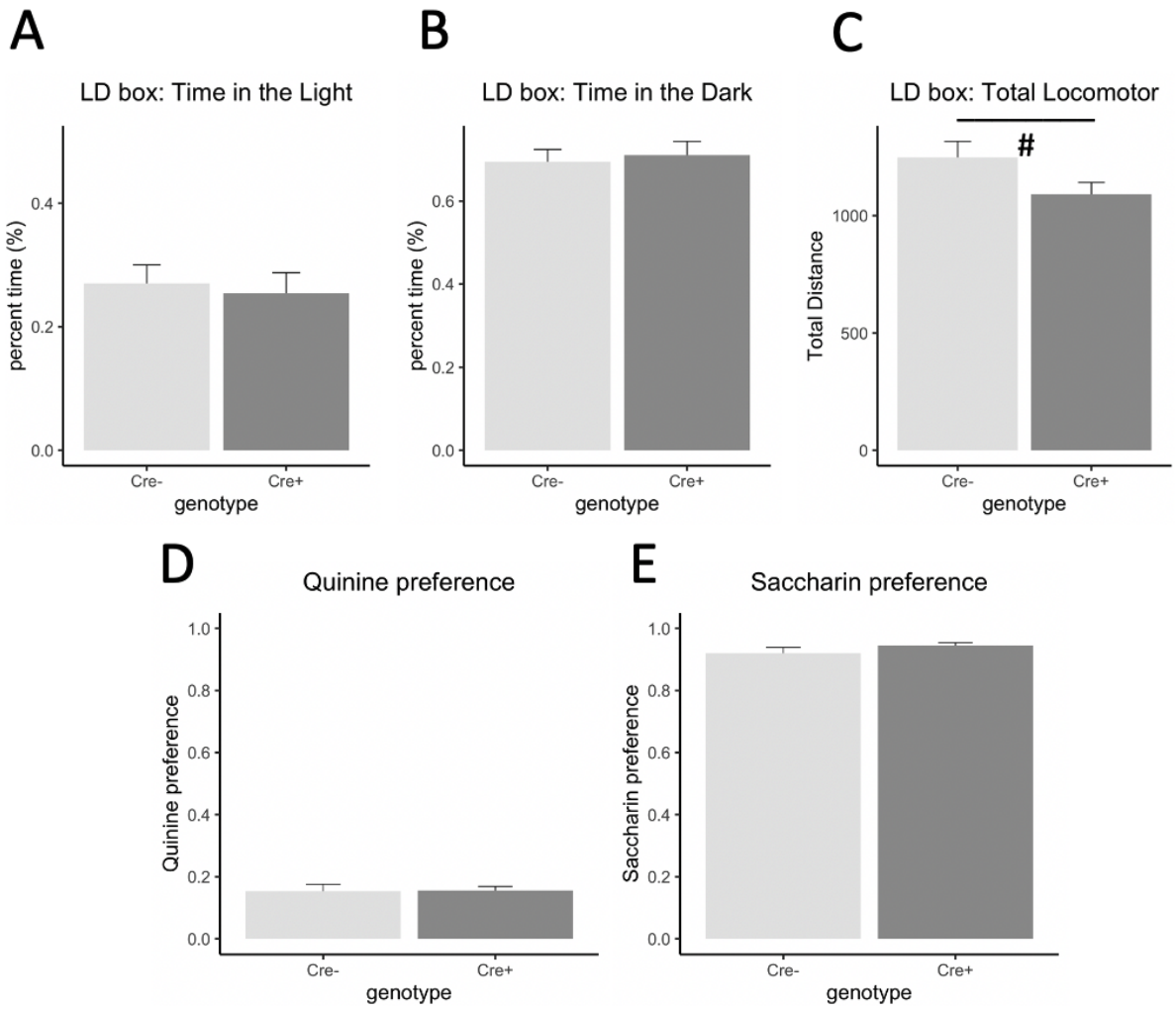

Figure 4.6: Control experiments for PCNdrg1 KO mouse line. (A) Time spent in the light side of the LD chamber (B) Time spent in the dark side of the LD chamber (C) Total locomotor activity recorded over the sesssion (D) Preference for quinine adulterated water relative to plain tap water (E) Preference for saccharin sweetened water to plain tap water. # denotes a suggestive P-value < 0.1.

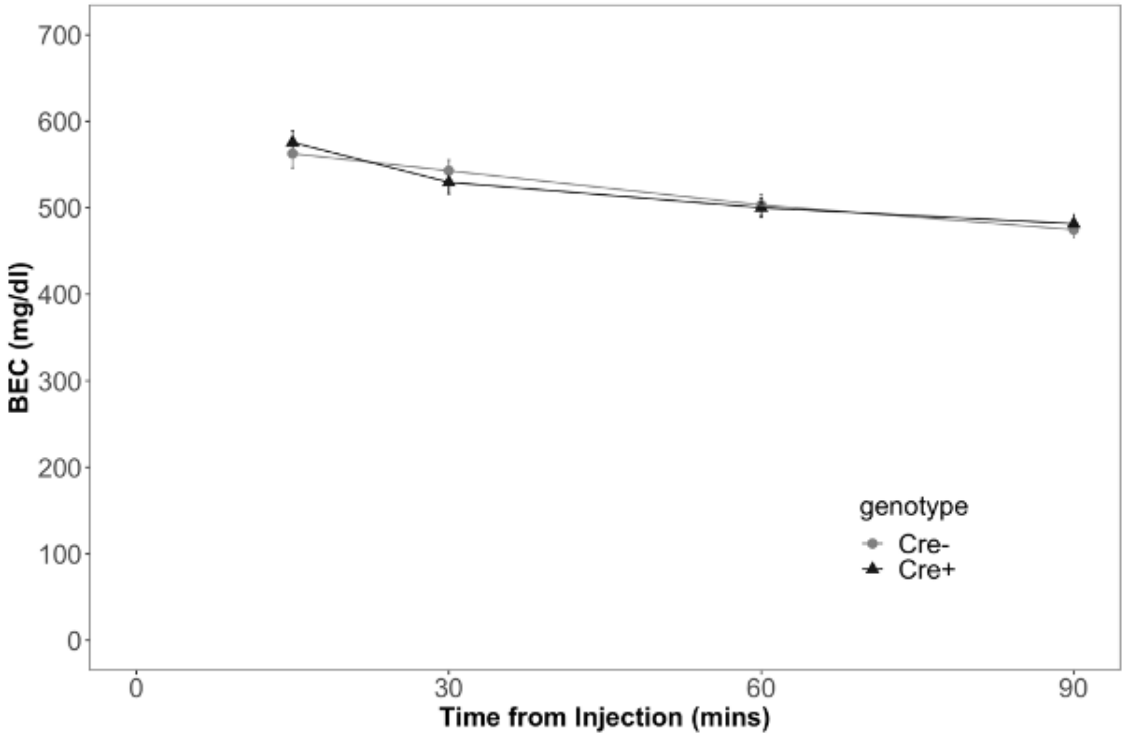

Figure 4.7: Ethanol pharmacokinetics: BEC time course following 4 g/kg of acute ethanol. Statistical analysis performed using linear mixed models. BEC was recorded at the following time points post-injection: 15, 30, 60, and 90 minutes. 2-way linear mixed model statistics were used.

4.5 Deletion of *Ndrg1* in Myelinating Cells Alters Ethanol-Related Behaviors

We evaluated the voluntary ethanol consumption of ethanol when presented with a 3-bottle choice drinking study for 5 total weeks. The study was well powered by combined two cohorts of PCNdrg1 mice (N = 10 - 16 per sex / per genotype). First, a simple Student's t-test revealed a very significant difference between the amount of ethanol consumed in female and male mice collapsed across genotypes. As expected, we found that the females, on average, consumed 37% ($P < 0.001$) more total ethanol than males per drinking day Figure 4.8A). Due to this sex effect, the following drinking related statistics and findings with regard to the *Ndrg1* deletion will consider sex separately. We found no significant alterations in average daily intake of ethanol across the entire 5 week study, but there was a suggestion of an increase total ethanol consumption ($P = 0.054$) in the male Cre+ mice (see Figure 4.8B).

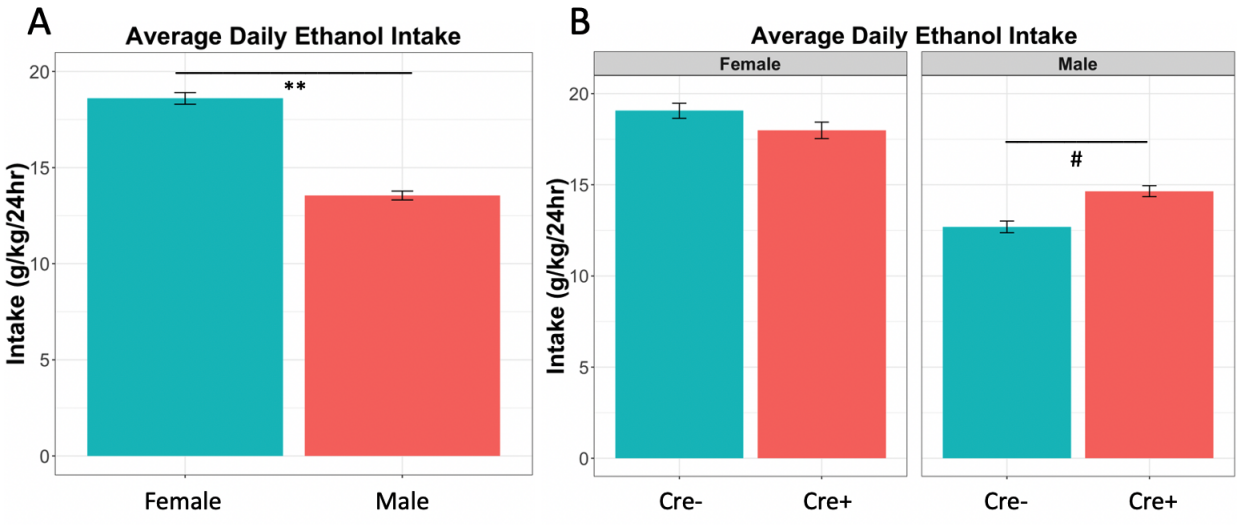

Figure 4.8: Comparison of male and female average daily ethanol (g/kg) in 3-bottle choice drinking. (A) Comparison of daily average intake all male and female mice, without considering genotype. (B) Comparison of daily average intake in Cre+ KO mice and Cre- control mice, separated by sex. Student's t-test (# $P < 0.1$; ** $P < 0.001$)

Further 2-way ANOVA analysis considered the average daily intake by bottle (15% vs. 30% consumed) and genotype for each sex separately. This statistical model revealed both male and female sex-specific alterations in drinking (see Figure 4.9A). Following post-hoc comparison with Tukey's HSD, we observed a significant decrease in 30% consumption in female Cre+ knockout mice ($P < 0.05$) relative to control, while an intake in 15% preference was observed in the male Cre+ knockout mice ($P < 0.05$) relative to control (see Figure 4.9A).

To analyze the alterations in drinking behavior that occur over the course of the 5 week drinking study, we utilized linear mixed model statistics. Here, we investigated total ethanol preference at the weekly level using a 3-way mixed model that considers the weekly preference averages, the genotype, and the sex of the mice. The individual mice are set as the error parameter, since each mouse is measured at every reading throughout the study. Our 3-way mixed model revealed a significant main effect of genotype ($F=6.701$, $P = 0.00964$) and week ($F = 185.074$, $P < 2.2E\text{-}16$), with no other effects or interactions. Therefore, we collapsed the sexes and further analyzed the data with a 2-way mixed model the only considered the week and the genotype. Here we found

that the Cre+ knockout mice maintained a significantly higher preference (F = 6.117, P = 0.0134) for ethanol over the duration of the 5 week study (see Figure 4.9B).

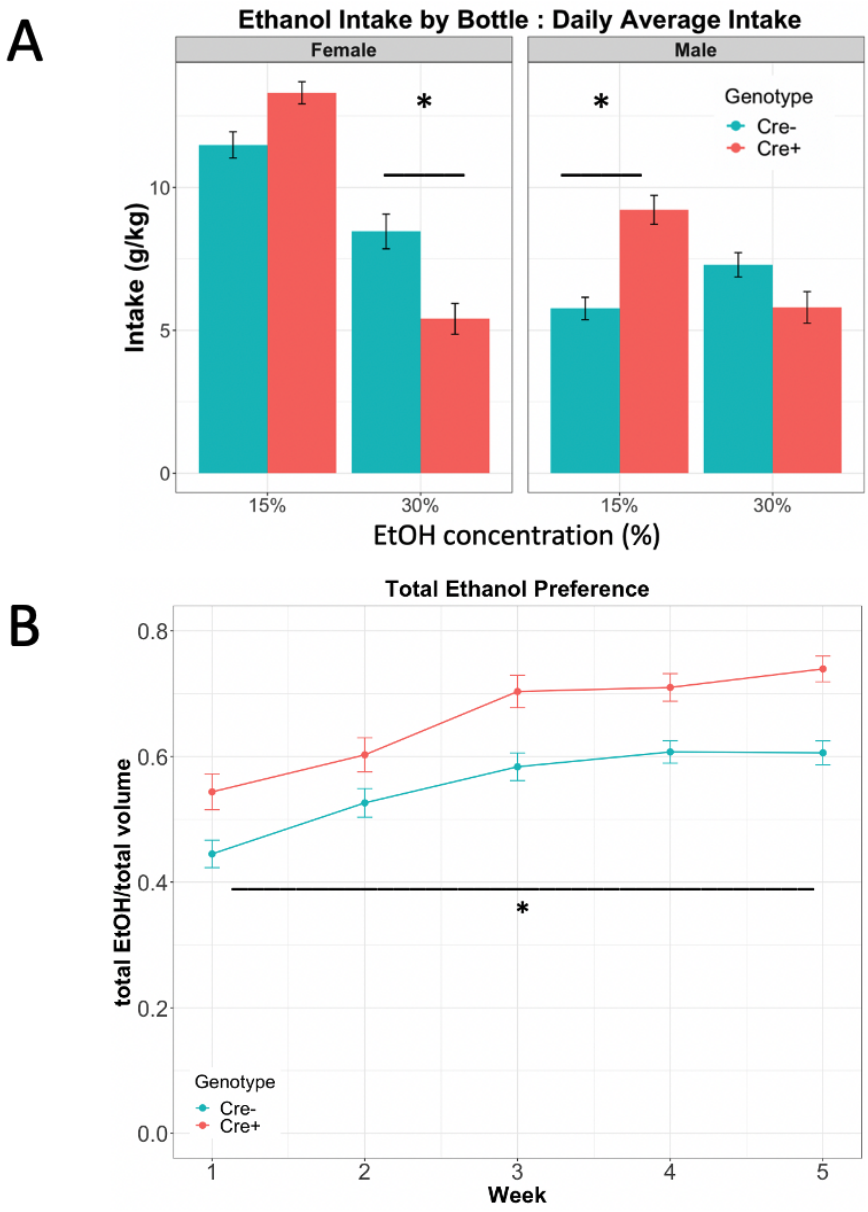

Figure 4.9: Average daily ethanol intake and average preference for ethanol by each drinking week. (A) Average daily ethanol intake for 3-bottle choice drinking, per alcohol concentration (15% or 30%) and sex. Left: Females. Right: Males (2- way ANOVA, * P < 0.05). (B) Weekly average ethanol preference by genotype. Linear mixed model statistics. Main effect of genotype highlighted by asterisk bar (P = 0.0134).

We investigated the effect of *Ndrg1* deletion on acute sensitivity to ethanol using the LORR protocol. We used mice of both sexes (N = 5 per genotype / per sex). Analysis was performed with Student's t-test. We found that neither the onset to LORR or the duration of LORR were significantly altered by *Ndrg1* deletion (see Figure 4.10A and Figure 4.10B). There was no effect of sex on either metric (not shown), so both sexes were collapsed to increase power. This resulted in a suggestion of a decrease in the onset time ($p < 0.1$) (see Figure 4.10A).

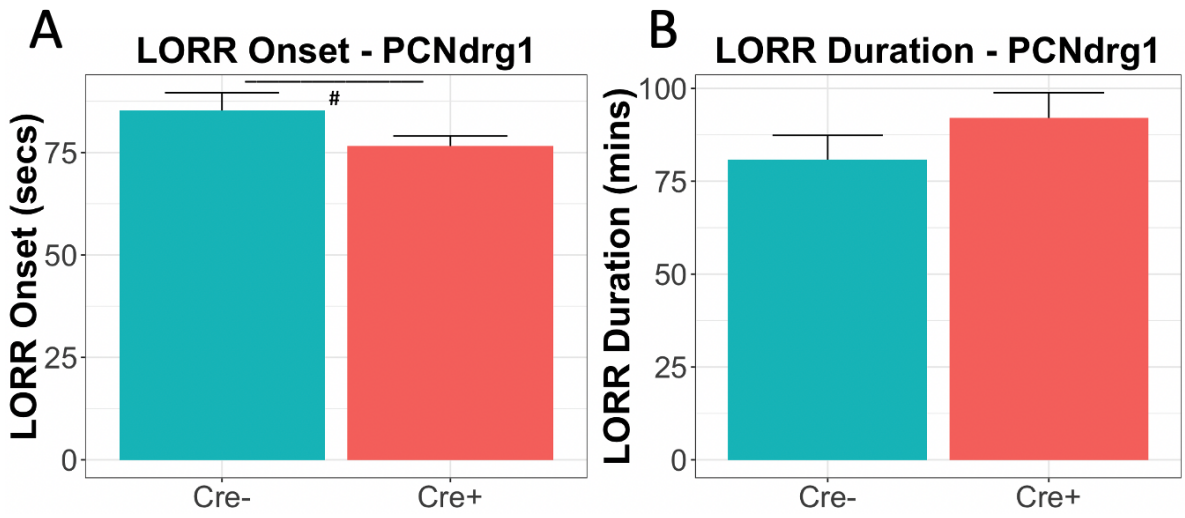

Figure 4.10: Loss of Righting Reflex (LORR) onset and duration. (A) time in seconds until the onset of LORR. (B) time in minutes until recovery of righting reflex. Student's t-test statistics (# P < 0.1)

4.6 Deletion of *Ndrg1* Results in Peripheral Nerve Dysfunction

4.6.1 Deletion of *Ndrg1* Leads to Long-Lasting Mechanical Hypersensitivity

Selective deletion of *Ndrg1* in myelinating cells produced long-lasting mechanical hypersensitivity as measured by Von Frey filaments. To begin, mice of both sexes (N = 6 Cre-; N = 8 Cre+) were tested for baseline mechanical sensitivity before Tamoxifen administration. Sexes were collapsed and simple Student's t-tests are used for statistical analysis. As shown in Figure 4.11, there was no difference between the mechanical thresholds for between the two genotypes ($P > 0.5$). By as little as two weeks post-Tamoxifen, there was development of significant hypersensitivity ($T = 2.931$, $P = 0.0199$) (see Figure 4.12A). By 2 months post-Tamoxifen, the hypersensitivity was

increased beyond the minimal detectable filament (T = 4.332, P = 0.00675) (see Figure 4.12B). Furthermore, this hypersensitivity is very long lived, as the knockout mice show hypersensitivity still at the minimal detectable filament force (T = 4.899, P = 0.0060) at least 8 months post-Tamoxifen (see Figure 4.13).

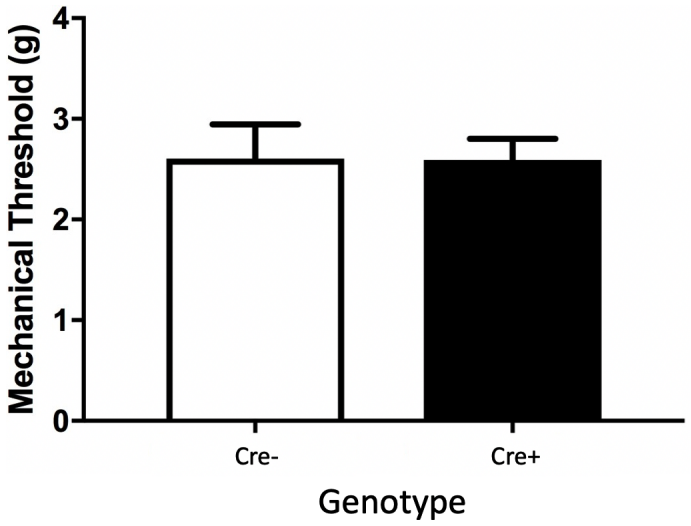

Figure 4.11: Baseline measurement of Cre+knockout mice and Cre- control mice of mixed sexes before the administration of Tamoxifen. Student's t-test (P > 0.5).

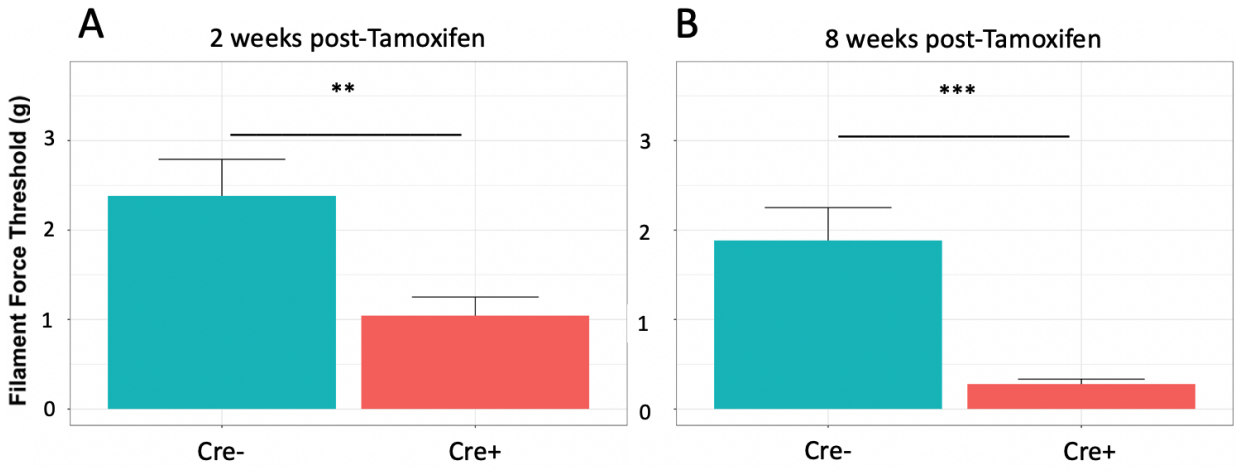

Figure 4.12: Time course for development of altered mechanical sensitivity following deletion of *Ndrg1*. (A) 2 weeks post-Tamoxifen. (B) 8 weeks post-Tamoxifen. Student's t-test (** P < 0.05; *** P < 0.01).

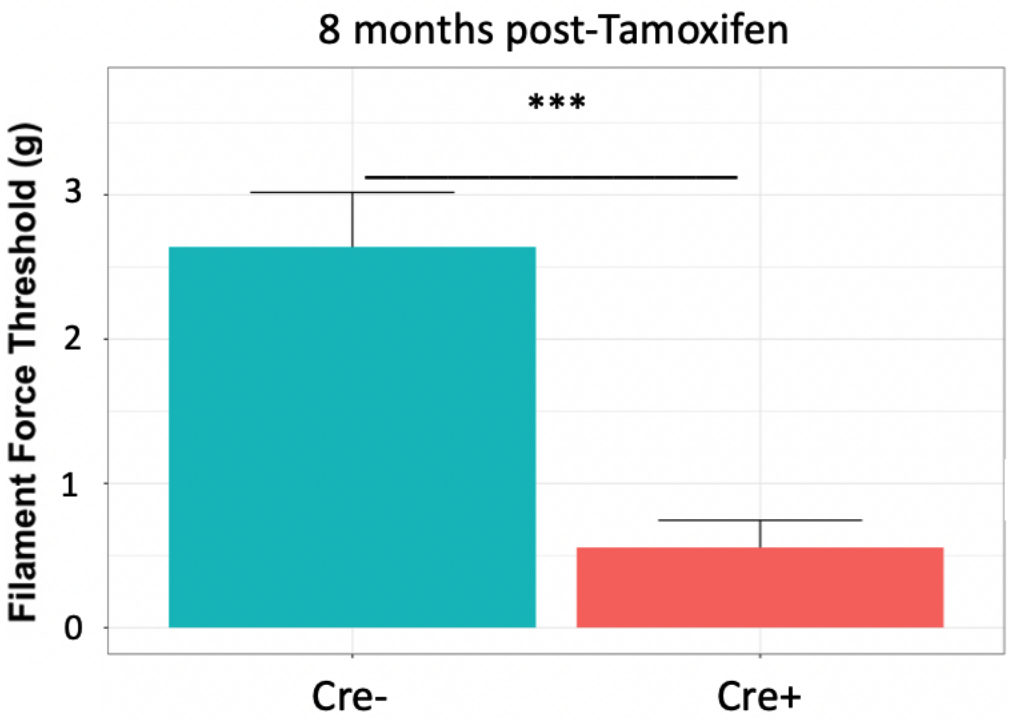

Figure 4.13: Heightened mechanical sensitivity is long lasting after *Ndrg1* deletion. Filament force measurements 8 months post-Tamoxifen. Student's t-test (*** $P < 0.01$).

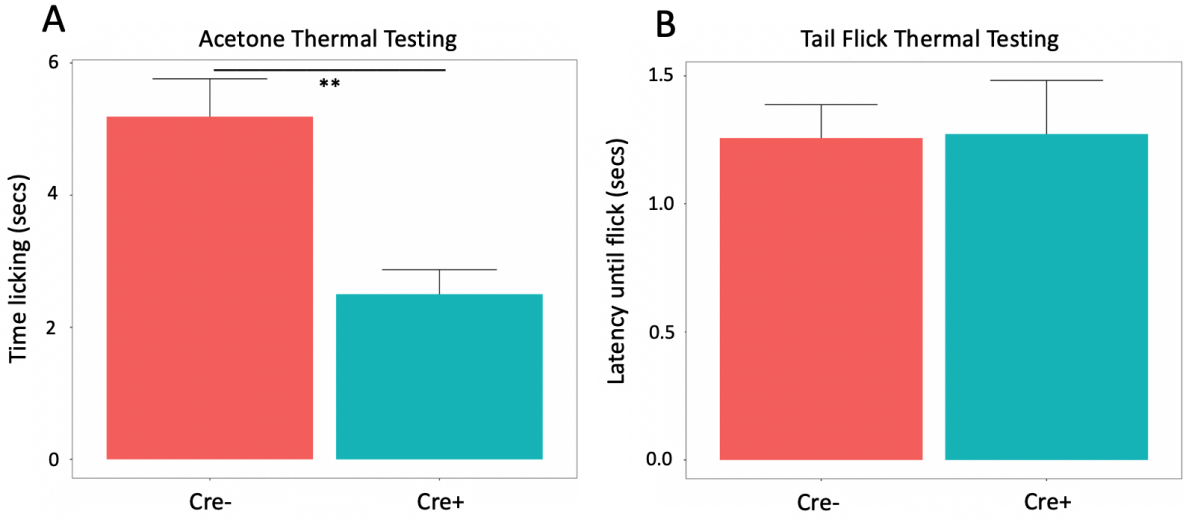

Figure 4.14: Thermal sensitivity testing of PCNdrg1 KO mice 3 months after *Ndrg1* deletion. (A) Acetone testing for cold sensitivity: average time spent licking paw after 20uL acetone on hind paws. (B) Tail flick assay for hot sensitivity: average latency until tail is withdrawn from 50C water bath. (Student's t-test, ** $P < 0.005$)

4.6.2 Homozygous Deletion of *Ndrg1* Causes Alterations of Thermal Sensitivity

Using the same cohort of mice from the above mechanical sensitivity study (see Figure 4.12), we tested for cold and thermal sensitivities at 3 months post-Tamoxifen administration. We found that Cre+ knockout mice spent significantly more time licking their paws after the application of acetone (T = -3.947, P = 0.000454), suggested increased sensitivity to cold stimulus (see Figure 4.14A). Conversely, we observed no differences (T = 0.0634, P = 0.951) in the latency to flick the tail out of a heated water bath between Cre+ and Cre- mice (see Figure 4.14B).

4.6.3 Heterozygous Deletion of *Ndrg1* does not Alter Sensitivity

In order to assess a possible gene dosage effect for *Ndrg1* loss-induced sensory modality changes, we studied heterozygous *Ndrg1* mice having one intact gene. We utilized both sexes of homozygous and heterozygous mice in this study. Statistical analysis was performed with 3-way linear mixed model that considered genotype (Cre+/Cre-), date measured, and group (Full KO or HET). While main effects of genotype and date measured were identified, we found no differences between heterozygous *Ndrg1* deleted mice with respect to mechanical or cold sensitivity (see Figure 4.15). The only group of mice that diverged from the Cre- control groups was the full homozygous deletion of *Ndrg1*, as noted in Figure 4.15. It is worth noting that all groups of mice developed some sensitivity to the assays due to over testing, which can result from too many mechanical measures in a short period of time. Regardless of this over testing effect, the homozygous *Ndrg1* deletion (Cre+/full KO) was the only group that significantly diverged from the control groups.

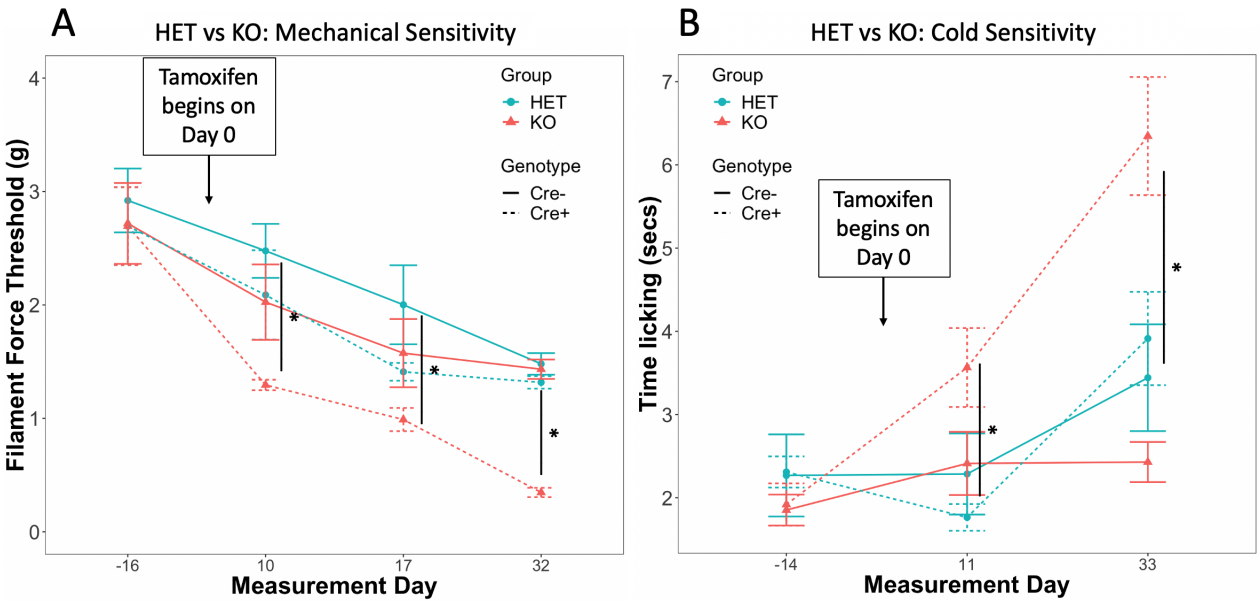

Figure 4.15: Tracking of mechanical and cold sensitivity over time in heterozygous *Ndrg1* KO mice. (A) Time course of development of mechanical sensitivity in HET and KO mice. Linear Mixed Model statistics, asterisks(*) at a measurement day indicates Cre+/KO was significantly different from at least one of the other three groupings (Tukey's adjusted p-value < 0.05). (B) Time course of development of cold sensitivity in HET and KO mice. Linear Mixed Model statistics, asterisks(*) at a measurement day indicates Cre+/KO was significantly different from at least one of the other three groupings (Tukey's adjusted p-value < 0.05). No other groupings (Cre-/KO, Cre+/HET, Cre-/HET) were significantly different from each other at any measurement day.

4.6.4 *Ndrg1* Deletion Results in Motor Skill Deficits, but Not Motor Learning

Since prior studies by other investigators have documented motor deficits with prolonged *Ndrg1* deletions in animal models (Okuda et al. 2004; Chandler et al. 2013), we commenced studies on these aspects of peripheral nerve function. Beginning at 2 months post-Tamoxifen, we began testing the Cre+ knockout mice for motor performance using a Romex rotarod machine. This experiment was conducted using the same cohort of mice that underwent the thermal sensitivity studies described above. At the first testing day, the Cre+ knockout mice remained on the rotarod for significantly less time than controls (Figure 4.16A). Retesting the same group of mice 2 weeks later revealed that both genotypes improved in their ability to stay on the rotarod for a longer amount of time. Interesting, the Cre+ show a larger degree of improvement relative to the Cre- control (Figure 4.16B). At the 3rd and final testing day, we found no additional improvement

in the Cre- group, but we did see that the Cre+ knockout mice continued to improve compared to their 8 week time point, and had no significant difference from the Cre- controls (Figure 4.16C).

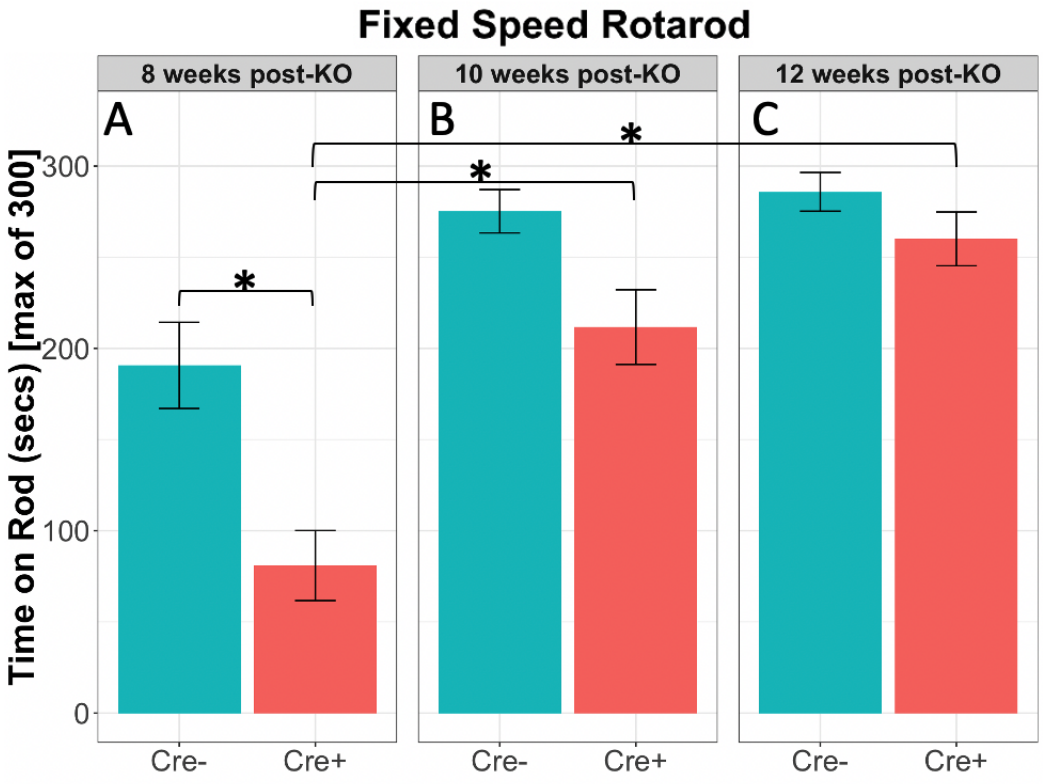

Figure 4.16: Performance on a fixed speed Rotarod protocol in KO mice over time. The Rotarod was tested at the following time points post-Tamoxifen: (A) 8 weeks, (B) 10 weeks, (C) 12 weeks. Linear Mixed Model statistics, asterisks (*) note relevant post-hoc contrasts (Tukey's adjusted p-value < .05)

4.6.5 *Ndrg* Deletion Adversely Affects Peripheral Nerve Conduction and Velocity

We found that both velocity and amplitude of peripheral nerve conduction was decreased by 6 months post-tamoxifen. We recorded the nerve conduction velocity of the cohort of mice that was tested for thermal sensitivities and Rotarod performance as described above. Statistical analysis was performed using Student's t-test. The sexes are analyzed separately as well as collapsed. As this 6 month time point, the decrease was found in both male and female mice, and in both cases we see a much greater decrease in amplitude than noted for the velocity measurements (Figure 4.17).

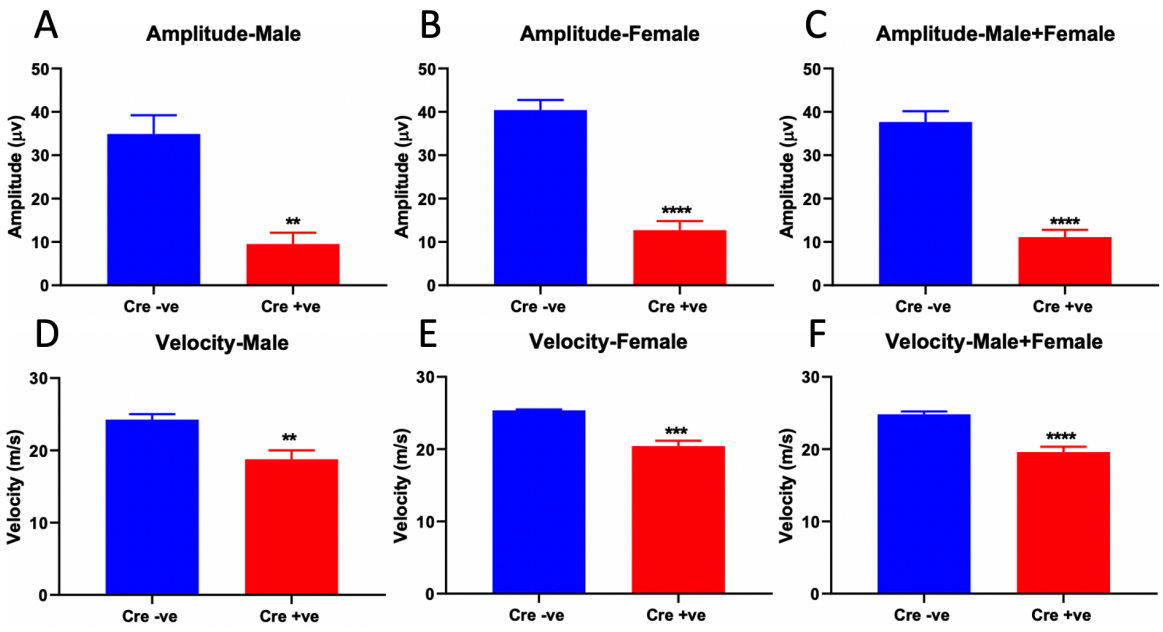

Figure 4.17: Nerve conduction and velocity testing 6 months port-Tamoxifen. Top row: Amplitude. Bottom row: Velocity. Left panel (males), middle panel (females), right panel (sexes collapsed). Student's t-tests (** $P < 0.01$; *** $P < 0.001$)

4.6.6 Sensitivity to Severity of Paclitaxel-Induced Neuropathies is Enhanced by *Ndrg* deletion

To directly prove that loss of *Ndrg1* expression altered the sensitivity to Paclitaxel-induced peripheral neuropathy, we employed a low dose Paclitaxel treatment that caused a submaximal and reversible increase in mechanical hypersensitivity. Here we utilized PCNdrg1 mice of both sexes, with the intent of collapsing sexes due to low N (N = 3 per sex / per genotype / per treatment). The experiment was analyzed with a 3-may linear mixed model that considered genotype (Cre+/Cre-), date measured, and treatment (Paclitaxel or saline). The low dose Paclitaxel study provided several pieces of information, including a clearer look at the time course for the development of mechanical sensitivity following *Ndrg1* deletion. First, we found no changes of the mechanical sensitivity of Cre- mice that received vehicle, establishing that the mice were not over-tested (see Figure 4.18, dashed blue line). As expected, based on the literature, we observed a transient development of hypersensitivity in Cre- control mice that received low dose Paclitaxel that resolved by the

end of the study (see Figure 4.18, solid blue line) . Regarding the time to develop dysfunction following *Ndrg1* deletion induction, we found that 1 week post-tamoxifen was the earliest we detected significant hypersensitivity in the vehicle treated Cre+ mice (Figure 4.18, dashed red line, d15). The vehicle treated *Ndrg1* deletion mice reached the floor of the Von Frey Filament testing by day 25, 2 weeks following the end of Tamoxifen treatment. In contrast, the Cre+ knockout mice that received low dose Paclitaxel began to show significant signs of sensitivity immediately after just 2 of the 4 doses of Paclitaxel (see Figure 4.18, solid red line, d11). These Cre+ Paclitaxel treated mice reach the floor of the Von Frey Filament testing by the day immediately after the 4th Paclitaxel injection (see Figure 4.18, solid red line, d15).

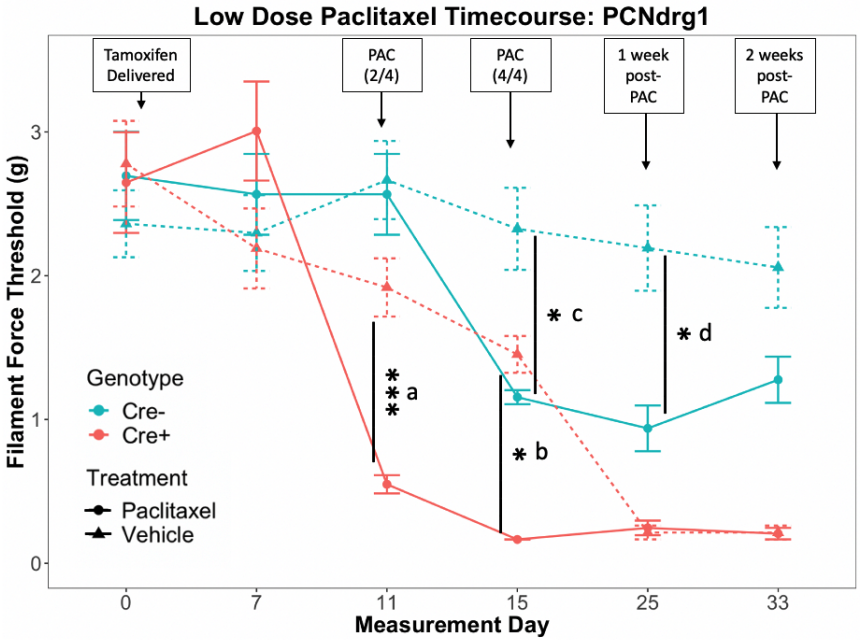

Figure 4.18: Tracking of mechanical sensitivity over time following Tamoxifen and low-dose Paclitaxel. The delivery date of the Tamoxifen and the measurement points are noted in the boxes at the top of the plot. 3-way linear mixed model statistics. Post-hoc testing was performed with Tukey's HSD. Relevant contrasts are highlighted in a-d. (a) After 2 of 4 PAC doses, the PAC treated Cre+ mice are significantly more sensitive than saline-treated Cre+ mice ($P < 0.001$). (b) After 4 of 4 PAC doses, the the PAC treated Cre+ mice are still significantly more sensitive than saline-treated Cre+ mice ($P < 0.05$). (c) After 4 of 4 PAC doses, the the PAC treated Cre- mice are significantly more sensitive than saline-treated Cre- mice ($P < 0.05$). (d) 1 week after completing of PAC treatment, the the PAC treated Cre- mice are still significantly more sensitive than saline-treated Cre- mice ($P < 0.05$). By this time point, both Cre+ treatment group were at the floor of the mechancial senstivity threshold for testing.

4.6.7 Repeated High Doses of Ethanol do not Alter the Development of Mechanical or Cold Sensitivity Following Deletion of *Ndrg1*

Given the augmentation of Paclitaxel-induced mechanical hypersensitivity by *Ndrg1* deletion, we sought to determine if the gene might also play a role in one of the most frequent causes of induced peripheral neuropathy – AUD. We thus conducted a pilot study similar in design to the low-dose Paclitaxel experiment described above. We assessed both acetone-induced cold hypersensitivity and mechanical hypersensitivity. The experiment used male mice only (N = 5 per genotype / per treatment) and we utilized a 3-way linear mixed model that considered genotype (Cre+/Cre-), date measured, and treatment (etOH or saline). We uncovered significant main effects of genotype (F = 39.63, P = 3.064E-10) and date measured (F = 194.35, P < 2.2E-16), but there was no effect of treatment group (F = 0.041, P = 0.841). We found no changes of the mechanical or cold sensitivity of Cre- mice that received only vehicle, establishing that the mice were not over-tested (see Figure 4.19, dashed blue line). However, we also did not observe any alterations in the ethanol treated Cre- control group in either cold or mechanical sensitivity over the course of the study (see Figure 4.19, solid blue line), suggesting a lack of ethanol-induced peripheral nerve dysfunction at this ethanol dose and time regimen. Following Cre induction by Tamoxifen, both vehicle- and ethanol-treated mice developed cold or mechanical hypersensitivity at 2 weeks post Tamoxifen (Figure 4.19, dashed and solid red line). Additionally, all Cre+ mice reached the floor of the Von Frey Filament testing by just 2 weeks following the end of Tamoxifen treatment.

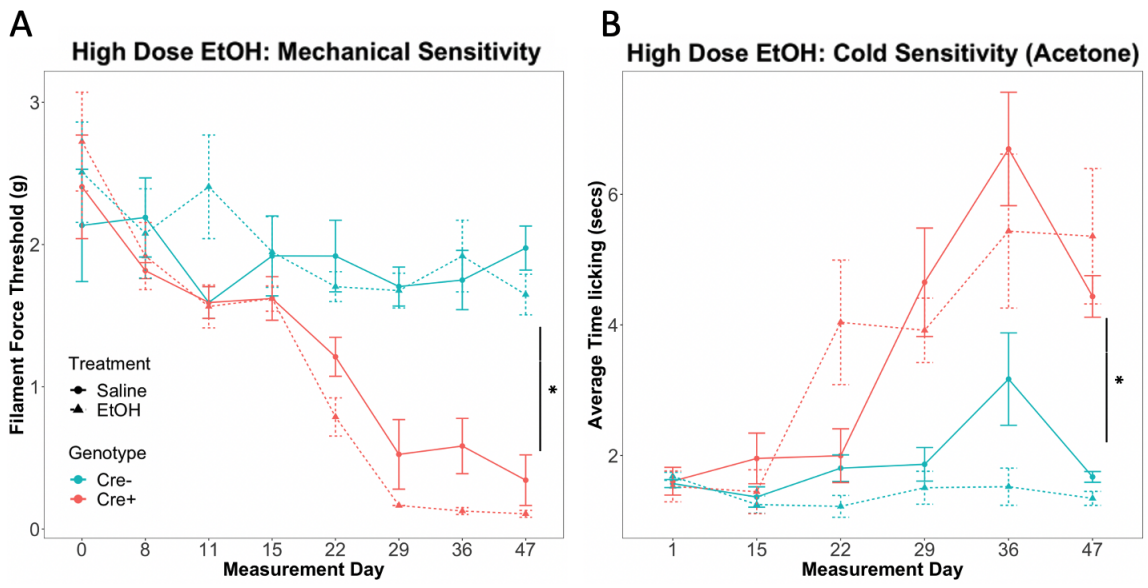

Figure 4.19: Tracking of mechanical and cold sensitivity over time following repeated high doses of following deletion of *Ndrg1*. (A) Tracking of mechanical sensitivity over time. (B) Tracking of cold sensitivity over time. Tamoxifen treatment began on measurement day 1 as indicated in (B). Linear mixed model statistics. * highlights the significant main effects of genotype and date measured. (* P, < 0.0001)

4.7 Discussion

We have identified numerous consequences that arise from deletion of *Ndrg1* in myelinating cells of the central or peripheral nervous system. We found changes in drinking behaviors and provided evidence that acute sensitivity is being subtly modulated by *Ndrg1* deletion (see Figure 4.8 and Figure 4.9). We have strong evidence that these differences in ethanol behaviors were not due to a typical experimental confounders (see Figure 4.6). We observed a very rapid increase in the mechanical sensitivity of the hind paws of KO mice (see Figure 4.12). This increased sensitivity is very long-lived and does not recover for at least 8 months following KO (see Figure 4.13). Other signs of nerve dysfunction, such as cold sensitivity, also developed rapidly while others, such as tail flick latency, did not (see Figure 4.14). Additionally, Cre+ KO mice had significantly decreased velocity and amplitude of nerve conduction by at least 6 months post-KO (see Figure 4.17). We found that mice that were heterozygous for floxed-*Ndrg1* mice did not show any signs of increased mechanical or cold sensitivity following Tamoxifen (see Figure 4.15). Importantly, we provided

fundamental evidence that levels of nerve *Ndrg1* are inversely correlated with the level of nerve dysfunction observed following Paclitaxel treatment (see Figure 4.18). Finally, we did not find any correlation between the levels of nerve *Ndrg1* and development of nerve dysfunction following repeated high doses of ethanol (see Figure 4.19).

It is worth noting that the nerve conduction velocity testing only recorded and measured the latency from the initial stimulus to the 1st peak. When measuring nerve conduction velocity, there are two peaks that can be measured. The first peak that arrives is from signal conduction along myelinated fibers, while the slower second peak is from signal conduction along unmyelinated fibers. Given the very rapid onset of mechanical sensitivity that follows *Ndrg1* deletion occurs well before any visible motor defects, it is possible that *Ndrg1* deletion is occurring in the unmyelinated Schwann cells which support unmyelinated fibers. Given that Von Frey filaments measure mechancial nocieption and that unmyelinated C fibers are the primary sensory receptor for mechanical stimulation, it is possible that the rapid onset of mechanical sensitivity is driven by dysfunction of C fibers soon after *Ndrg1* deletion. It would be very worthwhile to follow up with additional nerve conduction velocity that measures both peaks. If a more rapid degradation of the second peak occurs, then *Ndrg1* deletion is vital for the function for both myelinated nerves and unmyelinated sensory fibers.

Remarkably, the alterations in the consumption patterns of 15% and 30% ethanol consumption are strikingly similar to the lentiviral pilot data (see Figure 2.6). There is evidence that mPFC *Ndrg1* levels could in fact be the main driver of ethanol sensitivity and concentration preference, but this mouse model is not able to answer this question since the knockout is global in both the CNS and the PNS. In order to have this fine control, an injection of a MBP-Cre virus into the mPFC of floxed-*Ndrg1* mice would, for example, be able to provide the necessary localization. Additionally, it is wholly possible that the peripheral effects of Ndrg1 deletion could alter ethanol drinking through other means. If the mechanical sensitivity values are reflective of a pain-like state, there is evidence that male mice will escalate their ethanol consumption while female mice

do not alter their ethanol behaviors in response to a painful stimulus, such as CFA injection into hind paws (Yu et al. 2019).

We found that mechanical sensitivity develops very rapidly following the knockout of *Ndrg1*, suggesting that continuous expression of *Ndrg1* is necessary for the function of the peripheral nervous system at least in terms of this sensory modality (see Figure 4.12). It is also interesting that we begin to see some peripheral nerve recovery of *Ndrg1* at 6 months post-tamoxifen, but there is no recovery of the deletion-induced mechanical hypersensitivity at 8 months. This suggests that although there are adequate levels of myelin protein in the peripheral nerve (as *Ndrg1* deletion did not alter peripheral MBP protein expression – Figure 4.5), the function or the structure of myelin could have been perturbed sufficiently without *Ndrg1* expression that partial reestablishment of *Ndrg1* expression could not rescue nerve function over this time course. Perhaps this is because the axon suffers un-repairable damage without some potential tropic effects of *Ndrg1* contained in the adjacent myelin processes. As noted in the literature, *Ndrg1* clearly affected sensory and motor function in the PNS (Okuda et al. 2004). However, the fact that our Cre+ knockout mice were able to drastically improve their Rotarod performance suggests that motor skill learning is still intact (see Figure 4.16). Further studies into motor skill versus function could help establish more precise knowledge of the specific functions of *Ndrg1*.

Importantly, our work with low dose Paclitaxel administered during the active deletion of *Ndrg1* demonstrates the basal levels of nerve *Ndrg1* are essential for protection of the myelin and the nerve following a known peripherally toxic agent. This work assumes a fairly linear falloff of NDRG1 levels over the time post-tamoxifen. It also does not provide a steady reduced level of NDRG1 protein. Due to these assumptions and limitations, there would be an advantage to running this experiment with PCNdrg1 HET mice. Assuming that the HET mice do in fact have lower levels of NDRG1 protein, we would expect the HET mice to be more sensitive to Paclitaxel than the Cre+ vehicle-treated mice. Another point is the repeated testing of the mice in the nerve dysfunction assays. It is known that over testing of the sensory perception tasks can lead to altered and increased sensitivity. This can affect the measurements and confound the results. We expe-

rienced this with the HET experiment, as the mice saw much testing over a short period of time (acetone/Von Frey/Rotarod). There is the possibility that is occurred in our low dose Paclitaxel experiment and high dose ethanol study. However, the stability of the Cre- vehicle-treated groups over the course of that study suggests that the mice were not over-tested in the same manner as the HET data, where all mice increased their sensitivity over the course of the study.

While there was no short term effect of repeated high doses of ethanol on the development of mechanical and cold sensitivity, this does not mean there was no deleterious effect from these high dose ethanol exposures. Given that we do not see alterations in the nerve conduction and velocity of Cre+ knockout mice until 6 months after *Ndrg1* deletion, it would be worth taking several long-term measurements of mice that received the high doses ethanol. Perhaps nerve testing and cold sensitivity testing at 6 months would reveal larger deficits in Cre+ knockout mice that received the ethanol exposures. Additionally, it could be that too few ethanol injections were utilized to drive any acute toxic effects from the current regiment. It might also be wise to deliver the repeated doses of ethanol 2-3 months post-Tamoxifen, when the knockout is more robust and major motor deficits are beginning to occur. At that time, the already damaged peripheral nervous may have a much stronger response to the noxious levels of ethanol. Such future studies could have an important clinical impact by identification of a possible risk factor and mechanistic target (Ndrg1) for ethanol-induced peripheral neuropathy, which together with diabetes-related peripheral neuropathy, is one of the largest causes for clinical presentation of peripheral nerve disease.

Due to the large difference in the severity of PNS and CNS dysfunction following *Ndrg1* deletion, further studies into the transcriptome response differences between the CNS and PNS were planned. Tissue from both the mPFC and the Sciatic nerve were isolated and mRNA was extracted. We sought to investigate these differences using the latest generation of microarray technology (ClariomS Mouse Assay) from Affymetrix/Thermo-Fisher. In order to fully utlize the power of this microarray technology, a novel differential gene expression algorithm and package, GCSscore, was created and validated. The details of the algorithm/package and its validation are the subject of Chapter 5.

Chapter 5

GCSscore: a differential expression algorithm

5.1 Introduction

Despite the advent of RNAseq for transcriptomics analysis, microarrays continue to be widely used with an average of over 7000 PubMed citations per year in 2015-2019. A major commercial platform for microarray analysis, produced originally by Affymetrix and now by ThermoFisher, utilizes collections of oligonucleotides distributed across cognate genes to probe RNA expression by hybridization. Popular analysis methods for oligonucleotide arrays, such as the Robust Multiarray Analysis (RMA) method, produce expression values for given genes/transcripts/exons by summarizing hybridization intensities across all corresponding oligonucleotides (Irizarry et al. 2003). Since expression "differences" rather than absolute expression levels are generally the goal in microarray studies, our laboratory previously developed the S-score algorithm for analysis of Affymetrix oligonucleotide microarrays for detecting significant expression changes between paired samples (Zhang et al. 2002). This entailed comparing individual oligonucleotide probes within each probeset between two samples, after applying a heteroscedastic error correction model. The S-score method provided an easily interpretable standard normal distribution of expression differences between two samples for a given probeset, akin to a z-score transformation. Prior work demonstrated the advantage of the S-score method over probe summarization techniques such as RMA for Affymetrix microarray analysis, particularly for experiments having smaller numbers of replicates (Zhang et al. 2002; Kennedy, Archer, and Miles 2006). This advantage prompted development of a Bioconductor R package, sscore, for application of the original S-score method on Affymetrix microarrays (Kennedy, Archer, and Miles 2006). This algorithm has been utilized in publications across multiple laboratories for studies based on 3' IVT array technology (Kerns et al. 2005; Grice et al. 2007; Singh et al. 2011; Wolstenholme et al. 2011; Wolen et al. 2012; Paxson et al. 2013; Vaart et al. 2017; Bogenpohl et al. 2019). The original S-score relies on the differ-

ence between perfect match (PM) and cognate mismatch (MM) probes to correct for non-specific hybridization while calculating a measure of expression difference between two samples. MM probes were designed to capture array background noise (*rawQ*) and non-specific binding (NSB) of off-target transcripts. However, MM probes were subsequently shown to be an inconsistent measure of non-specific binding (Schuster et al. 2007). While the RMA method excluded MM probe data from the expression calculation and has come to be widely used, use of RMA summarization/normalization followed by appropriate statistical testing differential gene expression does not utilize probe-level information as with the S-score. Since NSB signal is strongly correlated with GC-content of the probe sequence, newer Affymetrix array technology eliminated the MM probes and instead utilized 16,943 antigenomic probes of varying GC-content on 25-mer oligonucleotide targets ranging from 3 (12% GC) to 25 (100 % GC) to estimate non-specific binding (Affymetrix 2005). This new technology, referred to as Whole Transcriptome (WT) arrays, allows probes to be grouped either in Transcript Cluster IDs (TCids) for a gene-level analysis or into Probe Selection Region IDs (PSRids) for an exon-level analysis. Subsequent arrays designs provide more detailed measures of exon expression and transcript splicing variants, via exon-exon Junction IDS (JUCids), that are on par with RNA-seq (Xu et al. 2011). These Transcriptome Assay chip types were released for human (HTA1.0/2.0), rat (RTA1.0), and mouse (MTA1.0). This fully featured design was further developed into the ClariomD chip type, available for human and mouse. An additional gene-level only chip type, the ClariomS, was created using only the ten best performing probes from each TCid present on the ClariomD/Transcriptome Assay (HTA/RTA/MTA) designs, which will be referred to as ClariomD/XTA arrays. Unfortunately, no generations of the WT-style arrays are compatible with the original S-score algorithm and existing sscore R package for probe-level analysis due to lack of MM probes on the new array designs. We have therefore developed an R package, GCSscore, with a new algorithm that enables the S-score probe-level analysis method for the newest generation of Affymetrix/ThermoFisher Clariom-style microarrays. We have also utilized updated data handling methods that improve the speed of the analysis considerably. We show here that GCSscore performed similarly to the originally published sscore R package for older type

microarrays (3' IVT) and added functionality for analysis of the newest Affymetrix/Fisher microarray types. Furthermore, our results suggest that use of the GCSscore package provides substantial benefit compared to existing methods in detection of differential gene expression (DEG) on these newer generation microarrays.

5.2 Implementation

5.2.1 Algorithm

The most fundamental change from the original algorithm is the introduction of background correction based on the median signal of antigenomic probes having the same GC-content as a the given PM probe, rather than relying on the cognate MM probe hybridization signal. The GCS-score algorithm is based upon the operations in equations (1) through (3). For a given probe grouping method, k, which is made up of N probes, the GCS-score, denoted as $GCSs_k$, is as follows:

$$GCSs_k = \sum_{i=1}^{N} \frac{l_{iB} - l_{iA}}{\varepsilon_i \sqrt{N}} \tag{1}$$

$$\varepsilon = \sqrt{\gamma^2 (l_{iB}^2 - l_{iA}^2) + SDT_A^2 + SDT_B^2} \tag{2}$$

$$SDT = 4 * rawQ * SF \tag{3}$$

- l_{iA} and l_{iB} : background corrected intensities of the i-th probe pair from array A and B, respectively.
- $N =$ number of probes in a probesetID or transcriptclusterID
- $\gamma =$ a scaler constant ($\gamma = .1$)
- $SDT = 4 * rawQ * SF$ for each array, A and B.

In the algorithm equations, l_{iA} and l_{iB}, represent the background corrected intensities of the i-th probe pair from array A and B, respectively. As defined in the Affymetrix MicroArray Suite (MAS) documentation, the significant difference threshold (*SDT*) is determined by the noise floor of each array and the chosen scaling factor. The noise floor (*rawQ*) is calculated from the standard deviation of the bottom 2% of the probe intensities across the array. The scaling factor (*SF*) for each array is a multiplier that scales the median intensities to a target value (default is 500). The gamma factor is set to 0.1 to prevent calculated Sscore values from being affected by gene expression levels (Zhang et al. 2002). The GCSscore package imports functions from the following CRAN/BioConductor packages: BiocManager, Biobase, utils, methods, RSQLite, devtools, dplR, stringr, graphics, stats, affxparser, and data.table. If it is desirable to pull datasets for GEO or perform the downstream analysis presented in this publication, the following additional packages are necessary: siggenes, GEOquery, and R.utils. All probe-level data and annotations utilized by the GCSscore package are parsed and sourced directly from the following chip specific BioConductor packages: platform design (.pd) and AnnotationDbi (.db). The resulting probe-level data file is packaged into a 'probefile' package, while the annotations are packaged into an additional 'annot' package. These packages are created on the fly and installed in the user's library by utilizing customized versions of the makeProbePackage function and package templates sourced from the AnnotationForge package (Carlson and Obenchain 2015).

While the theory of the GCS-score method can be applied to any modern Affymetrix ThermoFisher chip type, the R package was written for use with Clariom-style arrays, which include: ClariomS, ClariomD, and XTA assay chip types. This package fully supports all Clariom-style arrays and has support for two of the most widely used 3' IVT arrays: Mouse Genome 430 2.0 and Human Genome UG133 2.0. For older types of Affymetrix arrays, the original sscore package must be used. The GCS-score algorithm allows the user to calculate Sscore values for ClariomD/XTA arrays using two probe grouping methods: (1) utilizes TCids groupings for gene-level, (2) utilizes PSRids and JUCids for exon & alternate splicing-level. Since the ClariomS arrays only contain TCids, there is only a gene-level analysis method. Additionally, for supported 3' IVT chips, the

method refers to two background subtraction options: (1) utilizes the new GC-bkg method (2) utilizes the original PM-MM method. The GCSscore package allows for direct probe-level comparisons of two Affymetrix microarrays at a time. The user can either input two .CEL files directly into the function, or read in a formatted batch file that is setup to run pair-wise comparisons of multiple .CEL files in a single function call (see Table 5.1). For more information regarding the implementation, please refer to the workflow diagram (see Figure 5.1). In brief: .CEL files are scaled to have equivalent trimmed median intensities for the desired probe grouping method. The Sscores are calculated and normalized using the middle 98% of the raw scores. Finally, normalized results are combined with the annotation information parsed from the Bioconductor repository and are returned to the user's environment using the Biobase data structure, ExpressionSet. The user can also choose to save the GCSscore results to disk, as a .CSV file.

5.2.2 Statistical properties and analysis of GCSscore outputs

One principal advantage of the S-score based methods is the simple Gaussian-like statistics of the resulting output (see Figure 5.2). If no extreme differential expression exists between two .CEL files then the GCSscore output will have a mean of 0 and a SD of 1 (Zhang et al. 2002). Since, each run is essentially z-scored and normalized prior to output, each GCS-score becomes a representation of the standard deviation from the mean of a Gaussian-like distribution. Thus, the absolute values of S-scores greater than 1.8-2.0 are likely to be statistically significant and this can be determined by using statistical testing of biological replicates with correction for multiple testing, as done with the SAM method below.

5.2.3 Workflow for generating differential expression for downstream analysis

In our standard implementation, all treatment samples were run against all control samples in a pairwise fashion. For example, if there are 3 replicates for the treatment and 3 replicates for the control group, there will be 9 total pairwise comparisons (see Table 5.1). The Sscores were averaged for each treatment sample against all 3 control samples, producing 3 averaged Sscore values, one for each of the treatment samples. This was done to reduce noise with small sample sizes and to prevent over inflation of sample numbers that would occur from taking all of the

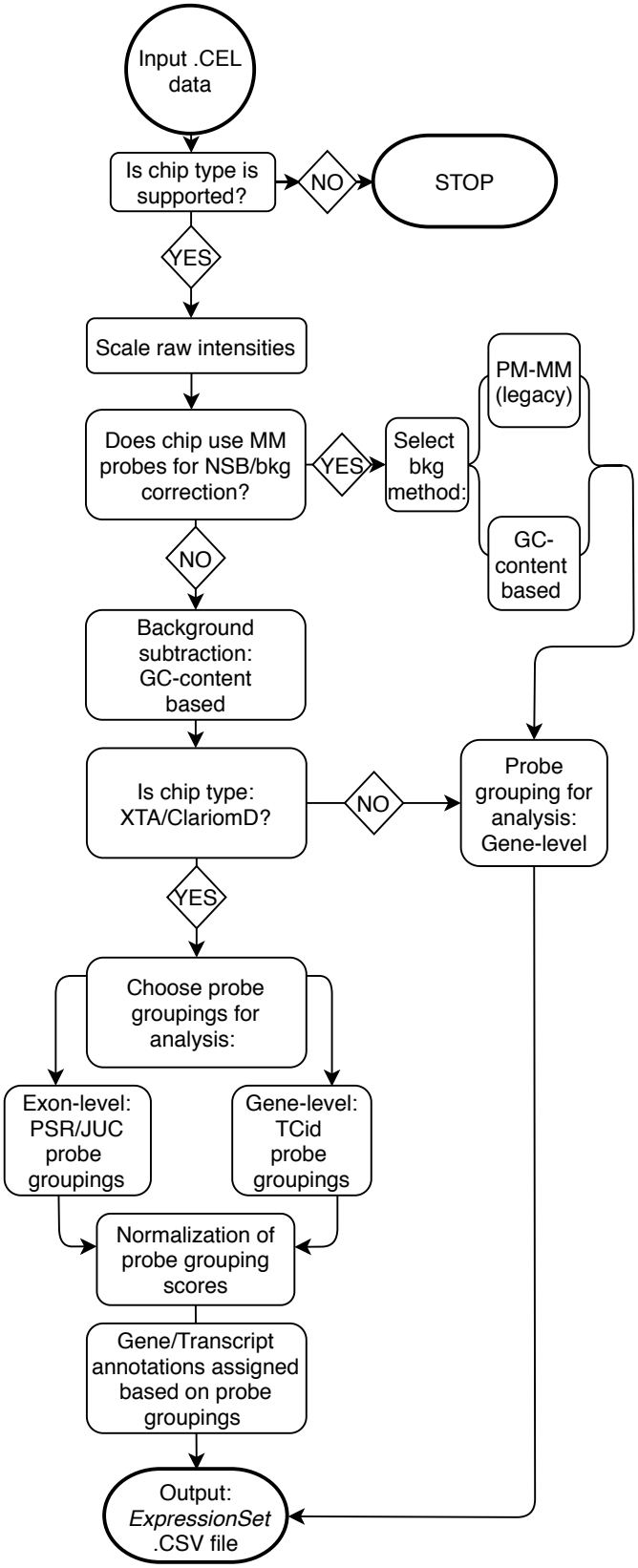

Figure 5.1: Workflow diagram for GCS-score algorithm.

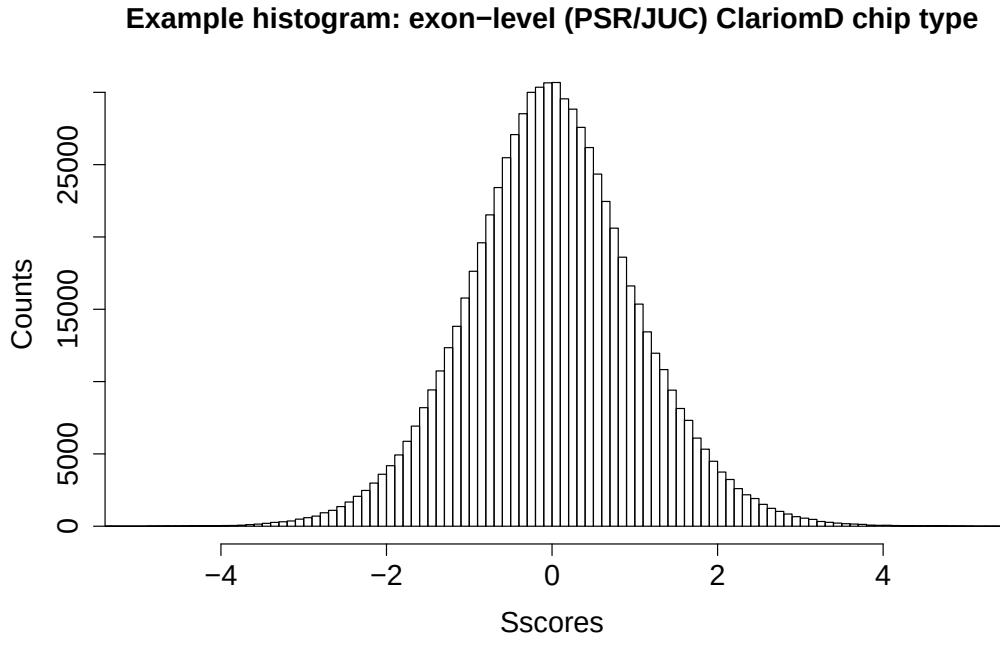

Figure 5.2: Example histogram for GCSscore output. Distribution of 785,000 exon targeted PSR probesetids. Note the normal distribution of the Sscores (mean=0.002, SD=1.031)

RunName	CelFile1	CelFile2
Tx01_v_Ctrl01	Tx01.CEL	Ctrl01.CEL
Tx01_v_Ctrl02	Tx01.CEL	Ctrl02.CEL
Tx01_v_Ctrl03	Tx01.CEL	Ctrl03.CEL
Tx02_v_Ctrl01	Tx02.CEL	Ctrl01.CEL
Tx02_v_Ctrl02	Tx02.CEL	Ctrl02.CEL
Tx02_v_Ctrl03	Tx02.CEL	Ctrl03.CEL
Tx03_v_Ctrl01	Tx03.CEL	Ctrl01.CEL
Tx03_v_Ctrl02	Tx03.CEL	Ctrl02.CEL
Tx03_v_Ctrl03	Tx03.CEL	Ctrl03.CEL

Table 5.1: A typical pairwise comparison of a case with 3 treatment samples and 3 control samples. Also demonstrates the formatting and structure of the BATCH input for generating multiple GCSscore comparisons in a single function call

pairwise comparisons into account (Farris and Miles 2013). Alternatively, random pairings of treatment/control samples can be used for generation of Sscores (Kerns et al. 2005). Differential expression analysis with multiple-testing correction can then be applied.

For the statistical analyses presented in this publication, the averages of each treatment replicate against all of the control samples were used as the input into a 1-class Significance Analysis of Microarrays (SAM) analysis to identify genes with GCSscore values statistically different from 0, as demonstrated in prior publications with the original S-score algorithm (Kerns et al. 2005; Wolen et al. 2012; Farris and Miles 2013). The SAM algorithm used here was provided by the siggenes package from Bioconductor. More complex experimental designs implement multiple group testing in SAM or other appropriate statistical methods, such as LIMMA (Ritchie et al. 2015). The average of these treatment replicate averages, denoted as *AvgSs*, was used as an additional stringent filter to decrease contributions from genes with exceedingly small fold-changes, as reported previously (Kerns et al. 2005; Wolen et al. 2012; Farris and Miles 2013). To determine significantly regulated gene lists, the following criteria were thus used: genes from the SAM output within a determined FDR cutoff (e.g. 0.0125-0.1) and genes who also have $|AvgSs| > 1.8$. In the Clariom array cases explored in Section 5.3.3 and Section 5.3.2, downstream analysis of the gene lists was performed using ToppFun suite for Gene Ontology/Functional enrichment analysis and Ingenuity Pathway Analysis (IPA) to find significantly altered signaling pathways. For the ToppFun analysis, only the gene symbols from the generated gene lists were input directly into the suite. For the IPA analysis, the TCids, *AvgSs*, and rawp values from the SAM output were used as the input.

5.3 Results

5.3.1 Comparison with original algorithm

Since the original S-score algorithm has been validated and utilized in previous publications, we initially compared the GCS-score algorithm against the original S-score method. In this example, previously published Mouse Genome 430 2.0 array data (GSE28515) from the prefrontal cortex of DBA2/J mice is used (Wolen et al. 2012). We utilized 3 biological replicates exposed to

acute i.p. ethanol (1.8 g/kg x 4 hours; treatment) and 3 biological replicates that received i.p. saline (control). The GCSscore package and algorithm was completely rewritten from the ground up to be much more efficient and add new functionalities. To confirm that the new algorithm performed as expected, we analyzed these 430 2.0 arrays first using the PM-MM method found in the GCSscore package with the original sscore package. For any given comparison between a treatment and a control, GCS-score (PM-MM method) and the original S-score method produced identical Sscore values (see Figure 5.3A), since the GCS-score algorithm simply utilizes individual MM probes instead of the GC-content based background (GC-bkg). The new GC-bkg method was also compared against the PM-MM method using the *AvgSs* metric described in Section 5.2. There was considerable variation between the two methods as the *AvgSs* values approached zero, where there was no detectable difference between treatment and the control groups (see Figure 5.3B). However, convergence of the two methods was observed for Sscore values beyond an empiric significance threshold of $|AvgSs| > 1.8$ (red lines in see Figure 5.3B). Previous studies have demonstrated that DBA2/J mice have many more genes that are upregulated than downregulated, especially in the medial prefrontal cortex (see Figure 3 from Kerns et al. 2005). This explains the dramatic skew towards positive significant *AvgSs* values, regardless of the background subtraction method. The results displayed in Figure 5.3 demonstrate that the new background subtraction method returned very similar results to the original PM-MM method for significantly regulated genes, validating the use of the new GC-based background subtraction method.

5.3.2 Comparison with RMA analysis of ClariomD/XTA assays

We then extended our characterization of GCS-score by comparing resulting analysis with a traditional RMA analysis for ClariomD/XTA arrays. In this use case, the GCS-score results were compared with RMA analysis results previously published in a study that utilizes ClariomD mouse arrays (aka MTA 1.0) to study effects of chronic diazepam (DZP) administration on gene expression in 3 mouse brain regions: cerebral cortex, hippocampus, and amygdala (Furukawa et al. 2017). The .CEL files used in the GCS-score analysis were pulled directly from the corresponding GEO dataset: GSE76700. For the purposes of this analysis of the GCS-score algorithm, we limited

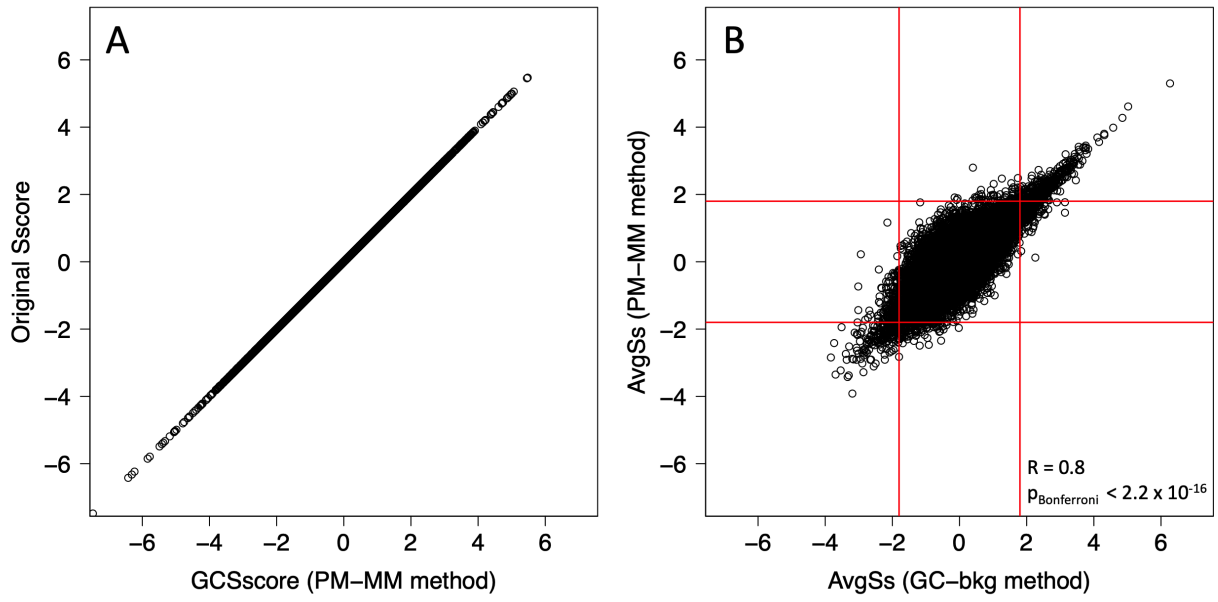

Figure 5.3: Comparison of results for original S-score algorithm (y-axis) and the GCS-score algorithm, using the PM-MM background correction method (x-axis). (B) Comparison of total averaged GCSscores (*AvgSs*) on the 3' IVT array, Mouse Genome 430 2.0 assay, for the GC-based background correction (x-axis) and the legacy PM-MM method (y-axis). The red lines denote the thresholds for significant Sscores ($|AvgSs| > 1.8$).

comparisons to just cerebral cortex. There were 3 biological replicates in both the treatment (DZP) and control group.

The original publication utilizes the standard workflow provided by Affymetrix's Transcriptome Analysis Console (TAC). Using statistical criteria without correction for multiple testing (ANOVA uncorrected p-value ≤ 0.05 and |log2 fold change| ≥ 1.5), the authors identify 57 total transcripts regulated by chronic diazepam in cerebral cortex (see Suppl. Table 1 from Furukawa et al. 2017). Additionally, the reported PANTHER gene ontology enrichment results show over-representation only for general large categories such as "binding" or "receptor activity" (see Figure 1.C from Furukawa et al. 2017). Only one gene, Lipocalin-2 (*Lcn2*), from the cortex results was replicated by quantitative PCR and used for further analysis, as it is the most strongly upregulated gene in all 3 brain regions investigated (Furukawa et al. 2017). Current literature reports suggest that *Lcn2* is implicated in innate immune responses via the sequestration of iron.

For the analysis of microarray data used the Furukawa publication, Sscores for the 3 treated and 3 control .CEL files were generated in the pairwise fashion described in Implementation. This results in 3 treatment replicate averages produced for each of 3 treatment sample against all of the control samples. These 3 treatment replicate averages were used as the input for SAM statistical analysis. The GCS-score algorithm produced 432 transcripts with the following criteria: SAM-based FDR $\leq .015$ and $|AvgSs| > 1.8$. Thus, the GCS-score method was able to produce many more significantly regulated transcripts with stringent multiple testing corrections, while the published RMA/LIMMA approach generated much smaller gene lists using uncorrected p values and modest fold changes produced from the standard TAC software. As expected, *Lcn2* (TC0200003303.mm.1) had very large positive Sscores for all comparisons, which resulted in an extremely high $AvgSs = 17.21$, replicating aspects of the results from the original publication. Strikingly, over-representation analysis of GCS-score results with ToppFun produced multiple categories directly related to diazepam/GABA biology (see Table 5.2), as should be expected from the experimental paradigm. GO categories of note included: drug binding, glutamate decarboxylase activity, synaptic signaling, GABAergic synapse, and GABA synthesis. Pathway analysis of

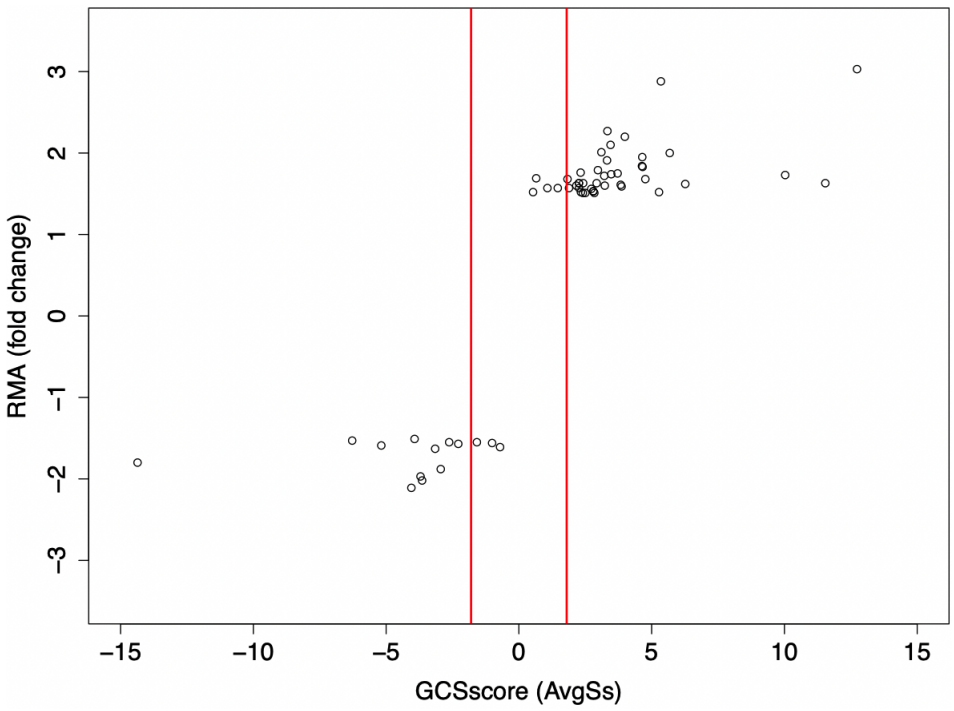

Figure 5.4: Fold change vs averaged GCSscore (*AvgSs*) for all publication-identified TCids in cerebral cortex from GEO dataset: GSE76700. The vertical red lines denote the significant threshold for the averaged GCSscore values ($|AvgSs| > 1.8$). 50 of the 57 identified TCids are also detected by the GCSscore method.

our GCS-score generated gene list via IPA produces multiple hits for immune-related signaling pathways, which supported the original findings from (Furukawa et al. 2017), in the context of the known functions of *Lcn2* (see Figure 5.5). Importantly, the top 20 pathways produced by IPA contained significant pathways for Glutamate degradation and GABA receptor signaling (see Figure 5.5). Furthermore, 50 of the 57 genes identified in Furukawa et al. 2017 had a study-wide $AvgSs > |1.8|$ and *AvgSs* values displayed a highly similar distribution to the originally published log2 fold-change values (see Figure 5.4).

The original publication also investigates *Lcn2* at the exon-level using the differential splicing functionality of the TAC software. The MTA 1.0 array has 15 PSRids (8 targeting exons) and 5 JUCids targeting splice junctions for the *Lcn2* transcript (see Table 5.3). The authors of the original publication deduce that the main transcript, *Lcn2*-201, is up-regulated rather than the only other protein-coding transcript variant, *Lcn2*-206 (see Figure 4.A from Furukawa et al. 2017).

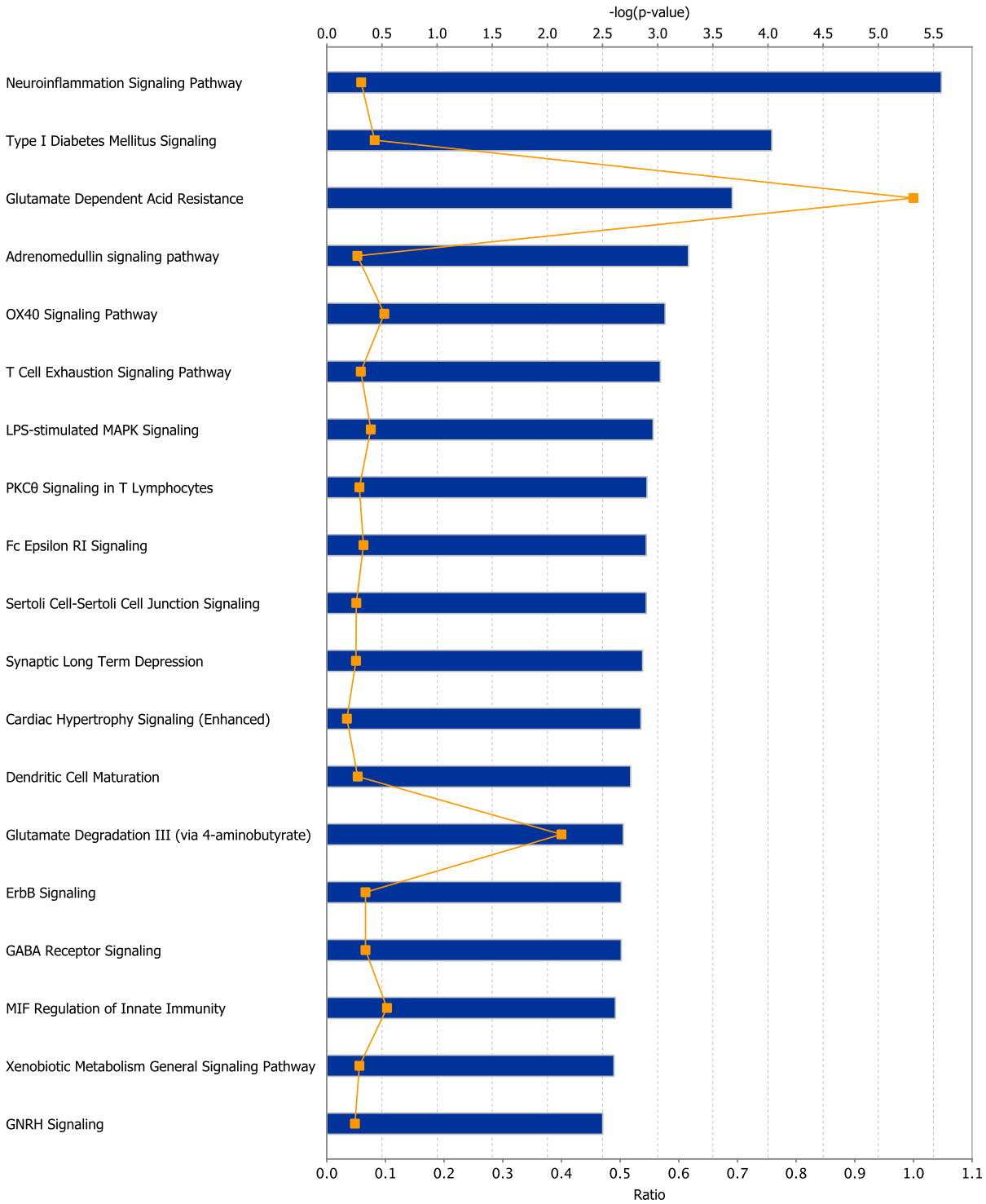

Figure 5.5: Functional pathway enrichment for GCS-score results for GEO dataset: GSE76700. Top 20 pathways returned from IPA

	ID	Name	p-value	FDR (B&H)
GO: Molecular Function				
	GO:0008144	drug binding	6.97e-05	2.11e-02
	GO:0032559	adenyl ribonucleotide binding	8.10e-05	2.11e-02
	GO:0030554	adenyl nucleotide binding	9.36e-05	2.11e-02
	GO:0051020	GTPase binding	1.03e-04	2.11e-02
	GO:0004351	glutamate decarboxylase activity	1.53e-04	2.13e-02
GO: Biological Process				
	GO:2001280	positive regulation of unsaturated fatty acid biosynthetic process	4.16e-06	1.91e-02
	GO:0045723	positive regulation of fatty acid biosynthetic process	1.62e-05	1.96e-02
	GO:0045923	positive regulation of fatty acid metabolic process	1.63e-05	1.96e-02
	GO:0099536	synaptic signaling	1.79e-05	1.96e-02
	GO:0098916	anterograde trans-synaptic signaling	3.25e-05	1.96e-02
GO: Cellular Component				
	GO:0030136	clathrin-coated vesicle	6.26e-07	3.52e-04
	GO:0045202	synapse	1.20e-05	2.68e-03
	GO:0030135	coated vesicle	1.43e-05	2.68e-03
	GO:0005938	cell cortex	2.67e-05	3.76e-03
	GO:0030054	cell junction	5.85e-05	5.70e-03
Pathway				
	1268766	Transmission across Chemical Synapses	2.54e-06	3.70e-03
	P00018	EGF receptor signaling pathway	2.70e-05	1.62e-02
	377263	GABAergic synapse	3.34e-05	1.62e-02
	M8353	Human Cytomegalovirus and Map Kinase Pathways	7.95e-05	2.90e-02
	1268763	Neuronal System	1.37e-04	3.30e-02
	83105	Pathways in cancer	1.52e-04	3.30e-02
	137938	IL2 signaling events mediated by PI3K	1.61e-04	3.30e-02
	1268775	GABA synthesis	2.02e-04	3.30e-02
Drug				
	ctd:D003024	Clozapine	4.37e-11	1.06e-06
	ctd:D020849	Raloxifene Hydrochloride	2.07e-10	2.01e-06
	ctd:D004390	Chlorpyrifos	2.49e-10	2.01e-06
	ctd:C548651	2-(1'H-indolo-3'-carbonyl)thiazole-4-carboxylic acid methyl ester	3.55e-09	2.15e-05
	CID000005637	U0126	9.57e-09	4.65e-05
Disease				
	C0027051	Myocardial Infarction	1.98e-06	6.85e-03
	C0006012	Borderline Personality Disorder	1.35e-05	2.29e-02
	C0917798	Cerebral Ischemia	2.32e-05	2.29e-02
	C0006287	Bronchopulmonary Dysplasia	2.65e-05	2.29e-02
	C0001430	Adenoma	5.34e-05	3.69e-02
	C0001973	Alcoholic Intoxication, Chronic	7.18e-05	4.14e-02

Table 5.2: Functional GO enrichment for GCS-score results for GEO dataset: GSE76700. Top 5 enrichments for the listed GO categories returned from ToppFun GO Suite

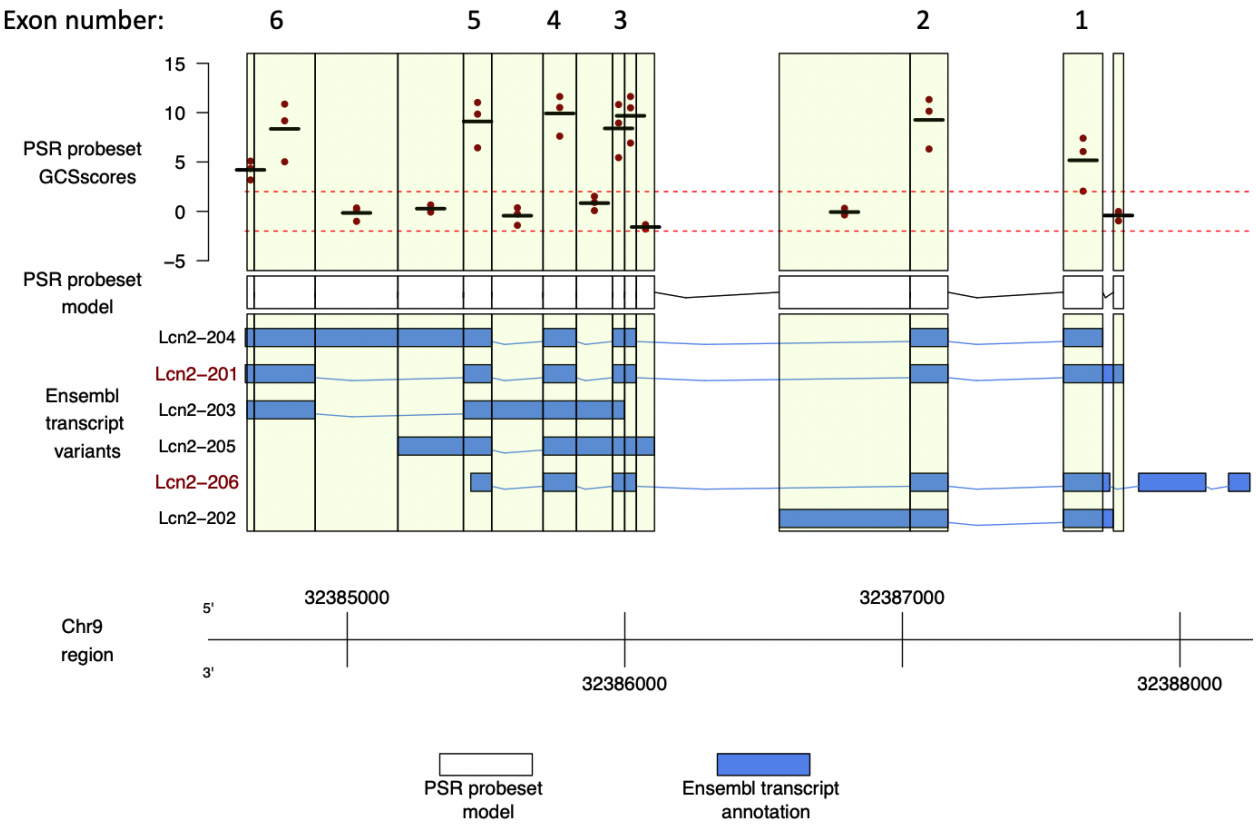

Figure 5.6: Exon- level GCGscores for *Lcn2* expression in GEO dataset: GSE76700. GCSscores for all PSRids assigned to *Lcn2*. The coverage segments of each PSRid is shown in the 'PSR probeset model' and in the highlighted segments of 'PSR probeset GCSscores' and 'Ensembl transcript variants'. *Lcn2* is on the negative strand, so exon 1 is on the right and exon 6 is on the left. Ensembl transcript variants that are 'protein-coding' are in red (*Lcn2*-201 and *Lcn2*-206). Figure demonstrates that PSRids in the introns of the *Lcn2*-201 are all non-significant, while all *Lcn2*-201 exons are upregulated. This rules out the non-coding transcript variants. There is significant upregulation of exon 6 of Ln2-201, which is not present in the other protein coding transcript, *Lcn2*-206.

probesetid	exon ID	GCSscore
PSR0200028082.mm.1	**exon6**	**4.201**
PSR0200028083.mm.1	**exon6**	**8.350**
PSR0200028084.mm.1	intron	-0.150
PSR0200028085.mm.1	intron	0.270
PSR0200028086.mm.1	**exon5**	**9.100**
PSR0200028087.mm.1	intron	-0.440
PSR0200028088.mm.1	**exon4**	**9.920**
PSR0200028089.mm.1	intron	0.830
PSR0200028090.mm.1	**exon3**	**8.400**
PSR0200028091.mm.1	**exon3**	**9.680**
PSR0200028092.mm.1	intron	-1.585
PSR0200028093.mm.1	intron	-0.071
PSR0200028094.mm.1	**exon2**	**9.260**
PSR0200028095.mm.1	**exon1**	**5.170**
PSR0200028098.mm.1	upstream intron	-0.420
JUC0200014167.mm.1	**exon5-exon6**	**5.100**
JUC0200014163.mm.1	**exon4-exon5**	**5.970**
JUC0200014164.mm.1	**exon3-exon4**	**6.190**
JUC0200014165.mm.1	**exon2-exon3**	**2.650**
JUC0200014166.mm.1	**exon1-exon2**	**4.420**

Table 5.3: GCS-score results for all 15 exon-level probesetids assigned to *Lcn2*. Probesetids in bold are either within an exon (PSR) or connect 2 exons (JUC).

Using the exon-level GCS-score method to analyze *Lcn2*, we found similar results to the original publication. The GCS-score method found that all 8 PSRids targeting exons were significantly upregulated, while none of the PSRids that targeted introns were altered (see Table-5.3 and Figure 5.4). Furthermore, all 5 of the JUCids were significantly upregulated in the GCS-score results. The genomic location of PSRids targeting introns suggest that the transcripts with retained introns (*Lcn*-202 to *Lcn2*-205) are unlikely to be regulated by the treatment (see Figure 4.A from Furukawa et al. 2017). Additionally, both PSRids in the final exon of Lcn-201 (exon 6), are significantly upregulated via the GCS-score method. Since exon 6 is not found in *Lcn2*-206, we could not fully eliminate the possibility of *Lcn2*-206 upregulation, but we confidently concluded that the main transcript, *Lcn2*-201, was upregulated and that *Lcn2* variants with retained introns were unlikely to be altered by diazepam treatment. This demonstrates the utility of GCS-score exon-level method for deducing which transcript variants are altered for the significantly regulated genes identified by the GCS-score gene-level method. These results implied that the GCSscore package a valuable

tool for both detecting significantly regulated genes and differential splicing analysis of exons for ClariomD/XTA type arrays.

5.3.3 Comparison with RMA analysis of ClariomS assays

A final comparison illustrates use of the GCS-score vs. RMA/LIMMA methods for analysis of published results with the ClariomS platform. As described in Wheeler et al. 2018, the original study utilizes ClariomS mouse arrays to investigate differential gene expression of mouse microglia cells 4 days after infection with the coronavirus, murine hepatitis virus (MHV). In this study, the authors generate a gene list using an FDR cutoff of 0.05 and a linear fold change with an absolute value greater than 2. The authors utilize IPA to produce enriched pathways for their significant genes (see figure 1.C from Wheeler et al. 2018). The authors find that interferon (IFN) signaling is the most upregulated pathway following infection, followed by 3 additional pathways linked directly to the immune system (Wheeler et al. 2018). They also report the expression metrics of 29 select genes from their gene list that were highly upregulated (see figure 1.D from Wheeler et al. 2018). All microarray data related to the microglial analysis in the Wheeler publication is available in GEO dataset: GSE103380. For GCS-score analysis, all 4 naïve (control) samples and all 4 infected samples in the GEO dataset were investigated, leading to 16 total pairwise comparisons of CEL files. As described above, the resulting 4 treatment replicate averages were interrogated by a 1-class SAM analysis to detect Sscores not equal to 0. This resulted in 486 genes that passed the determined selection criteria (FDR < 0.0125 and $|AvgSs| > 1.8$). The resulting gene list was input into both IPA and ToppFun for functional over-representation analysis as described in the Implementation section. The IPA analysis produced multiple pathways related to immune function, including the top pathways found in the original publication (see Figure 5.7). Of note, all top 10 pathways from the GCS-score analysis are related directly to immune response and function, which is an even stronger implication of the biological functions observed in the original published analysis (see Figure 1.C from Wheeler et al. 2018). Furthermore, 2 of the enriched pathways unique to the GCS-score results, “eIF2 Signaling” and “role of PKR in Interferon Induction and Antiviral Response”, are likely upstream of the interferon signaling pathways identified in both

methods. Recent literature has demonstrated that eIF2-alpha is integral for maximum production of inflammatory cytokines and type I interferons in response to microbial infection (Pierre 2019). This suggested that the GCS-score method was also able to identify potential important additional biological functions related to this experimental design. The ToppFun analysis was consistent with the IPA data, showing major enrichment for categories related to immune response and modulating interferon production during a viral infection (see Table 5.4). Additionally, *AvgSs* values displayed a high degree of correlation (see Figure 5.8) with the linear fold change values for significantly regulated genes identified by the authors of the original manuscript (S. Perlman, personal communication; data not shown). Finally, 24 of the 29 (83%) of the selected upregulated genes highlighted in the original publication (Figure 1.D from Xu et al. 2011) were also contained in the GCS-score derived gene list, demonstrating good overlap between the methods when the comparing the most differentially regulated transcripts that are identified by either method.

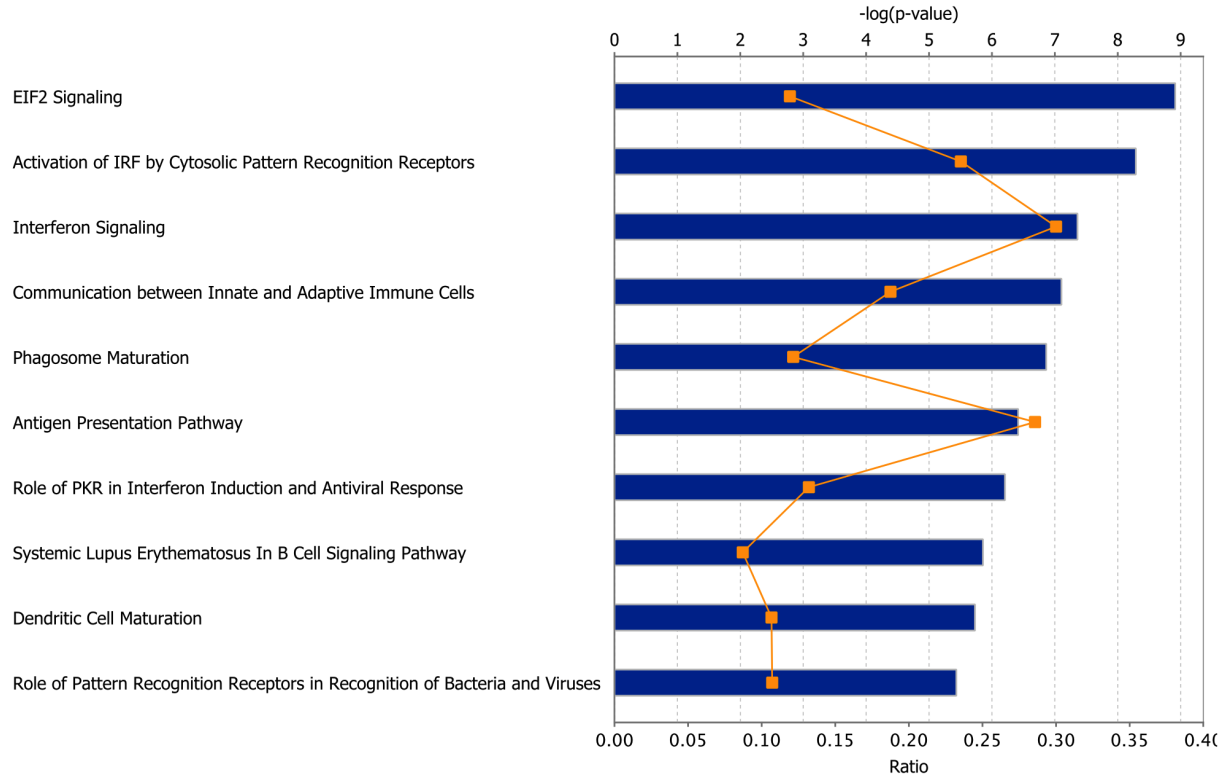

Figure 5.7: Top 10 enriched pathways via Ingenuity Pathway Analysis (IPA) for GCS-score analysis of GEO dataset: GSE103380

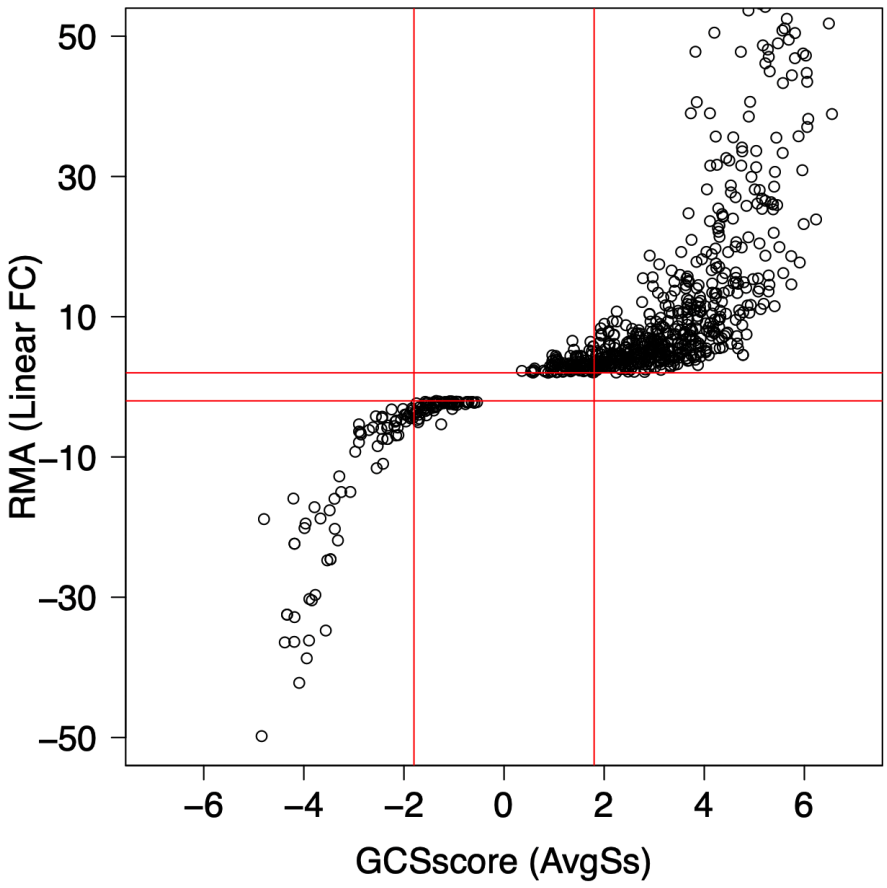

Figure 5.8: Correlation of *AvgSs* values with reported linear fold change (FC) for dataset: GSE103380. The vertical red lines denote the thresholds for significant Sscores ($|AvgSs| > 1.8$). The horizontal red lines denote the threshold for significant linear fold changes ($|\text{Linear FC})| > 2$).

	ID	Name	p-value	FDR (B&H)
GO: Molecular Function				
	GO:0003723	RNA binding	1.11e-10	1.18e-07
	GO:0017076	purine nucleotide binding	5.01e-08	2.16e-05
	GO:0003735	structural constituent of ribosome	6.07e-08	2.16e-05
	GO:0032555	purine ribonucleotide binding	1.48e-07	3.93e-05
	GO:0032553	ribonucleotide binding	2.09e-07	4.45e-05
GO: Biological Process				
	GO:0044403	symbiotic process	1.16e-35	6.36e-32
	GO:0016032	viral process	2.25e-35	6.36e-32
	GO:0044419	interspecies interaction between organisms	1.03e-34	1.93e-31
	GO:0051707	response to other organism	2.90e-32	3.06e-29
	GO:0009607	response to biotic stimulus	3.08e-32	3.06e-29
	GO:0043207	response to external biotic stimulus	3.25e-32	3.06e-29
	GO:0098542	defense response to other organism	9.85e-32	7.95e-29
	GO:0045087	innate immune response	3.58e-31	2.53e-28
	GO:0006952	defense response	4.28e-28	2.69e-25
	GO:0002252	immune effector process	3.18e-26	1.80e-23
GO: Cellular Component				
	GO:0022626	cytosolic ribosome	1.48e-15	1.01e-12
	GO:0005840	ribosome	2.06e-10	5.84e-08
	GO:0044391	ribosomal subunit	2.57e-10	5.84e-08
	GO:0005764	lysosome	4.85e-10	6.90e-08
	GO:0000323	lytic vacuole	5.05e-10	6.90e-08
Mouse Phenotype				
	MP:0005025	abnormal response to infection	5.88e-18	1.32e-14
	MP:0001793	altered susceptibility to infection	7.44e-18	1.32e-14
	MP:0002406	increased susceptibility to infection	3.38e-16	4.01e-13
	MP:0020185	altered susceptibility to viral infection	1.27e-14	1.13e-11
	MP:0002418	increased susceptibility to viral infection	2.17e-14	1.55e-11
Pathway				
	1269311	Interferon Signaling	1.95e-19	3.36e-16
	1269310	Cytokine Signaling in Immune system	4.81e-15	3.38e-12
	1269312	Interferon alpha/beta signaling	5.86e-15	3.38e-12
	1269108	Influenza Infection	3.72e-14	1.61e-11
	1268686	GTP hydrolysis and joining of the 60S ribosomal subunit	3.13e-13	7.91e-11
Disease				
	C0023893	Liver Cirrhosis, Experimental	1.08e-13	4.66e-10
	C0042769	Virus Diseases	1.34e-12	2.89e-09
	C0021400	Influenza	7.78e-12	9.47e-09
	C0024141	Lupus Erythematosus, Systemic	8.76e-12	9.47e-09
	C0019196	Hepatitis C	4.01e-11	2.90e-08

Table 5.4: Functional GO enrichment for GCS-score results for GEO dataset: GSE103380. Top 5 enrichments for the listed GO categories returned from ToppFun GO Suite

5.4 Discussion

Here we have described a new software methodology for analysis of the latest generation of Affymetrix/ThermoFisher microarrays, based upon a re-derivation of our original S-score algorithm that allows analysis of current oligonucleotide microarray platforms. Since microarray technology has inherent advantages for certain genomic studies compared to RNAseq, on the basis of costs and time required for analysis, such methodology development is of considerable significance. Furthermore, microarray studies continue to be utilized for thousands of publications in the published literature each year, thus documenting a sizeable ongoing scientific contribution. Our software development is an outgrowth of the original S-score method for probe-level analysis of Affymetrix arrays which has been previously validated as a sensitive method for differential gene expression analysis that was particularly valuable for studies employing low numbers of replicates (Zhang et al. 2002; Kennedy, Archer, and Miles 2006). Here we have presented three use cases to demonstrate that our new R package software and analysis algorithm, GCS-score, can provide analysis results equal to the prior S-score method for older generation (3' IVT) microarrays, while delivering substantial benefits compared to existing methods for analysis of the newest ClariomS/ClariomD/XTA arrays. We demonstrated that for 3' IVT arrays, GCS-score produced very similar differential gene expression analysis results compared to the original S-score method, which had been validated against multiple other algorithms, including RMA (Kennedy et al. 2006). We also found that the GCS-score method produced similar results to the existing RMA/LIMMA method for the ClariomS arrays. The results presented here suggest that GCS-score provides greater sensitivity for detection of DEG gene lists for the ClariomS assay, as evidenced by results of the IPA and ToppFun enrichments. In particular, the GCS-score method may provide more relevant pathways, including two potential upstream regulators of the interferon signaling identified in (Wheeler et al. 2018). Additionally, GCS-score produced a larger gene set than the methods used in (Xu et al. 2011) when using similar statistical thresholds (S. Perlman, personal communication; data not shown). Finally, we showed that GCS-score was far superior to the traditional RMA/LIMMA approach for analysis of ClariomD/XTA based studies. The GCS-score

algorithm was able to identify many significantly regulated transcripts that survived multiple test correction, while the RMA/LIMMA method returned very few transcripts, even with uncorrected p-values. Importantly, the GCS-score method led to increased biological insight that was consistent with the studied treatment, as evidenced by identification of multiple gene sets over-represented with functional groups and pathways related to GABA biology, as would be expected when profiling the cortex of chronically Diazepam-treated animals. In addition, the GCS-score exon-level analysis was capable of providing critical details regarding the regulation of individual transcript variants in genes that show significant regulation at the gene-level. Although not the object of this report, it is peculiar that the RMA/LIMMA methods appeared to work satisfactorily with ClariomS platforms, but failed to function sensitively for ClariomD/XTA assays. The ClariomS array is derived from the accompanying ClariomD/XTA array for each species (mouse, rat, human). In fact, multiple publications that use ClariomD/XTA arrays only report uncorrected p-values due to this limitation (Pierre 2019; Wolstenholme et al. 2017). The ClariomS arrays are composed of probes taken directly from the corresponding ClariomD/XTA array but utilizes only the 10 best performing probes for TCids that code for well annotated genes producing at least one protein-coding variant. Thus, ClariomD/XTA arrays target many more noncoding transcripts than protein-coding transcripts. Non-coding TCids on ClariomD/XTA arrays are the predominant probe type and tend to be expressed at very low or high levels compared to protein-coding gene probes (data not shown). We suggest that the LIMMA analysis of log2 RMA intensities from ClariomD/XTA arrays may be affected by the overwhelming number of noncoding transcripts found in these low and high intensity distributions. This disparate signal distribution might alter the normalization of RMA intensity results and thus increase signal/noise variance and thereby reduce statistically significant results from FDR analysis of these arrays. GCS-score is immune to this effect since it only considers the relative changes for each individual TCid/PSRid when making comparisons. These individual TCid/PSRid comparisons are independent of each other, so the coding transcripts are unaffected by the noncoding transcripts. Furthermore, we demonstrated that GCS-score is able to produce significant results for the ClariomD/XTA arrays with as few as 3 control and 3 treatment

arrays, which reduces the time and costs of genomic experiments that utilize this technology. These properties make the GCS-score method a powerful analysis tool for the most advanced array technology available on ClariomD/XTA arrays, as well as the ClariomS arrays. The new methodology described here also further supports the inherent strengths of the probe-level analysis provided by the GCS-score algorithm.

Chapter 6

Discussion, Conclusions, and Future Directions

6.1 Ethanol and Expression of *Ndrg1* in Oligodendrocytes

One of the most troubling questions regarding alcohol consumption is what drives some individuals to develop maladaptive and compulsive escalation of consumption of ethanol while other individuals are unaffected by early and even fairly regular consumption. As discussed in Chapter 2 and shown in Figure 2.1, basal levels of myelin expression in the frontal cortex are thought to play a role in acute behavioral sensitivity to ethanol, which is a risk factor for AUD, and myelin expression responses to ethanol are hypothesized as integral to the pathophysiology of brain maladaptation during chronic ethanol consumption (Schuckit et al. 1994; Costin and Miles 2014). Strong alterations in myelin related gene expression following ethanol exposures have been detected in both animal models and post-mortem human tissue (Lewohl et al. 2000; Kerns et al. 2005; Farris and Miles 2013; Bogenpohl et al. 2019). The genes that have been replicated across multiple studies and animal models, and the genes that have the strongest connectivity to other myelin related genes are promising candidates for mechanistic study in gene-targeted models of AUD. In studies described here, one such myelin-related gene, *Ndrg1*, was identified as a potential candidate gene that modulates ethanol-induced changes in myelin-related gene expression, acute behavioral sensitivity to ethanol, and long term ethanol consumption behavior.

This dissertation began by studying the localization of the NDRG1 protein within the mPFC, in terms of both cell type and sub-cellular localization. Here, our goal was to determine if NDRG1 was expressed in mPFC neurons, in addition to the known high expression in oligodendrocytes, given the preliminary lentiviral NDRG1 knockdown results described in Chapter 2. Those preliminary studies did not fully characterize the cellular site of lentiviral expression but it was presumed to largely be in neurons based upon preliminary immunolabeling of the injection site (see Figure 3.2). It was thus presumed that some NDRG1 expression must occur in neurons to explain

the alterations in ethanol behaviors seen after mPFC viral transduction. However, we ultimately determined that *Ndrg1* expression was exclusively within oligodendrocytes in the mPFC and likely the whole of the CNS, at least at the level detectable by immunofluorescence. This suggests that perhaps the lentiviral knockdown experiments described in Chapter 2 were altering *Ndrg1* expression in oligodendrocytes, since lentiviral vectors have been used to transduce multiple brain cell types. Single cell sequencing or qPCR would be a more sensitive technique to resolve this question ultimately. We also found that the localization of *Ndrg1* to cellular compartments or the myelin processes varied with phosphorylation at two different sites that are both phosphorylated by ethanol responsive kinase, *Sgk1*. Based on these findings, we wanted to explore how *Ndrg1* transcript and protein variants were altered by both acute and chronic ethanol.

6.2 Ethanol Modulates *Ndrg1* Expression Patterns

Previous works have shown that *Ndrg1* transcript and phosphorylation levels in the mPFC are altered following acute ethanol exposure in DBA2/J male mice (Kerns et al. 2005; Costin, Dever, and Miles 2013). However, the effects of chronic ethanol exposure on *Ndrg1* had not been previously studied prior to this work. Additionally, we conducted a more extensive probing of *Ndrg1* transcript and protein dynamics following acute ethanol. Furthermore, we also performed our studies in the C57BL/6J mouse strain to characterize *Ndrg1* responses in a strain widely used for studies on ethanol consumption behavior. DBA2/J mice consume only low levels of ethanol (Yoneyama et al. 2008). We found that acute ethanol induced *Ndrg1* transcript in the mPFC in female C57BL6/J mice at the highest ethanol dose (4 g/kg, i.p.), but not in male mice. Additionally, we observed a dose dependent decrease in levels of thr346-pNDRG1 in both sexes of mice following acute ethanol. Furthermore, we found a change in the nuclear/cytosol ratio of ser330-pNDRG1 in oligodendrocytes following acute ethanol (2 g/kg, i.p.) in male mice.

Conversely, little change in NDRG1 protein expression or phosphorylation was detected following chronic ethanol exposure. We recorded a significant induction of *Ndrg1* transcript in the mPFC following the 2-bottle choice drinking study, but failed to detect any changes in total or phospho-protein levels in the mPFC. Future works should follow-up with an IHC-based study to

detect any changes in the nuclear/cytosol ratio of pNDRG1 are present after chronic ethanol drinking. Evidence in Hela cells has suggested that the phosphorylation state as determined by electrophoretic mobility, from action of both *Sgk1* and *Gsk3*β, plays a role in the function of NDRG1 (Murray et al. 2004). While this group did not detect any changes of pNDRG1 localization in HeLa cells, others have reported the different phospho-forms of NDRG1 can display both cytoplasmic and nuclear localization (Lachat et al. 2002). As of the time of this dissertation work, neither the physiological functions of nuclear vs. cytoplasmic NDRG1 nor the role that phosphorylation plays on these functions is well understood.

One potentially interesting follow-up would be to design antibodies that target some of the residues that are phosphorylated by *Gsk3b*, since there are no commercially available antibodies that target residues phosphorylated by this kinase. However, we did not see any larger bands or true doublets when staining for NDRG1 following acute or chronic ethanol exposure, as was observed by Murray et al. 2004. This suggests that large changes in levels of GSK3B mediated phosphorylation of NDRG1 are not likely to occur following ethanol exposures.

6.3 *Ndrg1* Levels Modulate Ethanol-Related Behaviors

After characterizing the response of mPFC *Ndrg1* expression following both acute and chronic ethanol, the next major aim of this work investigated the effects of *Ndrg1* modulation in the myelin producing cells of the nervous system. Earlier preliminary lentiviral data demonstrated that knockdown of mPFC *Ndrg1* altered sensitivity to acute ethanol and shifted consumption to lower ethanol concentration solutions. Localization of the lentiviral vector expression suggested mainly neuronal localization (Figure 3.2), but close inspection of that data does identify occasional lentiviral expression in NeuN- cells (see Figure 3.2). Based upon data from the first aim of this thesis project, we were confident that *Ndrg1* expression was limited to oligodendrocytes in the mPFC. We therefore predicted that deletion of *Ndrg1* in oligodendrocytes might produce similar results to the lentiviral knockdown of *Ndrg1* in terms of ethanol behaviors. In fact, we did find very similar drinking behaviors regarding concentration preferences in a 3-bottle choice drinking model. It should be noted that the current studies included both male and female mice while the lentiviral studies only

utilized male mice. We did not replicate the acute ethanol sensitivity phenotype that was present in the lentiviral knockdown. We found no change in duration of LORR, but we did see a suggestion of a decrease in the onset time of the knockout mice. The LORR onset results do suggest that acute sensitivity to ethanol is in fact increased, while the acute functional tolerance is unchanged as indicated in the LORR duration data.

Several options exist to explain the apparent discrepancy between the prior lentiviral NDRG1 knockdown studies and the current studies reported in this thesis. It could be that the lentiviral shRNA is interacting with something off target in neurons to alter ethanol behavioral, since neurons were the overwhelming infected cell type in IHC validation (see Figure 3.2). However, as noted above, the lentiviral studies did appear to infect at least some non-neuronal cells. Unfortunately, further cell-type characterization of such cells was not done at the time. It could also be possible that the current studies producing a global knockout of *Ndrg1* in all myelinating cells resulted in a confounding behavioral phenotype that could be driving some of our results. It would also be worthwhile to conduct a LORR study at 3-6 months following the knockout of *Ndrg1*, instead of just one month. If there is a degradation of myelin function that is not recoverable following a re-population of *Ndrg1*-positive oligodendrocytes, then we could expect to see worse performance in the LORR challenge.

Additionally, the possible effect of the peripheral nerve dysfunction on the *Ndrg1* global myelin knockout cannot be ignored when considering the ethanol-related behaviors. Increased tactile hypersensitivity in the knockout could, for example, modify ethanol behaviors. A strong followup to this work would include experiments with a newly generated *Ndrg1*-floxed mouse line. Here, a Cre-expressing virus targeted to oligodendrocytes or neurons could be precisely delivered into the mPFC region by stereotactic injection. This would be of great use to help determine if the peripheral effects of *Ndrg1* deletion or the deletion of *Ndrg1* in other brain regions or cell types is driving some of our behavioral data.

6.4 *Ndrg1* Levels Modulate Peripheral Nerve Function

The effects of functional deletion of *Ndrg1* on the peripheral nervous system has been documented throughout this work. Previous studies with *Ndrg1* mutations or deletions in mice and humans have demonstrated that peripheral myelination proceeds normally until adolescence begins. The degradation of myelin at this later stage led experimenters to suggest that *Ndrg1* deletion leads to myelin degradation during myelination bursts in particular (Okuda et al. 2004). In this work, we generated a novel mouse line that allowed us to delete *Ndrg1* in adult mice following the myelination burst that occurs in adolescence. Ultimately, we found that deletion of *Ndrg1* led to rapid and permanent development of very high levels of mechanical and thermal sensitivity. We found that both the velocity and the amplitude of sciatic nerve conduction was diminished in *Ndrg1* knockout mice 6 months post deletion. This demonstrated that ongoing expression of *Ndrg1* is in fact essential for the maintenance of peripheral myelin and axonal function.

Additionally, we used our animal model to show that knockout mice that receive low doses of Paclitaxel shortly after the induction of *Ndrg1* deletion develop mechanical sensitivity much more rapidly than knockout mice that received vehicle or control mice treated with Paclitaxel. This novel study provided crucial experimental validation of a clinical observation that nerve levels of *Ndrg1* in human breast cancer patients was inversely correlated with severity of Paclitaxel induced neuropathy (Sundar et al. 2016).

In an effort to probe for cross-talk between the peripheral effects of *Ndrg1* and high levels of ethanol exposure, we attempted to ascertain if repeated high doses of ethanol could speed the development of nerve dysfunction following *Ndrg1* deletion. While we did not find any effect of acute high doses of ethanol on the development of mechanical or cold sensitivity, it was a limited experimental design that captured a very short time window. It could be that more chronic exposures to ethanol are needed to further drive nerve dysfunction. For both the low dose Paclitaxel and any additional ethanol exposure studies, it would be interesting to perform nerve conduction velocity testing at the 6 month point following knockout. It would not be surprising to see further deficits in both amplitude and velocity in knockout mice that received the experimental insults.

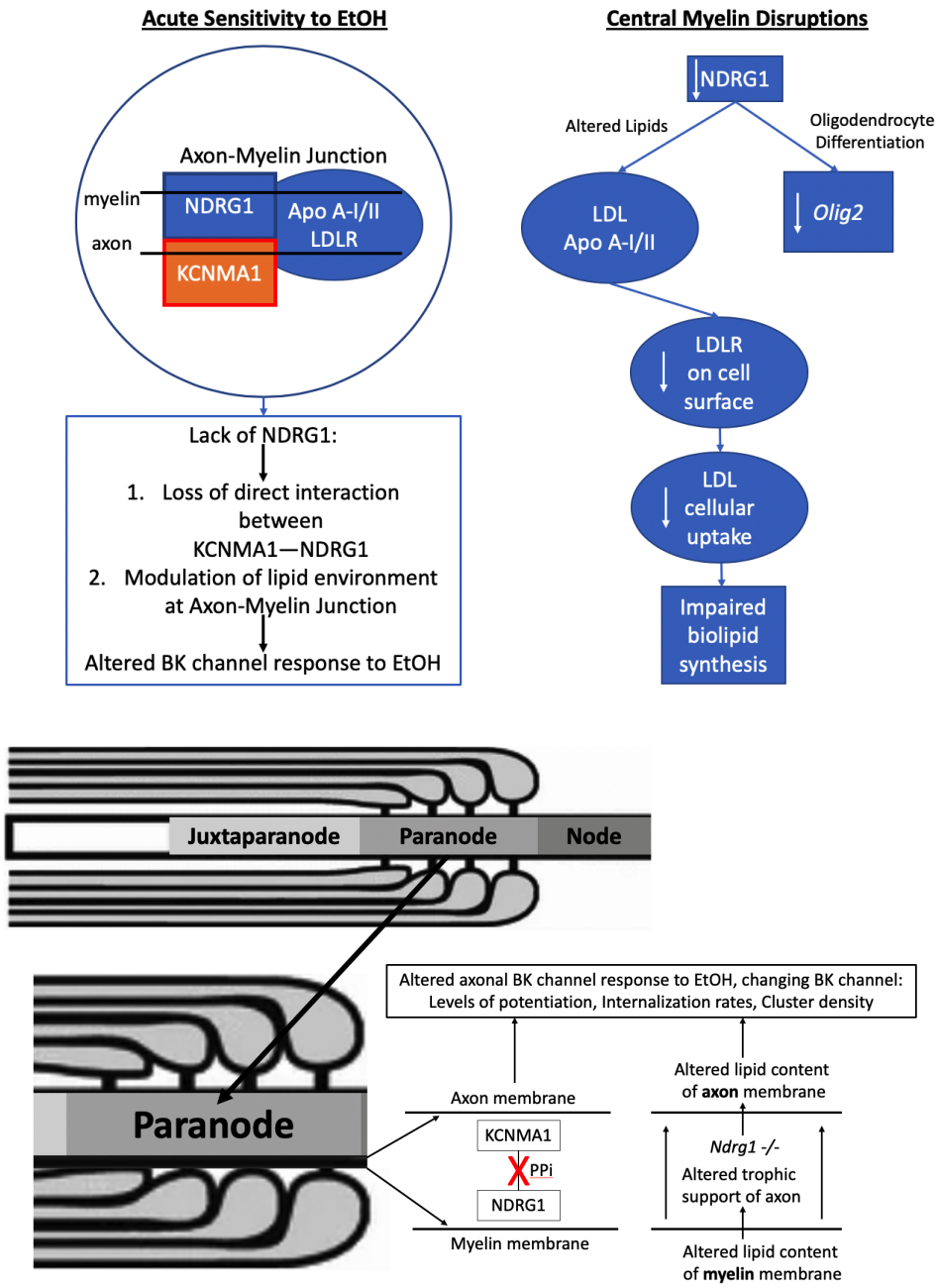

Figure 6.1: Theories for role of *Ndrg1* in modulation of acute ethanol sensitivity and normal myelin function. Top: Overview of proposed mechanisms for modulation of acute sensitivity to ethanol (left) and for the defects that occur in central myelin (right) following *Ndrg1* deletion. Bottom: Detailed view of proposed mechanism for modulation of ethanol sensitivity. Both NDRG1 and KCNMA1 have been identified in the paranodal region of CNS axons and direct protein-protein interactions (PPi) between KCNMA1 and NDRG1 have been observed. We propose that either the direct PPi of NDRG1 and KCNMA1, or the modulation axonal lipid environment surrounding KCNMA1 is responsible for the NDRG1-induced changes in acute ethanol sensitivity. Given that *Ndrg1* deletion did not change LORR onset or duration, we suggest that the possible *Ndrg1* induced modulation of the lipid content of the paranodal axonal membrane is more likely.

6.5 Theories for Observed Effects of *Ndrg1* Deletion

Given the number of diverse behavioral responses that are observed following *Ndrg1* deletion, it seems likely that multiple mechanisms are at play. Here, we suggest that two interconnected mechanisms are driving the two noted phenotypes: peripheral nerve dysfunction and altered sensitivity to ethanol. As described in detail in Chapter 2, there is ample evidence that *Ndrg1* is important for cellular bio-lipid metabolism. These deficits in metabolism in particular could be why dysfunction does not occur until myelin production is dramatically up-regulated during the myelination burst that occurs at adolescence. Thus, *Ndrg1* may truly be critical for ongoing myelin maintenance. Given the heavy lipid content of myelin, any deficits in lipid metabolism could result in a loss of stability to the myelin ultrastructure (see Figure 6.1).

Prior works have found that loss of function mutations in the NDRG1 homolog in *C. elegans* alters their acute functional tolerance to ethanol exposure (Farris et al., manuscript in preparation). This is very interesting given that *C. elegans* do not contain any myelin, but instead have an alternate glial-based support network for axons (Stout, Verkhratsky, and Parpura 2014). We know from prior works that one of the main modulators of acute sensitivity to ethanol in *C. elegans* is the *Slo1* calcium-activated potassium channel activity (*Kcnma1* in mice) along axons (Bettinger and Davies 2014). In this publication, Bettinger and Davies also noted that many previous studies had already determined that lipid environment surrounding the channel has large effects on the channel sensitivity to ethanol. Furthermore, a previous study that utilized co-immunoprecipitation with KCNMA1 as the bait found a unique protein-protein interaction with NDRG1, as shown in Figure 6.1 (Kathiresan et al. 2009).

Based on our results and the findings in the literature, we propose that *Ndrg1* affects the bio-lipid synthesis of the myelin producing cells and thus the lipid composition of myelin. NDRG1 is also localized to the myelin lamellar membrane processes, and it perhaps influences the trafficking of lipids to the myelin process. The lipid composition on the interface between the axon and the adjacent myelin membrane is responsible for the normal function and response of BK channels on the axon (see Figure 6.1), particularly in the presence of ethanol. In this way, the effect of *Ndrg1*

on lipid metabolism and trafficking is driving the degradation of peripheral nerve function as the Schwann cells cannot meet lipid demands. Conversely, in the CNS, *Ndrg1*-induced alterations in lipid dynamics of oligodendrocytes might directly modulate the BK channels along axons, which could result in significant changes in the sensitivity of the BK channel response to ethanol.

To begin testing these theories, it would be useful to utilize confocal IHC to determine overlap of anti-KCNMA1 antibody along axons with the anti-NDRG1 antibody along the myelin processes. We predict that a noted co-localization of these proteins will occur along the myelin process-axon junction. It would also be of interest to stain with additional markers, such as sodium channels, to further understand how *Ndrg1* interacts with various compartments of the axon it surrounds. Additionally, it is remarkable how much more severe (in terms of myelin structure) the peripheral effects of *Ndrg1* deletion are than the central effects. It is unknown if different pathways are affected or if compensatory mechanisms exist in the CNS relative to the PNS. We propose a microarray/RNAseq experiment that will analyze the transcriptome response to knockout of *Ndrg1* in both sciatic nerve and in the mPFC. The genomic study should help dissect which pathways and mechanisms are most affected in each region, providing a more clear understanding of the role of *Ndrg1* in both the PNS and the CNS.

6.6 Concluding Remarks

The work presented in this dissertation sought to illuminate the frontal cortex response to ethanol in relation to *Ndrg1* expression and how *Ndrg1* deletion alters ethanol-related behaviors. We also sought to answer questions of how temporal knockout of *Ndrg1* produces its most well characterized phenotype: peripheral neuropathy. Our findings demonstrate that *Ndrg1* expression and functional state, as determined by phosphorylation and localization, are clearly modulated by acute and/or chronic ethanol. We also found that deletion of *Ndrg1* in myelinating cells alters ethanol-related behaviors in a way that suggests sensitivity to ethanol is modified. The literature and our results suggest that cellular bio-lipids and lipid interactions with BK channels, such as *Kcnma1*, are key drivers for both the peripheral nerve dysfunction and the changes in ethanol sensitivity, but more studies are needed to prove this hypothesis. We demonstrated the impor-

tance of *Ndrg1* for peripheral nerve function and that decreasing levels of *Ndrg1* are a risk factor for increased toxic effects of chemotherapeutics. Ultimately, the works presented here demonstrate the biological importance of *Ndrg1* in the maintenance of peripheral nerve function and as an ethanol-related gene that modulates ethanol sensitivity, consumption, and risk for developing AUD.

References

Adkins, Daniel E, Shaunna L Clark, William E Copeland, Martin Kennedy, Kevin Conway, Adrian Angold, Hermine Maes, Youfang Liu, Gaurav Kumar, Alaattin Erkanli, Ashwin A Patkar, Judy Silberg, Tyson H. Brown, David M. Fergusson, L. John Horwood, Lindon Eaves, Edwin J. C. G. van den Oord, Patrick F Sullivan, and E. J. Costello. 2015. "Genome-Wide Meta-Analysis of Longitudinal Alcohol Consumption Across Youth and Early Adulthood." *Twin Research and Human Genetics* 18 (4): 335–347 (aug).

Affymetrix, Inc. 2005. "Exon Array Background Correction." *Affymetrix White Paper*, pp. 1–5.

American Psychiatric Association. 2013. *Diagnostic and statistical manual of mental disorders: DSM-5*. 5th ed. Washington, DC: Autor.

Belknap, John K., Pamela Metten, Ethan H. Beckley, and John C. Crabbe. 2008. "Multivariate analyses reveal common and drug-specific genetic influences on responses to four drugs of abuse." *Trends in Pharmacological Sciences* 29 (11): 537–543.

Berger, Philipp, Erich E. Sirkowski, Steven S. Scherer, and Ueli Suter. 2004. "Expression analysis of the N-Myc downstream-regulated gene 1 indicates that myelinating Schwann cells are the primary disease target in hereditary motor and sensory neuropathy-Lom." *Neurobiology of Disease* 17 (2): 290–299.

Bettinger, Jill C., and Andrew G. Davies. 2014. "The role of the BK channel in ethanol response behaviors: Evidence from model organism and human studies." *Frontiers in Physiology* 5 AUG (September): 1–9.

Blednov, Yuri A, Jillian M Benavidez, Mendy Black, and R Adron Harris. 2014. "Inhibition of phosphodiesterase 4 reduces ethanol intake and preference in C57BL/6J mice." *Frontiers in neuroscience* 8:129.

Blednov, Yuri A, Adriana J Da Costa, R Adron Harris, and Robert O Messing. 2018. "Apremilast Alters Behavioral Responses to Ethanol in Mice: II. Increased Sedation, Intoxication, and Reduced Acute Functional Tolerance." *Alcoholism, clinical and experimental research* 42 (5): 939–951.

Bogenpohl, James W., Maren L. Smith, Sean P. Farris, Catherine I. Dumur, Marcelo F. Lopez, Howard C. Becker, Kathleen A. Grant, and Michael F. Miles. 2019. "Cross-Species Co-analysis of Prefrontal Cortex Chronic Ethanol Transcriptome Responses in Mice and Monkeys." *Frontiers in Molecular Neuroscience* 12 (August): 1–18.

Carlson, Marc, and Valerie Obenchain. 2015. "AnnotationForge: Tools for building SQLite-based annotation data packages." *Bioconductor* 3.11 (R package version 1.28.0): 1–21.

Cen, Gang, Zhang Kundong, Jun Cao, and Zhengjun Qiu. 2017. "Downregulation of the N-myc downstream regulated gene 1 is related to enhanced proliferation, invasion and migration of

pancreatic cancer." *Oncology Reports* 37 (2): 1189–1195.

Chandler, David, Sash Lopaticki, Dexing Huang, Michael Hunter, Dora Angelicheva, Trevor Kilpatrick, Rosalind HM King, Luba Kalaydjieva, and Grant Morahan. 2013. "The stretcher spontaneous neurodegenerative mutation models Charcot-Marie-Tooth disease type 4D." *F1000Research* 2:46.

Chesler, Elissa J, Lu Lu, Siming Shou, Yanhua Qu, Jing Gu, Jintao Wang, Hui Chen Hsu, John D Mountz, Nicole E Baldwin, Michael A Langston, David W Threadgill, Kenneth F Manly, and Robert W Williams. 2005. "Complex trait analysis of gene expression uncovers polygenic and pleiotropic networks that modulate nervous system function." *Nature Genetics* 37 (3): 233–242 (mar).

Chopra, Kanwaljit, and Vinod Tiwari. 2012. "Alcoholic neuropathy: Possible mechanisms and future treatment possibilities." *British Journal of Clinical Pharmacology* 73 (3): 348–362.

Colville, A. M., O. D. Iancu, D. L. Oberbeck, P. Darakjian, C. L. Zheng, N A R Walter, C. A. Harrington, R. P. Searles, S. McWeeney, and R. J. Hitzemann. 2017. "Effects of selection for ethanol preference on gene expression in the nucleus accumbens of HS-CC mice." *Genes, brain, and behavior* 16 (4): 462–471.

Costin, Blair N, Seth M Dever, and Michael F Miles. 2013. "Ethanol regulation of serum glucocorticoid kinase 1 expression in DBA2/J mouse prefrontal cortex." *PloS one* 8 (8): e72979 (jan).

Costin, B.N., and M.F. Miles. 2014. "Molecular and neurologic responses to chronic alcohol use." Chapter 10 of *Handbook of clinical neurology*, Volume 125, 1, 157–171. Elsevier B.V.

Crabbe, John C, Richard L Bell, and Cindy L Ehlers. 2010. "Human and laboratory rodent low response to alcohol: is better consilience possible?" *Addiction biology* 15 (2): 125–44 (apr).

Crowley, John J, Steven N Treistman, and Alejandro M Dopico. 2003. "Cholesterol antagonizes ethanol potentiation of human brain BKCa channels reconstituted into phospholipid bilayers." *Molecular pharmacology* 64 (2): 365–72 (aug).

Dacković, J, M. Keckarević-Marković, Z. Komazec, V Rakocević-Stojanović, D. Lavrnić, Z. Stević, K. Ribarić, S. Romac, and S. Apostolski. 2008. "Hereditary motor and sensory neuropathy Lom type in a Serbian family." *Acta myologica : myopathies and cardiomyopathies : official journal of the Mediterranean Society of Myology* 27 (OCT.): 59–62 (oct).

Deehan, Gerald A., Mark S. Brodie, and Zachary A. Rodd. 2013. "What is in that drink: the biological actions of ethanol, acetaldehyde, and salsolinol." *Current topics in behavioral neurosciences* 13 (November 2011): 163–84.

Echaniz-Laguna, Andoni, Bertrand Degos, Céline Bonnet, Philippe Latour, Tarik Hamadouche, Nicolas Lévy, and Bruno Leheup. 2007. "NDRG1-linked Charcot-Marie-Tooth disease

(CMT4D) with central nervous system involvement." *Neuromuscular disorders : NMD* 17 (2): 163–8 (feb).

Edenberg, Howard J. 2007. "The genetics of alcohol metabolism: Role of alcohol dehydrogenase and aldehyde dehydrogenase variants." *Alcohol Research and Health* 30 (1): 5–13.

Farris, Sean P., and Michael F. Miles. 2013. "Fyn-dependent gene networks in acute ethanol sensitivity." *PLoS ONE* 8 (11): 1–17.

Fritz, B. M., N. J. Grahame, and S. L. Boehm. 2013. "Selection for high alcohol preference drinking in mice results in heightened sensitivity and rapid development of acute functional tolerance to alcohol's ataxic effects." *Genes, Brain and Behavior* 12 (1): 78–86.

Furukawa, Tomonori, Shuji Shimoyama, Yasuo Miki, Yoshikazu Nikaido, Kohei Koga, Kazuhiko Nakamura, Koichi Wakabayashi, and Shinya Ueno. 2017. "Chronic diazepam administration increases the expression of Lcn2 in the CNS." *Pharmacology Research & Perspectives* 5 (1): e00283 (feb).

Gilman, Jodi M, Vijay a Ramchandani, Tess Crouss, and Daniel W Hommer. 2012. "Subjective and Neural Responses to Intravenous Alcohol in Young Adults with Light and Heavy Drinking Patterns." *Neuropsychopharmacology* 37 (2): 467–477.

Goodwin, Donald W. 1974. "Drinking Problems in Adopted and Nonadopted Sons of Alcoholics." *Archives of General Psychiatry* 31 (2): 164 (aug).

Grice, Dorothy E, Ilkka Reenilä, Pekka T Männistö, Andrew I Brooks, George G Smith, Greg T Golden, Joseph D Buxbaum, and Wade H Berrettini. 2007. "Transcriptional profiling of C57 and DBA strains of mice in the absence and presence of morphine." *BMC genomics* 8 (1): 76 (mar).

Heller, Bradley A., Monica Ghidinelli, Jakob Voelkl, Steven Einheber, Ryan Smith, Ethan Grund, Grant Morahan, David Chandler, Luba Kalaydjieva, Filippo Giancotti, Rosalind H. King, Aniko Naray Fejes-Toth, Gerard Fejes-Toth, Maria Laura Feltri, Florian Lang, and James L. Salzer. 2014. "Functionally distinct PI 3-kinase pathways regulate myelination in the peripheral nervous system." *Journal of Cell Biology* 204 (7): 1219–1236.

Hirono, M., Y. Ogawa, K. Misono, D. R. Zollinger, J. S. Trimmer, M. N. Rasband, and H. Misonou. 2015. "BK Channels Localize to the Paranodal Junction and Regulate Action Potentials in Myelinated Axons of Cerebellar Purkinje Cells." *Journal of Neuroscience* 35 (18): 7082–7094 (may).

Hunter, Michael, Dora Angelicheva, Ivailo Tournev, Evan Ingley, Dick C Chan, Gerald F Watts, Ivo Kremensky, and Luba Kalaydjieva. 2005. "NDRG1 interacts with APO A-I and A-II and is a functional candidate for the HDL-C QTL on 8q24." *Biochemical and biophysical research communications* 332 (4): 982–92 (jul).

Irizarry, Rafael A, Bridget Hobbs, Francois Collin, Yasmin D Beazer-Barclay, Kristen J Antonellis, Uwe Scherf, and Terence P Speed. 2003. "Exploration, normalization, and summaries of high density oligonucleotide array probe level data." *Biostatistics (Oxford, England)* 4 (2): 249–64 (apr).

Jin, Runsen, Wensheng Liu, Sharleen Menezes, Fei Yue, Minhua Zheng, Zaklina Kovacevic, and Des R. Richardson. 2014. "The metastasis suppressor NDRG1 modulates the phosphorylation and nuclear translocation of ß-catenin through mechanisms involving FRAT1 and PAK4." *Journal of Cell Science* 127 (14): 3116–3130.

Kalsi, Gursharan, Carol A. Prescott, Kenneth S. Kendler, and Brien P. Riley. 2009. "Unraveling the molecular mechanisms of alcohol dependence." *Trends in genetics : TIG* 25 (1): 49–55 (jan).

Kathiresan, Thandavarayan, Margaret Harvey, Sandra Orchard, Yoshihisa Sakai, and Bernd Sokolowski. 2009. "A Protein Interaction Network for the Large Conductance Ca ²⁺ -activated K ⁺ Channel in the Mouse Cochlea." *Molecular & Cellular Proteomics* 8 (8): 1972–1987.

Kennedy, Richard E, Kellie J Archer, and Michael F Miles. 2006. "Empirical validation of the S-Score algorithm in the analysis of gene expression data." *BMC bioinformatics* 7 (jan): 154.

Kennedy, Richard E, Robnet T Kerns, Xiangrong Kong, Kellie J Archer, and Michael F Miles. 2006. "SScore: an R package for detecting differential gene expression without gene expression summaries." *Bioinformatics (Oxford, England)* 22 (10): 1272–4 (may).

Kerns, Robnet T, Ajay Ravindranathan, Sajida Hassan, Mary P Cage, Tim York, James M Sikela, Robert W Williams, and Michael F Miles. 2005. "Ethanol-responsive brain region expression networks: implications for behavioral responses to acute ethanol in DBA/2J versus C57BL/6J mice." *The Journal of neuroscience : the official journal of the Society for Neuroscience* 25 (9): 2255–66 (mar).

Kim, Kyung-Tae, Pat P Ongusaha, Young-Kwon Hong, Siavash K Kurdistani, Masafumi Nakamura, Kun Ping Lu, and Sam W Lee. 2004. "Function of Drg1/Rit42 in p53-dependent mitotic spindle checkpoint." *The Journal of biological chemistry* 279 (37): 38597–602 (sep).

King, Rosalind H M, David Chandler, Sash Lopaticki, Dexing Huang, Julian Blake, John R. Muddle, Trevor Kilpatrick, Michelle Nourallah, Toshiyuki Miyata, Tomohiko Okuda, Kim W. Carter, Michael Hunter, Dora Angelicheva, Grant Morahan, and Luba Kalaydjieva. 2011. "Ndrg1 in development and maintenance of the myelin sheath." *Neurobiology of Disease* 42 (3): 368–380.

Kitabayashi, Tamotsu, Shinichi Demura, Masahiro Noda, and Takayoshi Yamada. 2004. "Gender Differences in Body-Sway Factors of Center of Foot Pressure in a Static Upright Posture and under the Influence of Alcohol Intake." *Journal of PHYSIOLOGICAL ANTHROPOLOGY and Applied Human Science* 23 (4): 111–118.

Koike, H., K. Mori, K. Misu, N. Hattori, H. Ito, M. Hirayama, and G. Sobue. 2001. "Painful alcoholic polyneuropathy with predominant small-fiber loss and normal thiamine status." *Neurology* 56 (12): 1727–1732.

Koike, Haruki, Masahiro Iijima, Makoto Sugiura, Keiko Mori, Naoki Hattori, Hiroki Ito, Masaaki Hirayama, and Gen Sobue. 2003. "Alcoholic neuropathy is clinicopathologically distinct from thiamine-deficiency neuropathy." *Annals of Neurology* 54 (1): 19–29.

Kranzler, Henry R., Hang Zhou, Rachel L. Kember, Rachel Vickers Smith, Amy C. Justice, Scott Damrauer, Philip S. Tsao, Derek Klarin, Aris Baras, Jeffrey Reid, John Overton, Daniel J. Rader, Zhongshan Cheng, Janet P. Tate, William C. Becker, John Concato, Ke Xu, Renato Polimanti, Hongyu Zhao, and Joel Gelernter. 2019. "Genome-wide association study of alcohol consumption and use disorder in 274,424 individuals from multiple populations." *Nature Communications* 10 (1): 1499 (dec).

Kril, J. J., G. M. Halliday, M. D. Svoboda, and H. Cartwright. 1997. "The cerebral cortex is damaged in chronic alcoholics." *Neuroscience* 79 (4): 983–98 (aug).

Lachat, Pascale, Philip Shaw, Sandra Gebhard, Nico van Belzen, Pascal Chaubert, and Fred T. Bosman. 2002. "Expression of NDRG1, a differentiation-related gene, in human tissues." *Histochemistry and cell biology* 118 (5): 399–408 (nov).

Lee, Rico S C, Sylco Hoppenbrouwers, and Ingmar Franken. 2019. "A Systematic Meta-Review of Impulsivity and Compulsivity in Addictive Behaviors." *Neuropsychology review* 29 (1): 14–26 (mar).

Lewohl, J M, L Wang, M F Miles, L Zhang, P R Dodd, and R a Harris. 2000. "Gene expression in human alcoholism: microarray analysis of frontal cortex." *Alcoholism, clinical and experimental research* 24 (12): 1873–1882.

Liu, Jianwen, Joanne M Lewohl, R Adron Harris, Vishwanath R Iyer, Peter R Dodd, Patrick K Randall, and R Dayne Mayfield. 2006. "Patterns of gene expression in the frontal cortex discriminate alcoholic from nonalcoholic individuals." *Neuropsychopharmacology : official publication of the American College of Neuropsychopharmacology* 31 (7): 1574–82 (jul).

Liu, Wen, Fei Xing, Megumi Iiizumi-Gairani, Hiroshi Okuda, Misako Watabe, Sudha K. Pai, Puspa R. Pandey, Shigeru Hirota, Aya Kobayashi, Yin Yuan Mo, Koji Fukuda, Yi Li, and Kounosuke Watabe. 2012. "N-myc downstream regulated gene 1 modulates Wnt-β-catenin signalling and pleiotropically suppresses metastasis." *EMBO Molecular Medicine* 4 (2): 93–108.

Liu, Xiao, Yanan Wang, Di Wu, Shuangqiu Li, Chaoqun Wang, Zhen Han, Jingjing Wang, Kai Wang, Zhengtao Yang, and Zhengkai Wei. 2019. "Magnolol prevents acute alcoholic liver damage by activating PI3K/Nrf2/PPARγ and inhibiting NLRP3 signaling pathway." *Frontiers in Pharmacology* 10 (December): 1–11.

Matsuoka, T., M. Yashiro, N. Nishioka, K. Hirakawa, K. Olden, and J. D. Roberts. 2012. "PI3K/Akt signalling is required for the attachment and spreading, and growth in vivo of metastatic scirrhous gastric carcinoma." *British journal of cancer* 106 (9): 1535–42 (apr).

Mayfield, R. Dayne, Joanne M. Lewohl, Peter R. Dodd, Amy Herlihy, Jianwen Liu, and R. Adron Harris. 2002. "Patterns of gene expression are altered in the frontal and motor cortices of human alcoholics." *Journal of Neurochemistry* 81 (4): 802–813 (may).

McCaig, Catherine, Louisa Potter, Olga Abramczyk, and James T Murray. 2011. "Phosphorylation of NDRG1 is temporally and spatially controlled during the cell cycle." *Biochemical and biophysical research communications* 411 (2): 227–234.

Metten, P, T J Phillips, J C Crabbe, L M Tarantino, G E McClearn, R Plomin, V G Erwin, and J K Belknap. 1998. "High genetic susceptibility to ethanol withdrawal predicts low ethanol consumption." *Mammalian genome : official journal of the International Mammalian Genome Society* 9 (12): 983–90 (dec).

Misonou, Hiroaki, Milena Menegola, Lynn Buchwalder, Eunice W Park, Andrea Meredith, Kenneth J Rhodes, Richard W Aldrich, and James S Trimmer. 2006. "Immunolocalization of the Ca2+-activated K+ channel Slo1 in axons and nerve terminals of mammalian brain and cultured neurons." *The Journal of comparative neurology* 496 (3): 289–302 (may).

Mokdad, Ali H. 2004. "Actual Causes of Death in the United States, 2000." *JAMA* 291 (10): 1238 (mar).

Murakami, Yuichi, Fumihito Hosoi, Hiroto Izumi, Yuichiro Maruyama, Hiroki Ureshino, Kosuke Watari, Kimitoshi Kohno, Michihiko Kuwano, and Mayumi Ono. 2010. "Identification of sites subjected to serine/threonine phosphorylation by SGK1 affecting N-myc downstream-regulated gene 1 (NDRG1)/Cap43-dependent suppression of angiogenic CXC chemokine expression in human pancreatic cancer cells." *Biochemical and biophysical research communications* 396 (2): 376–81 (may).

Murray, James T, David G Campbell, Nicholas Morrice, Gillian C Auld, Natalia Shpiro, Rodolpho Marquez, Mark Peggie, Jenny Bain, Graham B Bloomberg, Florian Grahammer, Florian Lang, Peer Wulff, Dietmar Kuhl, and Philip Cohen. 2004. "Exploitation of KESTREL to identify NDRG family members as physiological substrates for SGK1 and GSK3." *The Biochemical journal* 384 (Pt 3): 477–88.

Neasta, Jérémie, Sami Ben Hamida, Quinn Yowell, Sebastien Carnicella, and Dorit Ron. 2010. "Role for mammalian target of rapamycin complex 1 signaling in neuroadaptations underlying alcohol-related disorders." *Proceedings of the National Academy of Sciences of the United States of America* 107 (46): 20093–8 (nov).

Neasta, Jérémie, Sami Ben Hamida, Quinn V. Yowell, Sebastien Carnicella, and Dorit Ron. 2011. "AKT signaling pathway in the nucleus accumbens mediates excessive alcohol drinking behaviors." *Biological Psychiatry* 70 (6): 575–582.

Nolen-Hoeksema, Susan. 2004. “Gender differences in risk factors and consequences for alcohol use and problems.” *Clinical psychology review* 24 (8): 981–1010 (dec).

Okuda, Tomohiko, Yujiro Higashi, Koichi Kokame, Chihiro Tanaka, Hisato Kondoh, and Toshiyuki Miyata. 2004. “Ndrg1-deficient mice exhibit a progressive demyelinating disorder of peripheral nerves.” *Molecular and cellular biology* 24 (9): 3949–3956.

Okuda, Tomohiko, Koichi Kokame, and Toshiyuki Miyata. 2008. “Differential Expression Patterns of NDRG Family Proteins in the Central Nervous System.” *Journal of Histochemistry and Cytochemistry* 56 (2): 175–182.

Osna, Natalia A., and Kusum K. Kharbanda. 2016. “Multi-Organ Alcohol-Related Damage: Mechanisms and Treatment.” *Biomolecules* 6 (2): 1–5 (apr).

Pardo, Marta, Adrienne J. Betz, Noemí San Miguel, Laura López-Cruz, John D. Salamone, and Mercè Correa. 2013. “Acetate as an active metabolite of ethanol: studies of locomotion, loss of righting reflex, and anxiety in rodents.” *Frontiers in behavioral neuroscience* 7 (JUN): 81.

Park, Kyung Chan, Sharleen V Menezes, Danuta S Kalinowski, Sumit Sahni, Patric J Jansson, Zaklina Kovacevic, and Des R Richardson. 2018. “Identification of differential phosphorylation and sub-cellular localization of the metastasis suppressor, NDRG1.” *Biochimica et biophysica acta. Molecular basis of disease* 1864 (8): 2644–2663 (aug).

Paxson, Julia A, Alisha M Gruntman, Airiel M Davis, Christopher M Parkin, Edward P Ingenito, and Andrew M Hoffman. 2013. “Age dependence of lung mesenchymal stromal cell dynamics following pneumonectomy.” *Stem cells and development* 22 (24): 3214–25 (dec).

Perez, Edith A. 1998. “Paclitaxel in breast cancer.” *Oncologist* 3 (6): 373–389.

Phillips, Tamara J., John C. Crabbe, Pamela Metten, and John K. Belknap. 1994. “Localization of Genes Affecting Alcohol Drinking in Mice.” *Alcoholism: Clinical and Experimental Research* 18 (4): 931–941 (aug).

Pierre, Philippe. 2019. “Integrating stress responses and immunity.” *Science* 365 (6448): 28–29 (jul).

Pietiäinen, Vilja, Boris Vassilev, Tomas Blom, Wei Wang, Jessica Nelson, Robert Bittman, Nils Bäck, Noam Zelcer, and Elina Ikonen. 2013. “NDRG1 functions in LDL receptor trafficking by regulating endosomal recycling and degradation.” *Journal of cell science* 126 (Pt 17): 3961–71 (sep).

Prescott, Carol A., and Kenneth S. Kendler. 1999. “Genetic and Environmental Contributions to Alcohol Abuse and Dependence in a Population-Based Sample of Male Twins.” *American Journal of Psychiatry* 156 (1): 34–40 (jan).

Regan, Rainy D, Judy E Fenyk-melody, Sam M Tran, Guang Chen, and Kim L Stocking. 2016. “Submental blood collection in mice Materials and Methods.” *Journal of the American Asso-*

ciation for Laboratory Animal Science 55, No 5 (5): 570–576.

Ritchie, Matthew E., Belinda Phipson, Di Wu, Yifang Hu, Charity W. Law, Wei Shi, and Gordon K. Smyth. 2015. "limma powers differential expression analyses for RNA-sequencing and microarray studies." *Nucleic Acids Research* 43 (7): e47–e47 (apr).

Rowinsky, Eric K., Lorranie A. Cazenave, and Ross C. Donehower. 1990. "Taxol: A novel investigational antimicrotubule agent." *Journal of the National Cancer Institute* 82 (15): 1247–1259.

SAMHSA. 2013. "Results from the 2013 National Survey on Drug Use and Health: Summary of National Findings." *Substance Abuse and Mental Health Services Administration*, vol. HHS Publication No. (SMA) 14-4863.

Schuckit, M A, J L Klein, G R Twitchell, and L M Springer. 1994. "Increases in alcohol-related problems for men on a college campus between 1980 and 1992." *J Stud Alcohol* 55 (6): 739–742.

Schuster, Eugene F., Eric Blanc, Linda Partridge, and Janet M. Thornton. 2007. "Estimation and correction of non-specific binding in a large-scale spike-in experiment." *Genome Biology* 8 (6): R126.

Sevinsky, Christopher J., Faiza Khan, Leila Kokabee, Anza Darehshouri, Krishna Rao Maddipati, and Douglas S. Conklin. 2018. "NDRG1 regulates neutral lipid metabolism in breast cancer cells." *Breast Cancer Research* 20 (1): 1–17.

Sharma, Sushil, Arain, Mathur, Rais, Nel, Sandhu, Haque, and Johal. 2013. "Maturation of the adolescent brain." *Neuropsychiatric Disease and Treatment*, apr, 449.

Shi, Xiao Hua, Jacob C. Larkin, Baosheng Chen, and Yoel Sadovsky. 2013. "The Expression and Localization of N-Myc Downstream-Regulated Gene 1 in Human Trophoblasts." *PLoS ONE* 8 (9): 1–11.

Sibold, Sonja, Vincent Roh, Adrian Keogh, Peter Studer, Céline Tiffon, Eliane Angst, Stephan A Vorburger, Rosemarie Weimann, Daniel Candinas, and Deborah Stroka. 2007. "Hypoxia increases cytoplasmic expression of NDRG1, but is insufficient for its membrane localization in human hepatocellular carcinoma." *FEBS letters* 581 (5): 989–94 (mar).

Singh, Sandeep K, Reetika Bhardwaj, Katarzyna M Wilczynska, Catherine I Dumur, and Tomasz Kordula. 2011. "A complex of nuclear factor I-X3 and STAT3 regulates astrocyte and glioma migration through the secreted glycoprotein YKL-40." *The Journal of biological chemistry* 286 (46): 39893–903 (nov).

Skedsmo, Fredrik S., Michael A. Tranulis, Arild Espenes, Kristian Prydz, Kaspar Matiasek, Gjermund Gunnes, Lene C. Hermansen, and Karin H. Jäderlund. 2019. "Cell and context-dependent sorting of neuropathy-associated protein NDRG1 - Insights from canine tissues and primary Schwann cell cultures." *BMC Veterinary Research* 15 (1): 1–17.

Stein, Susanne, Emily K Thomas, Birger Herzog, Matthew D Westfall, Jonathan V Rocheleau, Roger S Jackson, Mai Wang, and Peng Liang. 2004. "NDRG1 is necessary for p53-dependent apoptosis." *The Journal of biological chemistry* 279 (47): 48930–40 (nov).

Stout, Randy F, Alexei Verkhratsky, and Vladimir Parpura. 2014. "Caenorhabditis elegans glia modulate neuronal activity and behavior." *Frontiers in cellular neuroscience* 8:67.

Sun, Jing, Daohai Zhang, Dong Hun Bae, Sumit Sahni, Patric Jansson, Ying Zheng, Qian Zhao, Fei Yue, Minhua Zheng, Zaklina Kovacevic, and Des R. Richardson. 2013. "Metastasis suppressor, NDRG1, mediates its activity through signaling pathways and molecular motors." *Carcinogenesis* 34 (9): 1943–1954.

Sun, Yan, Suhua Chang, Fan Wang, Hongqiang Sun, Zhaojun Ni, Weihua Yue, Hang Zhou, Joel Gelernter, Robert T. Malison, Rasmon Kalayasiri, Ping Wu, Lin Lu, and Jie Shi. 2019. "Genome-wide association study of alcohol dependence in male Han Chinese and cross-ethnic polygenic risk score comparison." *Translational Psychiatry* 9, no. 1.

Sundar, Raghav, Anand Jeyasekharan, Kar Tong Tan, Thomas Choudary Putti, Lay Mui Poh, Huiling Yap, Nur Sabrina Binte Sapari, Richie Chuan Teck Soong, and Soo-Chin Lee. 2014. "Paclitaxel-induced severe sensory peripheral neuropathy is associated with NDRG-1 genetic variant and negative NDRG-1 expression in nerve tissue." *Journal of Clinical Oncology* 32 (15_suppl): 1054–1054.

Sundar, Raghav, Anand D. Jeyasekharan, Brendan Pang, Richie Chuan Teck Soong, Nesaretnam Barr Kumarakulasinghe, Samuel Guan Wei Ow, Jingshan Ho, Joline Si Jing Lim, David Shao Peng Tan, Einar P.V. Wilder-Smith, Aishwarya Bandla, Stacey Sze Hui Tan, Bernadette Reyna Asuncion, Zul Fazreen, Michal Marek Hoppe, Thomas Choudary Putti, Lay Mui Poh, Boon Cher Goh, and Soo Chin Lee. 2016. "Low Levels of NDRG1 in nerve tissue are predictive of severe paclitaxel-induced neuropathy." *PLoS ONE* 11 (10): 1–8.

Thompson, Warren, and Gregory Lande. 2018. "Alcoholism Follow-up." *Drugs & Diseases*, vol. Medscape.

Treistman, Steven N, and Gilles E Martin. 2009. "BK Channels: mediators and models for alcohol tolerance." *Trends in neurosciences* 32 (12): 629–37 (dec).

Tu, Lan Chun, Xiaowei Yan, Leroy Hood, and Biaoyang Lin. 2007. "Proteomics analysis of the interactome of N-myc downstream regulated gene 1 and its interactions with the androgen response program in prostate cancer cells." *Molecular and Cellular Proteomics* 6 (4): 575–588.

Umoh, Nsini A., Robin K. Walker, Mustafa Al-Rubaiee, Miara A. Jeffress, and Georges E. Haddad. 2014. "Acute alcohol modulates cardiac function as PI3K/Akt regulates oxidative stress." *Alcoholism, clinical and experimental research* 38 (7): 1847–64 (jul).

Vaart, Andrew D Van Der, Jennifer T Wolstenholme, Maren L Smith, Guy M Harris, Marcelo F Lopez, Aaron R Wolen, Howard C Becker, Robert W Williams, and Michael F Miles. 2017.

"The allostatic impact of chronic ethanol on gene expression : A genetic analysis of chronic intermittent ethanol treatment in the BXD cohort." *Alcohol* 58:93–106.

van der Vaart, Andrew, Xianfang Meng, M. Scott Bowers, Angela M. Batman, Fazil Aliev, Sean P. Farris, Jennifer S. Hill, Thomas A. Green, Danielle Dick, Jennifer T. Wolstenholme, and Michael F. Miles. 2018. "Glycogen synthase kinase 3 beta regulates ethanol consumption and is a risk factor for alcohol dependence." *Neuropsychopharmacology* 43 (13): 2521–2531.

Velázquez-Marrero, Cristina, Alexandra Burgos, José O. García, Stephanie Palacio, Héctor G. Marrero, Alexandra Bernardo, Juliana Pérez-Laspiur, Marla Rivera-Oliver, Garrett Seale, and Steven N. Treistman. 2016. "Alcohol regulates BK surface expression via Wnt/β-catenin signaling." *Journal of Neuroscience* 36 (41): 10625–10639.

Wheeler, D. Lori, Alan Sariol, David K. Meyerholz, and Stanley Perlman. 2018. "Microglia are required for protection against lethal coronavirus encephalitis in mice." *The Journal of clinical investigation* 128 (3): 931–943.

Wickham, Hadley. 2016. *ggplot2: Elegant Graphics for Data Analysis*. Springer-Verlag New York.

Wolen, Aaron R, Charles A Phillips, Michael A Langston, Alex H Putman, Paul J Vorster, Nathan A Bruce, Timothy P York, Robert W Williams, and Michael F Miles. 2012. "Genetic dissection of acute ethanol responsive gene networks in prefrontal cortex: functional and mechanistic implications." *PloS one* 7 (4): e33575 (jan).

Wolstenholme, Jennifer T., Jon A. Warner, Maria I. Capparuccini, Kellie J. Archer, Keith L. Shelton, and Michael F. Miles. 2011. "Genomic Analysis of Individual Differences in Ethanol Drinking: Evidence for Non-Genetic Factors in C57BL/6 Mice." *PLoS ONE* 6 (6): e21100 (jun).

Wolstenholme, Jennifer T, Tariq Mahmood, Guy M Harris, Shahroze Abbas, and Michael F Miles. 2017. "Intermittent Ethanol during Adolescence Leads to Lasting Behavioral Changes in Adulthood and Alters Gene Expression and Histone Methylation in the PFC." *Frontiers in molecular neuroscience* 10:307.

Xu, Weihong, Junhee Seok, Michael N. Mindrinos, Anthony C. Schweitzer, Hui Jiang, Julie Wilhelmy, Tyson A. Clark, Karen Kapur, Yi Xing, Malek Faham, John D. Storey, Lyle L. Moldawer, Ronald V. Maier, Ronald G. Tompkins, Wing Hung Wong, Ronald W. Davis, Wenzhong Xiao, and Inflammation and Host Response to Injury Large-Scale Collaborative Research Program. 2011. "Human transcriptome array for high-throughput clinical studies." *Proceedings of the National Academy of Sciences of the United States of America* 108 (9): 3707–12 (mar).

Yao, Yuxiao, Shaoyang Sun, Jingjing Wang, Fei Fei, Zhaoru Dong, Ai Wu Ke, Ruoyu He, Lei Wang, Lili Zhang, Min Biao Ji, Qiang Li, Min Yu, Guo Ming Shi, Jia Fan, Zhiyuan Gong, and Xu Wang. 2018. "Canonical Wnt signaling remodels lipid metabolism in zebrafish hepa-

tocytes following ras oncogenic insult." *Cancer Research* 78 (19): 5548–5560.

Yoneyama, Naomi, John C Crabbe, Matthew M Ford, Andrea Murillo, and Deborah A Finn. 2008. "Voluntary ethanol consumption in 22 inbred mouse strains." *Alcohol (Fayetteville, N.Y.)* 42 (3): 149–60 (may).

Yu, Waylin, Lara S Hwa, Viren H Makhijani, Joyce Besheer, and Thomas L. Kash. 2019. "Chronic inflammatory pain drives alcohol drinking in a sex-dependent manner for C57BL/6J mice." *Alcohol* 77 (jun): 135–145.

Yuan, Chunbo, Robert J. O'Connell, Robert F. Jacob, R. Preston Mason, and Steven N. Treistman. 2007. "Regulation of the Gating of BK Ca Channel by Lipid Bilayer Thickness." *Journal of Biological Chemistry* 282 (10): 7276–7286 (mar).

Zahr, Natalie M., and Adolf Pfefferbaum. 2017. "Alcohol's Effects on the Brain: Neuroimaging Results in Humans and Animal Models." *Alcohol research : current reviews* 38 (2): 183–206.

Zajaczkowską, Renata, Magdalena Kocot-Kępska, Wojciech Leppert, Anna Wrzosek, Joanna Mika, and Jerzy Wordliczek. 2019. "Mechanisms of chemotherapy-induced peripheral neuropathy." *International Journal of Molecular Sciences* 20, no. 6.

Zhang, Li, Long Wang, Ajay Ravindranathan, and Michael F Miles. 2002. "A new algorithm for analysis of oligonucleotide arrays: application to expression profiling in mouse brain regions." *Journal of molecular biology* 317 (2): 225–35 (mar).

Ziegler, Gabriel, Tobias U Hauser, Michael Moutoussis, Edward T Bullmore, Ian M Goodyer, Peter Fonagy, Peter B Jones, NSPN Consortium, Ulman Lindenberger, and Raymond J Dolan. 2019. "Compulsivity and impulsivity traits linked to attenuated developmental frontostriatal myelination trajectories." *Nature neuroscience* 22 (6): 992–999.

Vita

Guy Harris was born in Atlanta, Georgia on August 22, 1986. He grew up on a small farm outside of the city and received his B.S. in Physics from the Georgia Institute of Technology in 2009. After deciding to pursue a career in the field of medicine, Guy moved to Baton Rouge, Louisiana to work towards a Masters of Science in Medical and Health Physics at Louisiana State University. During the three years spent in Baton Rouge, Guy spent two years working at the program's clinical affiliate, Mary Bird Perkins Cancer Center. The clinical environment of Mary Bird Perkins Cancer influenced him to continue his education in translational research between basic and clinical sciences at Virginia Commonwealth University in Richmond, Virginia.